Theory and Phenomenology of Dirac Leptogeneis

by

Brooks D. Thomas

A dissertation submitted in partial fulfillment
of the requirements for the degree of
Doctor of Philosophy
(Physics)
in The University of Michigan
2007

Doctoral Committee:

Associate Professor James D. Wells, Chair
Professor Fred C. Adams
Professor Gordon L. Kane
Associate Professor Timothy A. McKay
Assistant Professor Aaron T. Pierce

From the digital fountains
To the analog mountains
Let the mirror express the room.

— David Berman

ACKNOWLEDGEMENTS

I would like to thank my advisor, James D. Wells, for all the help and guidance he's offered me over the past five years, and the members of my committee for all their assistance. I would also like to think all the colleagues in the MCTP with whom I've worked and interacted during my tenure as a graduate student, and especially my research collaborators David Morrissey and Manuel Toharia.

TABLE OF CONTENTS

LIST OF FIGURES

Figure

LIST OF TABLES

Table

LIST OF APPENDICES

Appendix

ABSTRACT

Theory and Phenomenology of Dirac Leptogenesis

by
Brooks D. Thomas

Chair: James D. Wells

Dirac leptogenesis, in which neutrinos are purely Dirac and develop small but nonzero effective masses without the aid of the see-saw mechanism, provides an interesting alternative to the standard leptogenesis picture. Here we review the theory and phenomenology of Dirac leptogenesis and show that it is a viable theory capable of simultaneously satisfying all relevant bounds from cosmology, neutrino physics, and flavor violation. In addition, we also explore several potential extensions of the model, such as the possibility of right-handed sneutrino dark matter and the potential for relating the leptogenesis mechanism to the origin of the μ-term. Theories with a heavy gravitino and gaugino masses generated by anomaly mediation emerge as one natural context for Dirac leptogenesis. In such models the lightest neutralino is often expected to be predominately wino or Higgsino, and is a viable dark matter candidate. We conclude with an examination of the prospects for detecting the effectively monoenergetic photon signal that results from the annihilation of such a dark matter particle in the galactic halo.

CHAPTER I

BARYOGENESIS AND LEPTOGENESIS

1.1 The Problem of the Baryon Asymmetry

The universe we live in is manifestly asymmetric between baryons and antibaryons. This statement can be quantified by introducing a parameter η, defined as $\eta = n_B/n_\gamma$. Here $n_B \equiv n_b - n_{\overline{b}}$, where n_b and $n_{\overline{b}}$ are the baryon density and antibaryon density of our universe, respectively, and n_γ is the present number density of photons. The value of η has recently been measured with great precision by WMAP [1] to be within the range

$$\eta = (6.1 \pm 0.3) \times 10^{-10}, \tag{1.1}$$

which implies that the relic density of baryonic matter in our universe is somewhere in the range

$$0.021 < \Omega_b h^2 < 0.025. \tag{1.2}$$

Since the standard cosmology is manifestly symmetric with respect to matter and antimatter, it must be supplemented with some additional physics which can account for the presence of a baryon asymmetry on the observed scale. The generic name for such scenarios is baryogenesis.

Any successful baryogenesis model must satisfy a set of three requirements which were originally pointed out by Sakharov [2]. The first and most self-evident of these conditions is that there must be baryon number violation; otherwise, a universe with an initial value of $\eta = 0$ could not evolve to one where $\eta \neq 0$. The second is that the charge conjugation symmetry C and its composition with parity CP must also be violated. If this were not the case, baryon number violation and antibaryon number violation would occur at the same rate, and hence no net baryon asymmetry would be created. Finally, one must have either a departure from thermal equilibrium or else posit that CPT, the composition of CP with the time evolution operator, is somehow violated during the early universe. This condition can be obtained by calculating the thermal average $\langle B \rangle$ of the baryon number, a dimensionless quantity defined by the $B \equiv (n_b - n_{\overline{b}})/s$ in terms of the entropy density

$$s = \frac{2\pi^2}{45} g_* T^3, \tag{1.3}$$

where T is the temperature of the thermal bath and g_* is the number of interacting degrees of freedom (in the minimal supersymmetric model (MSSM) during the baryogenesis epoch, $g_* \approx 205$). The result is [3]:

$$\langle B \rangle = \mathrm{Tr}[e^{-\beta H} B] = \mathrm{Tr}[(CPT)(CPT)^{-1} e^{-\beta H} B]. \tag{1.4}$$

If CPT commutes with the Hamiltonian, this becomes

$$\langle B \rangle = \mathrm{Tr}[e^{-\beta H} B] = \mathrm{Tr}[e^{-\beta H} (CPT)^{-1} B (CPT)] = -\mathrm{Tr}[e^{-\beta H} B], \tag{1.5}$$

which implies $B = 0$ (conversely, if thermal equilibrium is not maintained, all particle species will not have a common temperature, and trace cyclicity can no longer be invoked). If any of these three conditions is not met, η will not deviate from zero. In general, since Lorentz

invariance is believed to be necessary for the formulation of a consistent quantum field theory, this condition has been taken to imply a departure from thermal equilibrium rather than the presence of CPT-violation. The alternative, in which Lorentz invariance is temporarily, dynamically violated in the early universe, was originally explored in the spontaneous baryogenesis scenario of [4] and has been elaborated on in models like the radion-induced baryogenesis of [5] and the gravitational baryogenesis of [6], in which a net baryon number is produced via a CP-violating effective interaction between the baryon number current and the derivative of the Ricci Scalar. Indeed Lorentz invariance is violated whenever a tensor field receives a nonzero vacuum expectation value (VEV), and indeed may arise spontaneously in string theories, brane-world scenarios, and modified gravity models [7]. Still, no experimental signal of CPT violation has ever been detected [8, 9], and most theories of baryogenesis (including the one with which this work is principally concerned) assume that CPT is a good symmetry of the Hamiltonian and that the generation of a baryon number for the universe involves out-of-equilibrium dynamics rather than Lorentz violation.

1.2 Baryogenesis via Leptogenesis

1.2.1 Leptogenesis and the See-Saw Mechanism

A variety of viable baryogenesis models exist, including electroweak baryogenesis, in which CP-violation occurs at a bubble wall, or phase boundary, and Affleck-Dine baryogenesis [10], in which the baryon asymmetry is generated by moduli fields charged under $B - L$, where $L = (n_\ell - n_{\overline{\ell}})/s$ denotes the lepton number of the universe. In this paper, we will focus on models which achieve baryogenesis through a framework known as leptogenesis [11, 12], where

decays of heavy particles in the early universe which violate both CP and lepton number L produce an initial lepton asymmetry, which is then converted to a nonzero baryon asymmetry by sphaleron processes associated with the $SU(2)$ electroweak anomaly [13]. Leptogenesis is a particularly attractive model because in addition to its ability to yield a realistic value for η [14], it can also explain why the standard model neutrinos have small but nonzero masses. In its most common form, which we will call Majorana leptogenesis, the role of the heavy, decaying particles is played by the right-handed neutrinos ν_R required to fill out the multiplets housing the Standard Model fields in many grand unified groups. As they are gauge singlets, nothing prevents them from obtaining large (GUT-scale) Majorana masses M_{ν_R}, and such masses are inherently lepton-number-violating.

In the following brief review of Majorana leptogenesis, and for the remainder of this work, we will work under the assumption that the universe we live in is inherently supersymmetric, but that supersymmetry is broken at some high scale M_{SUSY}. Although leptogenesis certainly does not require supersymmetry, we choose to work in a supersymmetric framework for a variety of reasons. Supersymmetry naturally explains the stability of the weak scale against quadratic divergences [15, 16] and improves the outlook for the unification of the Standard Model gauge couplings [17, 18]. Furthermore, the assumption of conserved (or nearly conserved) R-parity makes the lightest supersymmetric particle (LSP) a convenient dark matter candidate [19].

In supersymmetric Majorana leptogenesis, the most general realizable superpotential one can write for the relevant fields is

$$\mathcal{W} \ni y_{\alpha\beta} L_\alpha N_\beta H_u + M_{\nu_R \alpha} N_\alpha N_\alpha, \tag{1.6}$$

where L_α and N_α represent the left- and right-handed neutrino superfields respectively, H_u is

the up-type Higgs superfield, and $y_{\alpha\beta}$ is a dimensionless trilinear coupling.[1] This superpotential contains both Majorana and Dirac masses for neutrinos (once the Higgs field gets a VEV) and yields a mass matrix

$$\overline{\nu}\mathbf{M}\nu = (\overline{\nu}_L \ , \ \overline{\nu}_R) \begin{pmatrix} 0 & m_D \\ m_D^T & M_{\nu_R} \end{pmatrix} \begin{pmatrix} \nu_L \\ \nu_R \end{pmatrix}, \tag{1.7}$$

where flavor indices have been suppressed to simplify notation. Since $m_D = yv \sin\beta$, where $\tan\beta = v_u/v_d$ denotes the ratio of the up- and down-type Higgs VEVs, the off-diagonal terms mixing ν_L and ν_R will be small compared to $M_{\nu_R\alpha}$. As a result, when this matrix is diagonalized, the mass spectrum of the theory contains three light neutrinos with masses

$$m_\nu = m_D \frac{1}{M_{\nu_R}} m_D^\dagger, \tag{1.8}$$

which are identified with the Standard Model neutrinos, as well as three heavy neutrinos with masses $\mathcal{O}(M_{\nu_R})$. This method for obtaining small but nonzero neutrino masses is known as the see-saw mechanism [20, 21], and the liaison it forges between the origin of the observed baryon asymmetry and the lightness of the Standard Model neutrinos is one of the most compelling aspects of leptogenesis scenarios.

One of the useful consequences of Majorana component to the light neutrino masses is that such a source of lepton number violation would be observable in neutrinoless double-β decay experiments [22]. The contribution to this process from a Majorana neutrino mass is shown diagrammatically in figure 1.2. It should be noted that a Majorana neutrino mass is not required for it to occur (certain other other beyond-the-Standard-Model sources of lepton number violation can also contribute), but if neutrinoless double-β decay were ever observed, it would serve as compelling evidence in favor of the see-saw mechanism.

[1] We have chosen to work in a basis where the $M_{\nu_R\alpha}$ are diagonal.

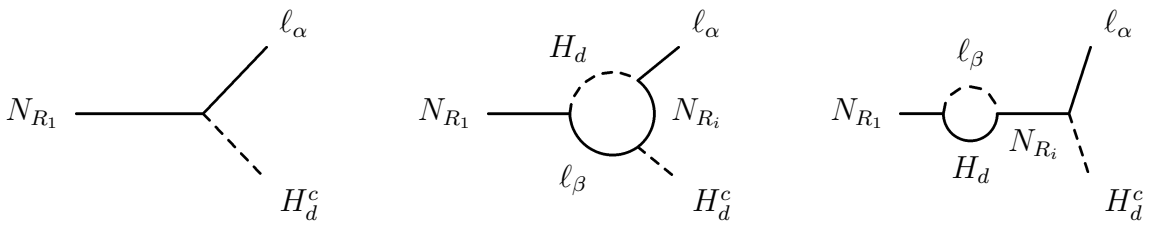

Figure 1.1: The diagrams whose interference yields the leading contribution to CP-violation from N_{R_1} decays in the traditional, Majorana version of leptogenesis. In a supersymmetric theory, the supersymmetrized versions of these diagrams must also be included.

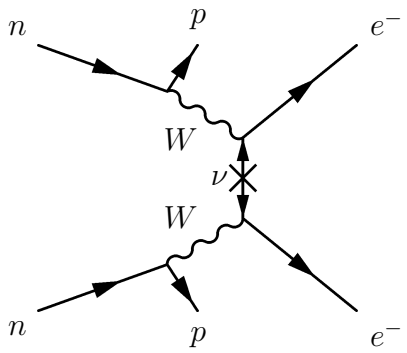

Figure 1.2: A diagrammatical representation of neutrinoless double-β decay.

The production of lepton number in Majorana leptogenesis occurs when the heavy right-handed neutrinos decay out of equilibrium. The leading CP-violating contribution comes from the interference between the diagrams shown in figure 1.1 (in supersymmetric models, the supersymmetrized versions of these diagrams must also be included), and results in the generation of a nonzero lepton number L for the universe in the traditional, Majorana version of leptogenesis. In the limit where there is a large splitting between the right-handed sneutrino masses ($M_{\nu_R 1} \ll M_{\nu_R 2},\ M_{\nu_R 3}$) The contribution from a single N_{R_1} decay is commonly called the decay

asymmetry and is given by [23]

$$\epsilon \approx \frac{3}{16\pi} \frac{\mathrm{Im}\left[y^*_{1\alpha} y_{i\beta} y^*_{1\beta} y_{i\alpha}\right]}{(y_{1\beta} y^*_{1\beta})} \left(\frac{M_{\nu_R 1}}{M_{\nu_R i}}\right) \tag{1.9}$$

where a sum over repeated indices is assumed. This translates into a net lepton number [11]

$$L = \kappa_W \frac{\epsilon}{g_*} \tag{1.10}$$

for the universe, where κ_W is a dimensionless, model-dependent prefactor included to account for the washout of lepton number by $2 \leftrightarrow 2$ lepton-number-violating processes, etc. that deplete the lepton number genrated during N_{R_1} decay. Whether Majorana leptogenesis is capable of reproducing the observed value of η depends both on ϵ and on κ_W.

1.2.2 Effects of the Electroweak Anomaly

So far we have seen that the leptogenesis mechanism is capable of generating a net lepton number $L \neq 0$ for the universe. A mechanism by which this lepton number can be transformed into a net baryon number is built into the Standard Model (SM) [24]. The baryon and lepton number currents

$$J^B_\mu = \frac{1}{3} \sum_i \left(\overline{q}_{L_i} \gamma_\mu q_{L_i} + \overline{u}_{R\alpha} \gamma_\mu u_{R\alpha} + \overline{d}_{R\alpha} \gamma_\mu d_{R\alpha}\right) \tag{1.11}$$

$$J^L_\mu = \frac{1}{3} \sum_i \left(\overline{\ell}_{L_i} \gamma_\mu \ell_{L_i} + + \overline{e}_{R_i} \gamma_\mu e_{R_i}\right), \tag{1.12}$$

where the sum is over generations, are anomalous due to the triangle anomaly, with divergence

$$\partial^\mu J^B_\mu = \partial^\mu J^L_\mu = \frac{N_f}{32\pi^2} \left(g_2^2 W^a_{\mu\nu} \tilde{W}^{a\mu\nu} + g_Y^2 F_{\mu\nu} \tilde{F}^{\mu\nu}\right). \tag{1.13}$$

Here, $W^a_{\mu\nu}$ and $F_{\mu\nu}$ are the respective field-strength tensors of the $SU(2)$ and $U(1)_Y$ gauge fields, g_2 and g_Y are the respective gauge coupling constants, N_f denotes the number of fermion

generations, and

$$\tilde{F}^{\mu\nu} = \frac{1}{2}\epsilon^{\mu\nu\rho\sigma}F_{\rho\sigma} \tag{1.14}$$

is the dual of $F^{\mu\nu}$ (the expression for $\tilde{W}^{a\mu\nu}$ is analogous). The change in baryon number over some duration t is then given in terms of the Chern-Simons number

$$N_{CS}(t) = \frac{g_2^3}{96\pi^2}\int d^3x\epsilon^{ijk}\epsilon_{abc}W_i^a W_j^b W_k^c(t) \tag{1.15}$$

by

$$\begin{aligned} B(t) - B(0) &= \int_0^t \int d^3x \partial^\mu J_\mu^B \\ &= N_f\left[N_{CS}(t) - N_{CS}(0)\right]. \end{aligned} \tag{1.16}$$

An analogous equation exists for lepton number.

This theory has an infinite number of quasi-degenerate vacua, in each of which the W_i^a are pure gauge and consequently N_{CS} becomes an integer. Equation (1.16) tells us that vacuum-to-vacuum transitions involve $\Delta B = \Delta L = N_f\Delta N_{CS}$, so the minimum change for such a transition in the SM, where $N_f = 3$, is $\Delta B = \Delta L = 3$. This corresponds to an effective 12-fermion interaction[2]

$$\mathcal{O}_{B+L} = \prod_i \left(q_{L_i}q_{L_i}q_{L_i}\ell_i\right), \tag{1.17}$$

where we have included the $B+L$ subscript to draw attention to another important consequence of equation (1.16): since the same equation describes the evolution of both baryon and lepton number, the combination $B - L$ is conserved in any process of the form (1.17), while $B + L$ is violated by at least 6 units. These effective interactions serve as the primary means of conversion between B and L in leptogenesis.

[2]The physical scale Λ associated with this effective operator is the inverse of the magnetic screening length $R_{Sph} \sim 1/(\alpha_2 T)$.

In calculating the transition rate for these interactions, we will make use of the fact that the potential energy of the electroweak theory between any pair of adjacent ($\Delta N_{CS} = 1$) vacua contains a saddle point, and that transitions through that point in field space should dominate over all others. This field configuration is known as the electroweak sphaleron, and the height of the potential barrier separating any two adjacent vacua is known as the sphaleron energy, usually denoted by E_{sph}. At zero temperature, the rate for such transitions is determined by the instanton action and turns out to be completely negligible [24]:

$$\Gamma_{inst} \sim e^{-S_{inst}} = e^{-1/g_2^2} \sim 10^{-165}. \tag{1.18}$$

At finite temperatures, however, the situation is modified by the possibility of thermal excitations over the barrier. For low temperatures $T < E_{sph}$, the rate calculation is reasonably straightforward and the result [25] is

$$\Gamma_{sph} = c \left[\frac{E_{sph}^3 M_W^4(T)}{T^6} \right] e^{-E_{sph}/T}, \tag{1.19}$$

where c is an $O(1)$ constant and $M_W(T)$ is the mass of the W boson as a function of temperature.

At higher temperatures $T > E_{sph}$, the calculation of the sphaleron interaction rate is somewhat difficult, but it can be estimated on dimensional grounds by examining the scales of the processes involved [26]. Non-perturbative fluctuations of the gauge field that mediate the sphaleron transition are associated with magnetic fluctuations with characteristic distance scale $R_{Sph} \sim 1/(\alpha_2 T)$ on the order of the magnetic screening length. If one naively assumes that the time scale for the process is of the same order, one obtains the result $\Gamma_{Sph} \sim \alpha_2^4 T$. However, when one takes into account damping effects in the plasma [27, 28] one finds that the time scale

is slowed to $t_{Sph} \sim 1/(\alpha_2^2 T)$, which leads to a rate[3]

$$\Gamma_{Sph} = (25.4 \pm 2.0)\alpha_2^5 T, \tag{1.20}$$

where $\alpha_2 \equiv g_2^2/4\pi \approx 1/30$ and the value given for the proportionality constant is the result of numerical calculations [30, 31].

Sphaleron interactions will be in equilibrium whenever the sphaleron transition rate Γ_{sph} exceeds the expansion rate of the universe, expressed by the Hubble parameter H. When the universe is radiation-dominated, the expansion rate is given by

$$H = 1.66 g_*^{1/2} T^2 / M_P. \tag{1.21}$$

From equations (1.19) and (1.20) we find that sphaleron interactions are in equilibrium when

$$100 \text{ GeV} < T < 10^{13} \text{ GeV}, \tag{1.22}$$

which means that the interconversion of B and L can be considered rapid perhaps during and certainly soon after the lepton number asymmetry L is built up by the decays of the heavy right-handed neutrino fields and will remain rapid down to around the weak scale.

In order to relate these baryon and lepton number asymmetries to each other in a quantitative way, we can take advantage of the set of conditions among the chemical potentials μ_i implied by equilibrium conditions among the species i present in the thermal bath. If chemical equilibrium is established between particle species $a_1, a_2 \ldots, a_m, b_1, b_2, \ldots b_n$ by sufficiently rapid interactions of the form $a_1, a_2 \ldots a_f \leftrightarrow b_1 b_2 \ldots b_f$, their chemical potentials obey the relation

$$\sum_{i=1}^{m} \mu_{a_i} = \sum_{i=1}^{n} \mu_{b_i}. \tag{1.23}$$

[3]It has been argued [29] that the characteristic time scale of these processes may also have a logarithmic suppression, so that $\Gamma_{sph} \sim [\alpha_2^5 T \ln(1/\alpha)]$. Since what is of interest to us is the numerical result for the rate of baryon-number-changing transitions, we can remain agnostic on this issue.

For example, when sphaleron interactions are in equilibrium, equation (1.17) implies that

$$\sum_i (3\mu_{q_i} + \mu_{\ell_i}) = 0. \tag{1.24}$$

Similarly, $SU(3)$ QCD instanton processes and global hypercharge conservation respectively require that

$$\sum_i (2\mu_{q_i} - \mu_{u_i} - \mu_{d_i}) = 0 \tag{1.25}$$

$$\sum_i \left(\mu_{q_i} + 2\mu_{u_i} - \mu_{d_i} - \mu_{\ell_i} - \mu_{e_i} + \frac{2}{N_f}\mu_H\right) = 0, \tag{1.26}$$

and from the fermion Yukawa interactions

$$\sum_i (2\mu_{q_i} - \mu_H - \mu_{d_i}) = 0 \tag{1.27}$$

$$\sum_i (2\mu_{q_i} + \mu_H - \mu_u) = 0 \tag{1.28}$$

$$\sum_i (2\mu_{\ell_{Li}} - \mu_H - \mu_{e_i}) = 0. \tag{1.29}$$

Since particles of different generations will also be in equilibrium with one another at high temperatures, we can take $\mu_{q_i} = \mu_{q_L}$, $\mu_{u_i} = \mu_u$, $\mu_{d_i} = \mu_d$, $\mu_{\ell_i} = \mu_\ell$, $\mu_{e_i} = \mu_e$ and solve this system of equations for one of the μ_i (we choose μ_ℓ). The resulting chemical potentials are

$$\begin{gathered}\mu_e = \frac{2N_f+3}{6N_f+3}\mu_\ell \quad \mu_d = -\tfrac{6N_f+1}{6N_f+3}\mu_\ell \quad \mu_u = \frac{2N_f-1}{6N_f+3}\mu_\ell \\ \mu_q = \frac{1}{3}\mu_\ell \quad \mu_H = \tfrac{4N_f}{6N_f+3}\mu_\ell,\end{gathered} \tag{1.30}$$

and since the values of B and L are related to these chemical potentials (see equation (B.5) in appendix B) by

$$B = \frac{1}{g_{*s}T}\sum_{i=baryon} g_i\mu_i = \frac{N_f}{g_{*s}T}(2\mu_q + \mu_u + \mu_d) \tag{1.31}$$

$$L = \frac{1}{g_{*s}T}\sum_{i=baryon} g_i\mu_i = \frac{N_f}{g_{*s}T}(2\mu_\ell + \mu_e), \tag{1.32}$$

one finds that

$$B = \frac{8N_f + 4}{22N_f + 13}(B - L) \qquad\qquad L = -\frac{14N_f + 9}{22N_f + 13}(B - L) \tag{1.33}$$

in the Standard Model. From this, we can state the relationship between baryon and lepton number when sphaleron interactions are in equilibrium:

$$B = \frac{28}{51}L. \tag{1.34}$$

In the MSSM, things are modified by the presence of a second Higgs doublet, and the result becomes result is

$$B = \frac{8}{23}L. \tag{1.35}$$

In Majorana leptogenesis, we know that since $B - L$ is conserved by sphalerons and violated only by the lepton-number-producing decays of N_{R_1}, the initial value $(B - L)_{init} = -L_{init}$ generated during the leptogenesis epoch and the present value will be equal; hence (in the MSSM)

$$B_{today} = -\frac{8}{23}L_{init} = -\frac{8}{23}\,\kappa_W\,\frac{\epsilon}{g_*} \tag{1.36}$$

and the universe receives a nonzero baryon number.

1.2.3 An Alternative Leptogenesis Scenario

Although it is not our aim to discuss the details of Majorana leptogenesis models, we note that they have been shown to be able to yield a realistic value of η, reproduce the observed light neutrino spectrum, and evade problems associated with relevant astrophysical constraints (for recent reviews, see [14, 23, 32, 33]). In this form, leptogenesis emerges as a viable phenomenological theory. There may be other forms of leptogenesis that are just as successful, however.

The aim of this work is to conduct a thorough examination of one such alternative, supersymmetric Dirac leptogenesis, and to show that it is also a phenomenologically viable model. We will begin by discussing the symmetries and field content which determine the form of superpotential and discuss the consequences of that superpotential for baryogenesis and neutrino masses in chapter II. In chapter III, we enumerate the phenomenological constraints on Dirac leptogenesis and construct a simple, theoretically-motivated model. In chapter IV, we solve the Boltzmann equations for the evolution of baryon and lepton number in the early universe numerically and discuss the consequences of these results on the model parameters. We investigate some potentially promising extensions of the model in chapter V, and in chapter VII.

CHAPTER II

DIRAC LEPTOGENESIS

2.1 Superpotential and Fields

While Majorana leptogenesis is a certainly successful model, it is not the only way in which leptogenesis can be realized. There are several reasons why exploring potential alternatives is a worthwhile endeavor, and in particular why it is advantageous to have a viable leptogenesis mechanism in a model without Majorana neutrinos. One is that the non-observation of neutrinoless double-β decay at future experiments [22, 34] could significantly constrain the parameter space of Majorana leptogenesis to the point where severe model tensions might arise between such constraints and others from astrophysics, flavor-physics, etc. Another is that it is not at all obvious that massive right-handed neutrinos emerge naturally from a string-theory context. While landscape surveys, even for particular classes of models and specified orbifold compactifications, are limited by computational complexity, preliminary results [35] performed for heterotic BSL_A models on the Z_3 orbifold suggest that a see-saw mechanism in the traditional sense is not a generic feature of otherwise phenomenologically promising string models.

For all these reasons, it would be useful if one could find a way to link the smallness of the physically-observed neutrino masses to a successful baryogenesis mechanism without having to introduce singlet neutrinos with Majorana masses. It is indeed possible to do this in the context of a scenario that has come to be known as Dirac leptogenesis or Dirac neutrinogenesis [36, 37]. In this scenario, an additional symmetry (the precise form of which is not terribly important or stringently constrained by the model framework) is introduced, and charges are assigned under this new symmetry in a manner which forbids, at tree level, both the Majorana and Dirac neutrino mass terms appearing in (1.6). A set of heavy, vector-like pairs of fields introduced whose couplings to the standard model fields contain nontrivial, CP-violating phases are also introduced. These fields will play the role that heavy right-handed neutrinos play in Majorana leptogenesis, and their decays during the early universe will lead to the buildup of equal and opposite lepton asymmetries L_ℓ and L_{ν_R} in the left-handed lepton and right-handed neutrino sectors, while conserving the overall lepton number for the universe $L_{tot} = L_\ell + L_{\nu_R} = 0$. The equilibration rate between these stores is suppressed by the smallness of the effective neutrino Dirac mass term; as a result, the electroweak sphaleron processes which convert L_ℓ into a baryon asymmetry B effectively shut off before L_ℓ and L_{ν_R} have a chance to equilibrate. Consequently, unlike in Majorana leptogenesis, the universe ends up with a net positive lepton number as well as a net positive baryon number—a result which is depicted schematically in figure 2.1.

We will begin by writing down the superpotential for Dirac leptogenesis,[1] which is modified from that of the MSSM only in the lepton sector. The field content and charge assignments of the model are essentially the same as those presented in [37]. Of the usual quark and lepton supermultiplets of the MSSM, the left-handed lepton multiplets L_α (α is a family index) and

[1]Once again, we remark that Dirac leptogenesis does not require supersymmetry and functions perfectly well without it [36].

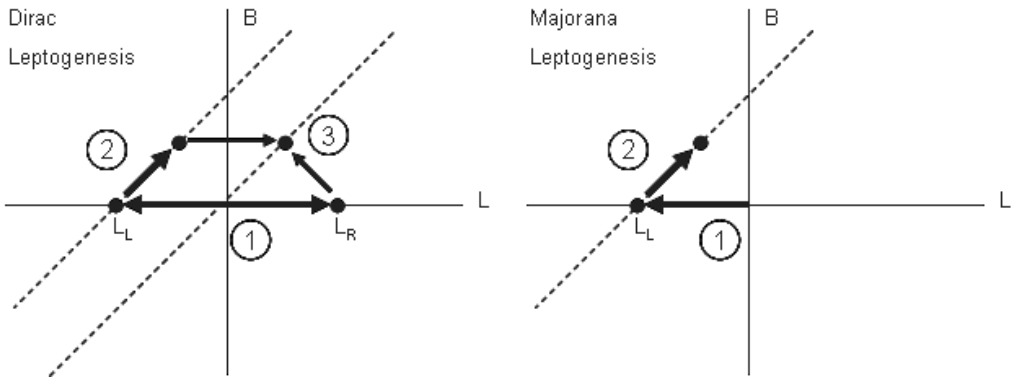

Figure 2.1: A schematic representation, after [36, 38], of the evolution of baryon number B (vertical axis) and lepton number L (horizontal axis) in Dirac and Majorana leptogenesis. In Dirac leptogenesis (left panel), the evolution of B and L_{tot} proceeds in three steps: first, two stores of lepton number L_ℓ (stored in left-handed neutrinos) and L_{ν_R} (stored in right-handed neutrinos) are produced during heavy particle decays; second, sphaleron processes (which act along lines of constant $B-L$) mix L_ℓ and B while leaving L_{ν_R} alone; third, after sphaleron interactions have effectively shut off, equilibration between L_ℓ and L_{ν_R} results in a net positive B and L for the universe. This is qualitatively quite different from the situation in Majorana leptogenesis (right-hand panel). Here, lepton-number-violating heavy particle decays first build up a single, nonzero store or lepton number $L_\ell = L_{tot}$; second, sphalerons transmute this lepton number into a nonzero baryon number for the universe. Only one store of lepton number is created, and the result is a universe with negative L_{tot} and positive B.

the Higgs multiplets H_u and H_d will be pertinent to leptogenesis. We also include a right-handed neutrino superfield N_α for each family, an exotic chiral multiplet χ, and a number N_Φ of vector-like pairs of chiral multiplets Φ_i and $\overline{\Phi}_i$. While at least two such pairs are required for leptogenesis, any $N_\Phi \geq 2$ is in principle allowed from a baryogenesis standpoint. We also need to introduce an additional symmetry to forbid Majorana masses for the N_α, which we choose to be an additional global $U(1)$ we will call $U(1)_N$, due to the fact that the right-handed neutrinos are charged under it. The charge configurations of these fields under this additional $U(1)$, as well as the rest of the relevant symmetries of the theory, are shown in table 2.1.[2] The

[2]With the field content given in table 2.1, the global $U(1)_N$ is anomalous. To deal with this issue, one

Field	$U(1)_L$	$U(1)_N$	$SU(2)$	$U(1)_Y$	P_M
N	-1	+1	**1**	0	-1
L	+1	0	**2**	$-\frac{1}{2}$	-1
H_u	0	0	**2**	$\frac{1}{2}$	+1
H_d	0	0	**2**	$-\frac{1}{2}$	+1
ϕ	+1	-1	**2**	$-\frac{1}{2}$	-1
$\overline{\phi}$	-1	+1	**2**	$\frac{1}{2}$	-1
χ	0	-1	**1**	0	+1

Table 2.1: One possible set of charge assignments, taken from [37], that leads to the Dirac leptogenesis superpotential given in (2.1). Here the additional symmetry employed is a $U(1)$ (which may in principle be either global or local). Only the charges of the fields relevant to leptogenesis, which include the Higgs doublets H_u and H_d, the left-handed lepton superfield L, the right-handed neutrino superfield N, the heavy fields Φ and $\overline{\Phi}$, and the additional field χ, have been included. Here, $U(1)_L$, $SU(2)$, and $U(1)_Y$ respectively denote lepton number, $SU(2)$, and $U(1)$ hypercharge quantum numbers, P_M denotes matter parity, and $U(1)_N$ denotes the charge under the additional $U(1)$.

most general superpotential that can be constructed out of this set of fields is

$$\mathcal{W} \ni \lambda_{i\alpha} N_\alpha \Phi_i H_u + h_{i\alpha} L_\alpha \overline{\Phi}_i \chi + M_{ij} \Phi_i \overline{\Phi}_j + \mu H_u H_d, \tag{2.1}$$

where α is a family index, $\lambda_{i\alpha}$ and $h_{i\alpha}$ are Yukawa couplings, M_{ij} is a matrix of supersymmetry-respecting mass terms coupling the Φ_i and $\overline{\Phi}_i$ fields, and μ is the usual Higgs mass parameter. We note that we can always choose to work in a basis where the the mass are diagonal and real, and hence from this point onward, without loss of generality, we will adopt the convention that $M_{ij}\Phi_i\Phi_j = M_{\Phi_i}\Phi_i\Phi_i$ and absorb all phases into the coupling matrices $\lambda_{i\alpha}$ and $h_{i\alpha}$.

can modify the theory at high energies by introducing additional heavy fields, appealing to the Green-Schwarz mechanism [39], etc. Alternatively, one may modify the field content of the low-energy effective theory and introduce a set of fields with the appropriate charges to cancel the $U(1)_N$ anomalies. We will explore one such choice in section 5.3.

2.2 Dirac Leptogenesis, Baryogenesis, and Neutrino Masses

In order for successful baryogenesis to occur, we must satisfy the Sakharov criteria discussed in section 1.1. The out-of-equilibrium condition is satisfied during the decays of the component fields in Φ and $\overline{\Phi}$ (both the scalar and fermionic components of the Φ and $\overline{\Phi}$ supermultiplets, which we denote by ϕ, $\overline{\phi}$, ψ_Φ, and $\psi_{\overline{\Phi}}$ will play the role that the ν_R play in Majorana leptogenesis). The mass of the lightest $\Phi - \overline{\Phi}$ pair, which we will denote M_{Φ_1}, defines the leptogenesis scale. Since the parameters $\lambda_{i\alpha}$, and $h_{i\alpha}$ may in general be complex (as may the elements of (M_{ij}) in a general basis), they will in general contain nontrivial CP-violating phases that cannot be rotated away. This allows us to satisfy the CP-violation criterion. As in Majorana leptogenesis, a source of baryon number violation is provided by electroweak sphaleron processes. The primary difference between the two models is that explicit lepton-number-violating terms are present in equation (1.6) but absent in equation (2.1). Unlike in Majorana leptogenesis, where L is explicitly violated by the decays of heavy fields, here the overall values of B and the total lepton number L_{tot} are altered only by sphaleron processes, and $B - L$ is never violated.

When the temperature of the thermal bath drops below the leptogenesis scale M_{Φ_1}, both the scalar and fermionic components of the Φ_1 and $\overline{\Phi}_1$ superfields will decay, generating a net CP asymmetry and building up stores of lepton number in the lepton fields ν_R and ℓ, and in the associated slepton fields $\tilde{\nu}_R$, $\tilde{\ell}$. The leading contribution to CP-violation arises due to the interference of tree-level and one-loop-level diagrams. Those relevant to ϕ and $\overline{\phi}$ decay are shown in figure 2.2; the fermion fields ψ_{Φ_1} and $\psi_{\overline{\Phi}_1}$ undergo similar decays, but in the approximation of unbroken supersymmetry the amplitudes (and resultant CP-asymmetries) in

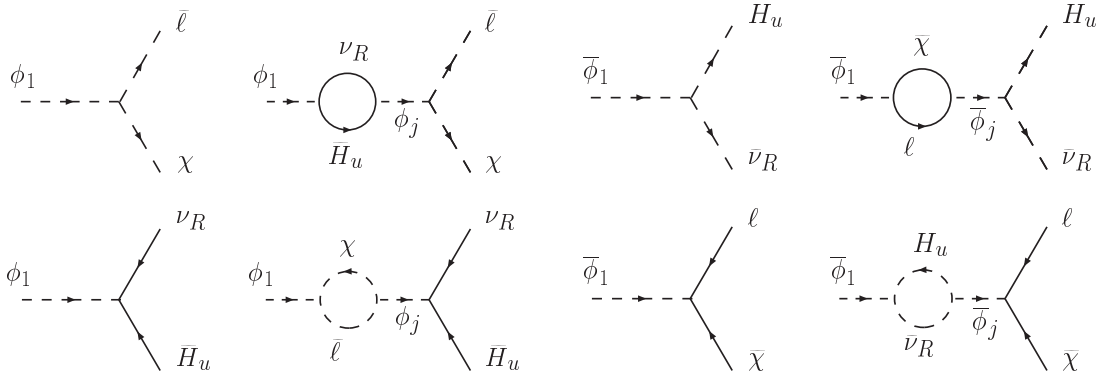

Figure 2.2: Diagrams that give the leading contribution to the CP asymmetry from decays of the scalar fields ϕ_1 and $\overline{\phi}_1$. Similar CP asymmetries are generated during the decay of the fermionic fields $\psi_{_{\Phi_1}}$ and $\psi_{_{\overline{\Phi}_1}}$.

the fermion case will be the same as those for the scalar case, so the rates need not be separately evaluated. For completeness, we have included contributions involving the scalar component of H_d, which start to become important when the supersymmetric Higgs mass parameter μ is of the same order as the M_{Φ_i}, but in what follows we will assume that $\mu \ll M_1$ and hence the contribution from these diagrams is negligibly small.

For purposes of illustration, let us begin by examining a simple toy model. We will consider the case where there are only two sets of Φ and $\overline{\Phi}$, the minimum number required for CP-violation, in which case [40], one may parameterize the associated lepton number violation by defining a single decay asymmetry ϵ, which represents the amount of lepton number generated in any particular lepton-number-carrying species by the decay of a single heavy particle. This

implies the relations

$$\Gamma(\Phi_1 \longrightarrow N_\alpha^c H_u^c) - \Gamma(\Phi_1^c \longrightarrow N_\alpha H_u) \equiv \epsilon\Gamma_D \tag{2.2}$$

$$\Gamma(\Phi_1 \longrightarrow L_\alpha \chi) - \Gamma(\Phi_1 \longrightarrow L_\alpha^c \chi^c) \equiv -\epsilon\Gamma_D \tag{2.3}$$

$$\Gamma(\overline{\Phi}_1 \longrightarrow L_\alpha^c \chi^c) - \Gamma(\overline{\Phi}_1^c \longrightarrow L_\alpha \chi) \equiv \epsilon\Gamma_D \tag{2.4}$$

$$\Gamma(\overline{\Phi}_1 \longrightarrow N_\alpha H_u) - \Gamma(\overline{\Phi}_1^c \longrightarrow N_\alpha^c H_u^c) \equiv -\epsilon\Gamma_D \tag{2.5}$$

among the rates for the processes depicted in figure 2.2, where Γ_D is the total decay width of any of the heavy fields in the Φ_1 or $\overline{\Phi}_1$ supermultiplets, and we have used the superfield notation for Φ_1, N, etc. because in the assumption of unbroken supersymmetry, the supersymmetrized versions of the diagrams appearing in fig. 2.2 yield the same result as the unsupersymmetrized ones. Explicit calculation of Γ_D and ϵ yields

$$\Gamma_D = \frac{1}{16\pi} M_{\Phi_1} \sum_\alpha \left(|\lambda_{1\alpha}|^2 + |h_{1\alpha}|^2 \right). \tag{2.6}$$

and

$$\epsilon = \frac{\mathrm{Im}(\lambda_{1\alpha}^* \lambda_{2\alpha} h_{1\beta}^* h_{2\beta} M_{\Phi_1} M_{\Phi_2}^*)}{4\pi(|M_{\Phi_2}|^2 - |M_{\Phi_1}|^2)(|\lambda_{1\gamma}|^2 + |h_{1\gamma}|^2)}, \tag{2.7}$$

where in both equations, a sum over the repeated indices α, β and γ is implied. It will be convenient to define a parameter $\delta \equiv |M_{\Phi_1}|/|M_{\Phi_2}|$, and in terms of δ,

$$\epsilon = \frac{\mathrm{Im}(\lambda_{1\alpha}^* \lambda_{2\alpha} h_{1\beta}^* h_{2\beta} e^{i\psi})}{4\pi(|\lambda_{1\gamma}|^2 + |h_{1\gamma}|^2)} \left(\frac{\delta}{1-\delta^2} \right), \tag{2.8}$$

where ψ is the relative phase between M_{Φ_1} and M_{Φ_2}. This tells us that for small values of δ, the final baryon-to-photon ratio will be approximately proportional to δ. Since ℓ_α and $n_{R\alpha}$ have equal and opposite charges under the global $U(1)_L$ symmetry, the individual L_ℓ and L_{ν_R} lepton numbers respectively stored in left-handed leptons and right-handed neutrinos will likewise be

equal and opposite. Supersymmetry enforces a similar condition $L_{\tilde{\ell}} = -L_{\tilde{\nu}_R}$ in the sneutrino sector, and consequently no net lepton number is produced by the decays of Φ_1 and $\overline{\Phi_1}$.

In order to discuss the subsequent evolution of these stores of lepton number, we must now take a moment to examine how things look at temperatures far below the leptogenesis scale M_1. Here, the theory can be described by an effective superpotential $\mathcal{W}_{\mathit{eff}}$ in which the heavy Φ_i and $\overline{\Phi}_i$ have been integrated out:

$$\mathcal{W}_{\mathit{eff}} \ni \frac{\lambda_{i\alpha} h^*_{i\beta}}{M_{\Phi_i}} \chi L_\beta H_u N_\alpha + \mu H_u H_d. \tag{2.9}$$

If we arrange for the scalar component of the χ superfield to acquire a VEV $\langle\chi\rangle$, an effective Yukawa matrix for neutrinos, proportional to the ratio $\langle\chi\rangle/M_{\Phi_1}$ will result; then, when H_u acquires its VEV during electroweak symmetry breaking, this will translate into a neutrino mass matrix with entries given by

$$m_{\nu\alpha\beta} = \langle\chi\rangle v \sin\beta \sum_i \frac{\lambda_{i\alpha} h^*_{i\beta}}{M_{\Phi_i}}. \tag{2.10}$$

If $\langle\chi\rangle \ll M_1$, this setup ostensibly yields small but nonzero masses for neutrinos, even when the elements in $\lambda_{i\alpha}$ and $h_{i\alpha}$ are $\mathcal{O}(1)$, and thus stands as an alternative to the traditional see-saw mechanism. Additionally, since the mass matrix in (2.10) has a reasonably simple structure, it can yield interesting predictions about the mass hierarchy among the standard model neutrinos, especially when certain additional, well-motivated constraints are applied, as we shall see in section 3.2.

We have so far said nothing about how χ receives its requisite VEV, but there are a variety of ways of engineering such a thing. One workable example is the O'Raifeartaigh-type model employed in [41], in which the F-term of χ acquires a large VEV $\langle F\rangle \simeq m_{3/2} M_P$, and supergravity effects give rise to a nonzero VEV $\langle\chi\rangle \simeq 16\pi m_{3/2}\kappa^{-3}$ for the scalar component of

χ, where κ is an undetermined dimensionless coupling constant. Another, in which the VEV is induced by introducing new superpotential couplings involving χ with additional exotic superfields charged under $U(1)_N$ and no F-term VEV develops for χ, is presented in chapter V. For the moment, we will not concern ourselves with the precise manner in which a χ VEV comes about, but it will be important to distinguish theories based on the presence or absence of a large F-term VEV $\langle F_\chi \rangle$. The reason for this is that when $\langle F_\chi \rangle$ is nonzero, the interaction lagrangian resulting from (2.9) includes an effective A-term

$$\mathcal{L}_{eff} \ni \frac{\langle F_\chi \rangle}{M_{\Phi_i}} \lambda i \alpha h_{i\beta} H_u \tilde{\ell}_\beta \tilde{\nu}_\alpha + c.c. \tag{2.11}$$

through which left- and right-handed sneutrinos can equilibrate. When $\langle F_\chi \rangle$ is large, this interaction will result in the lepton number asymmetries $L_{\tilde{\ell}}$ and $L_{\tilde{\nu}_R}$ stored in the slepton sector being rapidly equilibrated away; when it is small or vanishing, these two stores of lepton number do not equilibrate until late times. This effective A-term can induce potentially large flavor-violating effects, as will be addressed in chapter III.

As discussed in chapter one, B and L are not separately conserved in the early universe due to the electroweak anomaly, and as we saw in section 1.2.2, sphaleron processes associated with that anomaly will intermix the two, conserving $B - L$ and violating $B + L$. Since the net lepton number for the universe is zero in Dirac leptogenesis, we would normally expect these processes to wash out B, but this conclusion can be avoided if the individual stores of lepton number we have generated in charged (s)leptons and (s)neutrinos do not have a chance to equilibrate among themselves until well below the scale of electroweak phase transition T_c, at which point sphalerons have effectively shut off. For simplicity's sake, let us begin by assuming that any lepton number stored in sleptons and sneutrinos is rapidly annihilated through an effective A-term of the sort described above. In this case, there are only two stores of lepton

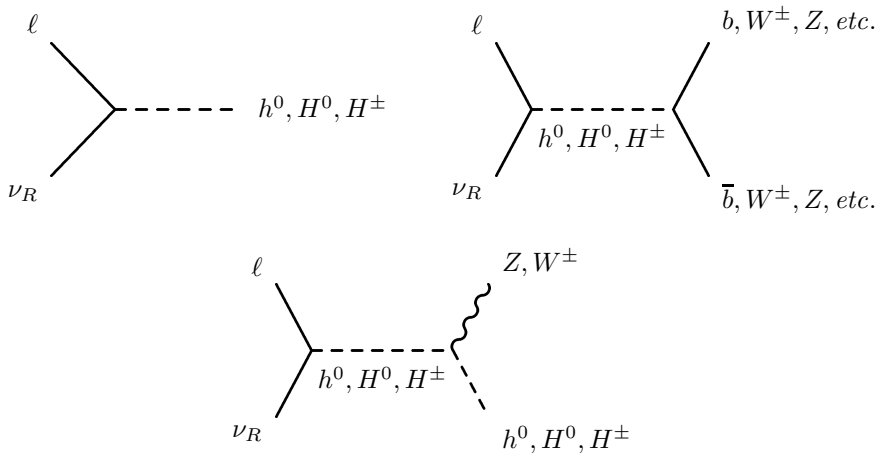

Figure 2.3: Diagrams corresponding to the leading order contribution to the equilibration of left-handed leptons with right-handed neutrinos. These include, from left to right, Higgs decays and inverse decays, scatterings off Standard Model fermions and electroweak gauge bosons through a virtual Higgs, and scattering off a Higgs boson in conjunction with the emission of an electroweak gauge boson. The right two diagrams also have t-channel equivalents. The amplitude associated with each diagram is proportional to the (small) effective neutrino Yukawa given in equation (2.9).

number L_ℓ and L_{ν_R} present. Since the ℓ fields are charged under $SU(2) \times U(1)_Y$ whereas ν_R are not, sphaleron effects will act on L_ℓ only, transmuting this store of lepton number into a nonzero baryon number along lines of constant $B - L_\ell$ in the manner described in section 1.2.2, while leaving L_{ν_R} untouched. As discussed above, when L_ℓ and L_{ν_R} finally do equilibrate, a net baryon number for the universe will already have frozen in, and the universe will end up with net positive B and L, as shown in figure 2.1.

The leading contributions to the equilibration rate between left- and right-handed neutrinos are shown in figure 2.3. The amplitude for each of these processes is proportional to the effective Higgs coupling term in equation (2.9), and hence suppressed by $\langle\chi\rangle/M_{\Phi_1}$. In order for Dirac leptogenesis to work, we must ensure that the net equilibration rate does not become significant

compared to the expansion rate of the universe until well after the electroweak phase transition. The equilibration rate may be estimated on dimensional grounds to be

$$\Gamma_{eq} \sim \frac{|\lambda|^2|h|^2\langle\chi\rangle^2}{M_{\Phi_1}^2} g_{sc}^2 T, \tag{2.12}$$

where g_{sc} is an $\mathcal{O}(1)$ gauge or top Yukawa coupling (see figure 2.3) and T is temperature. Requiring that $\Gamma_{eq} < H$ for $T > T_c$ leads to the condition

$$\frac{|\lambda||h|\langle\chi\rangle}{M_{\Phi_1}} \leq 10^{-8}, \tag{2.13}$$

which is easily satisfied, as it is essentially a recapitulation of the statement that neutrino masses must be small. This limit can be translated into a bound on the neutrino mass using equation (2.10)

$$m_\nu \leq 1.74\,(\sin\beta)\ \text{keV} \tag{2.14}$$

and thus the stipulation that left-right equilibration happen only well below T_c is satisfied automatically when neutrinos are given realistic masses.

In addition to this constraint, there are several other consistency checks which Dirac leptogenesis must pass in order to be considered a legitimate baryogenesis model. One of these is that the Sakharov criterion that the abundances of ϕ_1 and $\overline{\phi}_1$ depart from their equilibrium values must be satisfied. In order for this to occur, the decay rate Γ_D (2.6) must be slower than the rate of the expansion of the universe $H(T)$ (1.21) evaluated at the temperature $T \sim M_{\Phi_1}$ when ϕ_1 can no longer be treated as effectively massless and its abundance begins to fall off, or in other words

$$\frac{\Gamma_D}{H(M_{\Phi 1})} = 9.97 \cdot 10^{-2} g_*^{-1/2} \frac{M_P}{M_{\Phi_1}} \sum_\alpha (|\lambda_{1\alpha}|^2 + |h_{1\alpha}|^2) \lesssim 1. \tag{2.15}$$

This constraint also favors small couplings and large M_{Φ_1}. However, in addition to these two requirements, we must ensure that the present value of η satisfies the bounds in equation (1.1). To do this properly, one must solve the full system of Boltzmann equations, which we do in chapter IV, though a rough estimate can be made using the "drift-and-decay" approximation [42], in which we assume that the heavy particle decays occur well out of equilibrium and that the effects of inverse decays and $2 \leftrightarrow 2$ processes where $\Delta L_\ell \neq 0$ are negligible. Including contributions from both scalar and fermion decays, this gives the result

$$L_\ell = \frac{2\epsilon n_{\phi_1}^{init}}{s} = \frac{90\epsilon}{\pi^4 g_*} K_2(1) = 7.32 \times 10^{-3}\epsilon, \tag{2.16}$$

where $n_{\phi_1}^{init}$ is the initial number density of ϕ, $K_2(x)$ denotes the modified Bessel function of the second kind, evaluated at x, and ϵ is the decay asymmetry given in (2.7). Since the final baryon-to-entropy ratio B (related to η by $B = \eta/7.04$) generated by sphaleron processes will be on the same order ($B \simeq 0.35 L_\ell$), this can serve as a rough estimate for B. Thus even if equation (2.15) is satisfied, the final baryon-to-entropy ratio of the universe will be proportional to ϵ; and from equation (2.7), we see that for ϵ to be large, either the couplings must be large or the splitting between M_{Φ_1} and M_{Φ_2} must be small.

The upshot of all this is that while there are tensions among the model parameters in Dirac leptogenesis, they are not difficult to reconcile—in part because relevant physical scales in the theory are determined by the interplay of a large number of model parameters: (M_{Φ_1}, δ, $\langle\chi\rangle$), and the elements of the complex coupling matrices $\lambda_{i\alpha}$ and $h_{i\alpha}$. Unlike in Majorana leptogenesis, where neutrino masses are determined solely from the neutrino Yukawa y_ν matrix and the masses of the heavy fields according to the see-saw mechanism, neutrino masses in Dirac leptogenesis (2.10) depend not only on the superpotential couplings λ and h and the masses M_{Φ_i}, but also on $\langle\chi\rangle$. Consequently, the model parameters of Dirac leptogenesis are

far less constrained. Of course this versatility comes at the price of introducing an additional intermediate scale, though we will show that it is possible to relate $\langle\chi\rangle$ to other physical scales, for example the Higgs μ-term, in chapter V.

So far the constraints we have discussed have been limited to those which function as consistency checks on the model. The real tensions among M_{Φ_1}, δ, $\lambda_{i\alpha}$, $h_{i\alpha}$, and $\langle\chi\rangle$ are not those inherent in the Dirac leptogenesis framework, however, but those that arise when we demand that the model respect the full battery of additional constraints from neutrino physics, flavor physics, and cosmology. We now turn to address these constraints and their implications for Dirac leptogenesis.

CHAPTER III

CONSTRAINTS ON THE MODEL

3.1 Astrophysical Constraints

3.1.1 Baryogenesis and the Gravitino Problem

So far, we have seen that a simple toy model of Dirac leptogenesis is capable of yielding a nonzero baryon-to-photon ratio for the universe and explaining the observed scale of neutrino masses, but we have not yet shown that this scenario is a viable phenomenological model. To do this satisfactorily, we must first ensure that none of the modifications we have made disrupt the standard cosmology, i.e. that it is compatible with Big Bang nucleosynthesis (BBN), cosmic inflation, etc. [38]. Furthermore, we must investigate whether the theory is simultaneously capable of yielding a realistic neutrino spectrum and avoiding all current bounds on flavor-violation in the lepton sector [43]. At the same time, we must show that the theory is capable of reproducing the value of η observed by WMAP (1.1) once all these constraints are applied.

There are two primary ways supersymmetric Dirac leptogenesis could potentially disrupt BBN. First, constraints on the light element abundances place a bound on the number of

additional light neutrino species [44]

$$\Delta N_\nu \leq 0.3 \tag{3.1}$$

might cause one to worry that the presence of three additional light, sterile neutrino fields $\nu_{R\alpha}$ in the theory would violate this bound. However, the $\nu_{R\alpha}$ are not in thermal equilibrium with the bath during the BBN epoch; hence their contribution to ΔN is suppressed by and entropy factor

$$\Delta N = 3\left(\frac{T_{\nu_R}}{T_{bath}}\right)^4 = 3\left(\frac{g_*(1\text{ MeV})}{g_*(\text{MSSM}+N_i)}\right) = 0.02, \tag{3.2}$$

and thus the bound in (3.1) is respected. The second way in which supersymmetric Dirac leptogenesis can impact BBN is that, as in any supersymmetric theory, energy and entropy released during late decays of heavy sparticles (gravitinos will be of particular concern) could potentially distort the light element abundances from their observed values. This merits an in-depth discussion, as gravitino physics can place quite stringent constraints on the leptogenesis scale M_{Φ_1}.

The connection between leptogenesis and gravitino physics, which might not at first seem intimately interrelated, occurs through the reheating temperature T_R associated with cosmic inflation. Since leptogenesis requires that a thermal population of Φ_1 and $\overline{\Phi}_1$ be generated from the thermal bath during reheating, we require that $M_{\Phi_1} \lesssim T_R$; hence an upper bound on T_R translates into an upper bound on M_{Φ_1}. On the other hand, if $m_{3/2} \lesssim T_R$ heavy gravitinos will also be generated from the thermal bath, and one must take care that they do not cause problems for the standard cosmology. There are two distinct varieties of gravitino problem that must be addressed. First, as alluded to above, late gravitino decays can disrupt BBN by releasing energy in the form of photons and other energetic particles into the system; second, as the assumption of R-parity conservation implies that at least one LSP will be produced at

the end of the decay chain resulting from each late gravitino decay, the potentially large, non-thermal population of stable particles produced in this manner could overclose the universe—or if the right amount is produced, could make up the majority of cold dark matter (CDM). Both of these issues are contingent on the gravitino lifetime $\tau_{3/2}$, and for cases where $m_{3/2} \gg m_s$ (where m_s is the rough scale of the MSSM sparticle masses), this lifetime is approximated by [45]

$$\tau_{3/2} = 4.0 \times 10^8 \left(\frac{m_{3/2}}{100\text{GeV}}\right)^{-3} \text{s}. \tag{3.3}$$

Careful analysis of the BBN constraints (see, for example, [46] and references therein) reveals that unless $m_{3/2} \gtrsim 10^5$ GeV, T_R cannot be greater than around 10^8 GeV, and for $m_{3/2} \lesssim 5 \times 10^3$ GeV, cannot exceed 10^6 GeV. In models where $m_{3/2}$ is at the PeV scale, however, $\tau_{3/2} \sim 10^{-4}$ s, which implies that gravitinos produced in the thermal bath decay long before the BBN epoch (at $t_{universe} \sim 1$ s), and thus there is no gravitino problem of the former type for models with $m_{3/2}$ at or above these scales. However, since a weakly interacting LSP decouples on a timescale $t_f \sim 10^{-11}$ s, it will have long frozen out by the time gravitino decay occurs unless $m_{3/2}$ is larger than around 10^8 GeV; hence in theories with smaller gravitino masses (including simple PeV-scale supersymmetry with anomaly-mediated gaugino masses), LSPs produced by gravitino decay will be unable to thermalize and the latter type of gravitino issue cannot be ignored.

In order to avoid any complications from late gravitino decay, we require not only that the LSP not overclose the universe, but that its surviving relic density Ω_{LSP} must be less than (or ideally, if the LSP is to constitute the majority of cold dark matter, equal to) the relic density of CDM as measured by WMAP [47],

$$\Omega_{\text{CDM}} h^2 = 0.11 \pm 0.01 \text{ (WMAP 68\% C.L.)}. \tag{3.4}$$

In general, Ω_{LSP} will have both a thermal and a non-thermal component, so that $\Omega_{LSP} = \Omega_{LSP}^{Th} + \Omega_{LSP}^{NT}$. The thermal component Ω_{LSP}^{Th} may be ascertained by solving the relevant set of Boltzmann equations for the LSP abundance at freeze-out. The results, for the case where the LSP is essentially either a pure Wino or Higgsino, are [48]

$$\Omega_{LSP}^{Th} h^2 = 0.02 \left(\frac{|M_2|}{\text{TeV}} \right) \qquad \text{for Wino LSP} \tag{3.5}$$

$$\Omega_{LSP}^{Th} h^2 = 0.09 \left(\frac{|\mu|}{\text{TeV}} \right) \quad \text{for Higgsino LSP.} \tag{3.6}$$

Of course it is also possible that the gravitino itself is the LSP, in which case the primary concerns are that next-to-lightest supersymmetric particle (NLSP) decays to gravitino do not disrupt BBN and that the gravitino abundance does not exceed the WMAP bound (3.4). In Gauge-Mediated supersymmetry breaking and other theories where the gravitino is exceedingly light (with a mass on the order of a few keV or less), the gravitino contribution to the energy density of the universe during the BBN epoch [49] is also a concern. It has been shown [50] that these constrains can be translated to a reheating temperature limit $T_R \lesssim 10^7$ GeV, which, as we shall see in section 4.2.2 turns out to be incompatible with Dirac leptogenesis. When the gravitino is reasonably heavy, with a mass of $\mathcal{O}(100$ GeV), the gluino mass is around 500 GeV, and the NLSP is Higgsino-like (the best-case scenario) the constraints from NLSP decay and Ω_{CDM} conspire to produce a reheating temperature bound $T_R \lesssim 10^9$ GeV [51], which will also turn out to be problematic for the theory. It thus appears that a gravitino LSP is essentially incompatible with Dirac leptogenesis; thus we shall henceforth focus our efforts on models in which the gravitino is not the LSP.

Now we turn to evaluating Ω_{LSP}^{NT}. We begin by addressing the regime in which there is no significant reduction in Ω_{LSP}^{NT} from LSP annihilations. Assuming for the moment that the

dominant contribution to the non-thermal relic abundance comes from late gravitino decays and that all the LSPs produced from such decays survive until present day, Ω_{LSP}^{NT} is given by

$$\Omega_{LSP}^{NT} = \frac{m_{LSP}\zeta(3)T_0^3}{\pi^2\rho_{crit}}Y_{3/2}(T_{3/2}), \tag{3.7}$$

where ρ_{crit} is the critical density of the universe, T_0 is the present temperature of the universe, and $Y_{3/2}(T_{3/2})$ is the number of gravitinos per co-moving volume at the characteristic temperature $T_{3/2}$ at which the gravitino decays, which is given by [52]

$$Y_{3/2}(T_{3/2}) = 0.856 \times 10^{-11}\left(\frac{T_R}{10^{10}\text{GeV}}\right)\left(1 - 0.0232\ln\left(\frac{T_R}{10^{10}\text{GeV}}\right)\right). \tag{3.8}$$

Substituting this into equation (3.7) yields

$$\Omega_{LSP}^{NT}h^2 = 2.96 \times 10^{-4}\left(\frac{m_{LSP}}{\text{GeV}}\right)\left(\frac{T_R}{10^{10}\text{GeV}}\right)\left(1 - 0.0232\ln\left(\frac{T_R}{10^{10}\text{GeV}}\right)\right). \tag{3.9}$$

In figure 3.1, we plot the contours corresponding to the WMAP upper and lower bounds from equation (3.4) on the total relic abundance of a Wino LSP, as well as the simple overclosure bound $\Omega_{LSP}h^2 = 1$, taking into account both thermal and non-thermal contributions, as a function of m_{LSP} and T_R. The gently-sloping portion of each contour corresponds to the nonthermal abundance in equation 3.9, which becomes significant when T_R is large; the nearly vertical portion on the right side of the graph corresponds to the thermal abundance given in 3.5. In the region above and to the right of the WMAP upper bound given in (3.4), dark matter is overproduced and hence excluded. In the narrow strip between the upper and lower WMAP bounds, the thermal LSP abundance and the nonthermal LSP abundance resulting from late gravitino decay conspire to reproduce the observed value for Ω_{CDM}. In the region below and to the left of the lower WMAP contour, the experimental upper bound is not violated and hence this region of parameter space is phenomenologically allowed, provided there are other sources

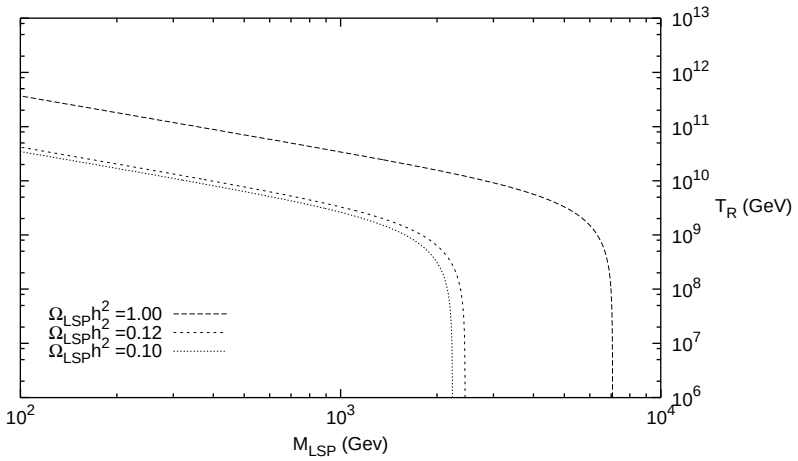

Figure 3.1: Contours of $\Omega_{LSP}h^2$ [38] corresponding to the upper and lower bounds from WMAP (3.4), as well as a simple overclosure bound, as a function of the LSP mass m_{LSP} and the reheating temperature T_R associated with cosmic inflation for a Wino LSP. The requirement that Ω_{LSP} not overclose the universe severely constrains T_R, and hence the temperature scale of thermal leptogenesis, for a theory like PeV-scale loop-split supersymmetry, in which the LSP is particularly heavy. For a Higgsino LSP, the results are similar, but the contours move slightly to the left.

of dark matter to make up the deficit between Ω_{LSP} and Ω_{CDM}. These sources could include other non-thermally-generated contributions to Ω_{LSP} or contributions, contributions from other exotic particles, or some combination of both. It can be seen from figure 3.1 that when m_{LSP} is large enough that $\Omega_{LSP}^{Th} \approx \Omega_{CDM}$ and CDM is essentially thermal in origin, the ceiling on T_R is quite low–around 10^9 GeV. In regions of parameter space where m_{LSP} is smaller and the majority of CDM is generated non-thermally, T_R may be raised a bit, but is still constrained to be below $\sim 5 \times 10^{10}$ GeV. As we shall see in chapter IV, $T_R \gtrsim 10^9$ GeV turns out to be problematic for Dirac leptogenesis (in terms of the final baryon-to-photon ratio generated), largely due to the out-of equilibrium condition in (2.15). This implies that if we want to raise T_R above 10^9 GeV and still have the LSP relic density dominate Ω_{CDM}, the majority of the dark matter abundance (be it from late gravitino decays or something else) must be essentially

non-thermal in origin.

We now turn to address the regime where LSP annihilations do play a role in reducing Ω_{LSP}^{NT}, and thus the upper bound on T_R may be raised. This effect becomes important when $m_{3/2} \gg m_{LSP}$. When it is taken into account [53], the non-thermal LSP relic density is modified to

$$\Omega_{LSP}^{NT} = \min\left(\Omega_{LSP}^{NT(0)}, \Omega_{LSP}^{NT(ann)}\right), \tag{3.10}$$

where $\Omega_{LSP}^{NT(0)}$ is the relic density given in equation (3.9), and $\Omega_{LSP}^{NT(ann)}$ is the relic density obtained by solving the full system of Boltzmann equations for the LSP. For a Wino LSP, $\Omega_{LSP}^{NT(ann)}$ is given by

$$\begin{aligned} \Omega_{LSP}^{NT(ann)} &= 2.41 \times 10^{-2} \frac{(2-x_W)^2}{(1+x_W)^{3/2}} \left(\frac{m_{LSP}}{100\text{GeV}}\right)^3 \left(\frac{m_{3/2}}{100\text{TeV}}\right)^{-3/2} \\ &\times \left(1 - \left(\frac{m_{LSP}}{m_{3/2}}\right)\right)^3 \left(1 + \frac{1}{3}\left(\frac{m_{LSP}}{m_{3/2}}\right)\right), \end{aligned} \tag{3.11}$$

where $x_W \equiv m_W/m_{LSP}$; for a Higgsino LSP, which annihilates far less efficiently, $\Omega_{LSP}^{NT(ann)}$ will be even higher.

In figure 3.2, we show the relationship between $\Omega_{LSP}^{NT(ann)}$ and m_{LSP} for several values of $m_{3/2}$. The horizontal line corresponds to the WMAP upper bound on Ω^{CDM}. From this plot it is evident that annihilations are only effective in reducing the LSP relic abundance below this bound when $m_{3/2}$ is much larger than m_{LSP}. However, when $m_{3/2}$ is increased beyond around 10^8 GeV, $\tau_{3/2}$ becomes short enough that gravitino decay occurs before LSP freeze-out, and Ω_{LSP}^{NT} drops to zero regardless of what the ratio of m_{LSP} to $m_{3/2}$ is, and nonthermal LSP overproduction from late gravitino decays no longer remains a concern.

While the problems that can arise for small gravitino masses have now been thoroughly addressed, the caveats associated with extremely large $m_{3/2}$ should also be mentioned. As has

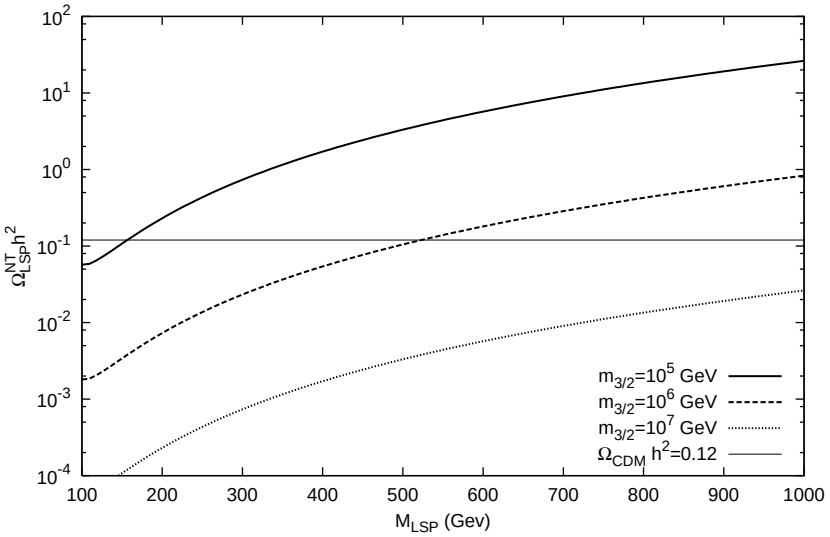

Figure 3.2: Here, we show the variation of $\Omega_{LSP}^{NT(ann)}$ (the improved expression for the LSP relic density that accounts for the effect of LSP annihilations) with LSP mass for several different values of $m_{3/2}$ [38]. The horizontal line corresponds to the WMAP upper bound on Ω_{CDM}. For a given choice of $m_{3/2}$, portions of the contour that fall below the horizontal line respect the WMAP constraint and are phenomenologically allowed, and the reheating temperature T_R be increased beyond the naive upper bound from figure 3.1. Portions that lie above it overproduce the LSP and are excluded (for example, when $m_{3/2} = 10^6$ GeV, an LSP mass $m_{LSP} \geq 500$ GeV is excluded).

been shown in [54], split supersymmetry models with a large hierarchy between the gravitino and gaugino masses can suffer from phenomenological problems associated with the overproduction of gluinos, including the distortion of both the CMB and the light element abundances through their late decays. Since gluinos will be bound into R-hadrons at temperatures below the scale Λ_{QCD} associated with the QCD phase transition, a precise analysis of their decay rate at late times has not yet been performed. Still, while a precise ceiling for $m_{3/2}$ must wait until the decay of R-hadrons is better understood, it is known that this ceiling falls somewhere in the $m_{3/2} \simeq 10^{10} - 10^{12}$ GeV range. For this reason, one should be wary about making the gravitino mass arbitrarily large. There are also caveats associated with the gravitino-producing decays

of scalar sparticles in models where one or more scalars has a mass larger than $m_{3/2}$ [55].

As discussed above, bounds on the reheating temperature in supersymmetric theories can be viewed as bounds on the leptogenesis scale M_{Φ_1}. This is not in any way peculiar to Dirac leptogenesis either: in a Majorana leptogenesis model, the constraints still apply with the lightest right-handed neutrino mass M_{ν_R} in place of M_{Φ_1}. In figure 3.3, we display these constraints graphically. For light gravitinos ($m_{3/2} \lesssim 10^5$ GeV), BBN limits severely constrain T_R, and hence M_{Φ_1}. For slightly heavier gravitinos (10^5 GeV $\lesssim m_{3/2} \lesssim 10^8$ GeV), there are still constraints on T_R from nonthermal decays which are only alleviated (via LSP annihilations) when $m_{LSP} \ll m_{3/2}$. For extremely heavy gravitinos, with mass $m_{3/2} \gg 10^{10}$ GeV, decays to gluinos become worrisome, and when $m_{3/2} \gg 10^{12}$ GeV they will almost certainly become problematic.

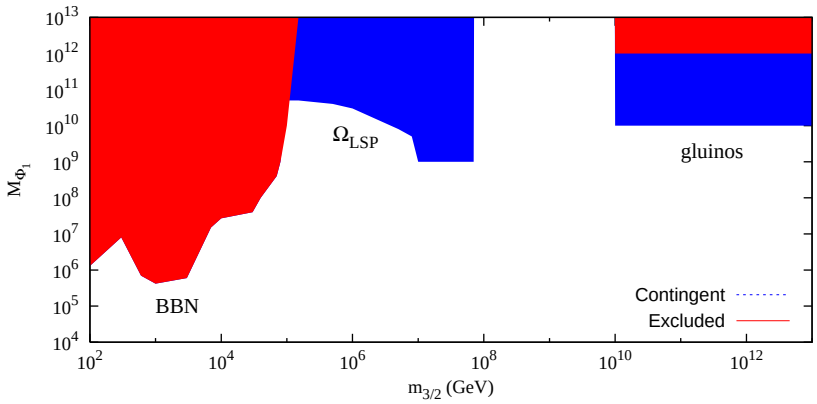

Figure 3.3: A schematic representing the bounds on the leptogenesis scale M_{Φ_1} from gravitino physics as a function of the gravitino mass $m_{3/2}$. When $m_{3/2} \lesssim 10^5$ GeV, constraints from BBN are quite severe. In the range 10^5 GeV $\lesssim m_{3/2} \lesssim 10^8$ GeV, M is still limited by nonthermal decays to the LSP. For $m_{3/2} < 10^{10}$ GeV, decays to gluinos are a concern. This leaves a window 10^5 GeV $\lesssim m_{3/2} \lesssim 10^{10}$ GeV within which, depending on the mass of the LSP, Dirac leptogenesis can be successful.

While we have not said much about other constraints on M_{Φ_1}, but it is not difficult to see that substantial model tension arises when the reheating temperature is constrained to be below

around 10^{10} GeV. The out-of-equilibrium condition (2.15) demands that $\lambda_{1\alpha}$ and $h_{1\alpha}$ be at most $\mathcal{O}(10^{-4})$ for $M_{\Phi_1} \sim 10^{10}$ GeV; on the other hand, (2.7) and (2.16) imply that unless there is a large hierarchy among the Yukawa couplings to different sets of Φ and $\overline{\Phi}$ (so that $\lambda_{1\alpha} \ll \lambda_{2\alpha}$ for all α), decreasing the $\lambda_{i\alpha}$ and $h_{i\alpha}$ below $\mathcal{O}(10^{-4})$ will yield insufficient baryon number—and we have not yet taken into account the effects of $2 \leftrightarrow 2$ processes and inverse decays.[1] Furthermore, engineering $\lambda_{i\alpha}$ and $h_{i\alpha}$ to be extremely small while the rest of the trilinear couplings in the superpotential are $\mathcal{O}(1)$ seems to defeat the purpose of leptogenesis, the advantage of which was its ability to explain the smallness of neutrino masses without resorting to arbitrary fine-tuning. While any precise statement about the value of M_{Φ_1} must wait until after we solve the Boltzmann equations governing the development of B and L during the leptogenesis epoch, leptogenesis seems to become difficult or contrived when $M_{\Phi_1} \lesssim 10^{10}$ GeV. This means that when $m_{3/2} \lesssim 10^8$ GeV and LSP annihilations are ineffective, substantial tensions arise among the out-of-equilibrium decay criterion, overclosure bounds related to the reheating temperature T_R, the equation that determines the decay asymmetry ϵ, etc., and problems are likely to arise. We shall confirm these suspicions in chapter IV.

The indication that $m_{3/2}$ must be quite large in order for Dirac leptogenesis to work suggests that the model could be quite successful in the context of split supersymmetry [56, 48]. In this scenario, a hierarchy generated between the gaugino masses and the masses of the scalar sparticles in which the latter are elevated to a high scale in order to evade unwanted flavor violation effects, while the former are kept at the TeV scale or below to constitute dark matter. The gravitino mass also tends to be quite large in split supersymmetry, hence it would provide a solution to the model tensions that gravitino cosmology presents Dirac leptogenesis. It will

[1] One can also get around this by making M_{Φ_1} and M_{Φ_2} essentially degenerate. We will elaborate on this possibility in section 4.4.

soon be made clear that Dirac leptogenesis and split supersymmetry are indeed compatible models.

As a case in point, a particularly simple and phenomenologically interesting split supersymmetry scenario in which it is difficult (though not impossible) to get Dirac leptogenesis to work is the PeV-scale supersymmetry of [57], sometimes also referred to as loop-split supersymmetry, in which anomaly mediation is invoked in the gaugino sector, but not in the scalar sector. One assumes that the messenger fields X responsible for transmitting the effects of supersymmetry-breaking to the visible scale are charged under some symmetry, and consequently, while the scalar masses are still given by

$$m_s^2 = c\frac{F_X^\dagger F_X}{M_P^2}, \tag{3.12}$$

where c is an $\mathcal{O}(1)$ constant, the term which normally yields dominant contribution to the gaugino masses

$$\int d^2\theta \frac{X}{M_P} W^a W^a \rightarrow \frac{F_X}{M_P}\lambda^a\lambda^a \tag{3.13}$$

is not longer gauge-invariant. The leading contribution arises at one loop, via the anomaly-mediated expression

$$M_\lambda = \frac{\beta_{g_\lambda}}{g_\lambda}\left(\frac{\langle F_X^\dagger F_X\rangle}{M_P^2}\right)^{1/2}. \tag{3.14}$$

If we assume that supersymmetry is broken at an intermediate scale, around $\sim 10^5 - 10^7$ GeV, then all scalars in the theory, (with the exception of one light Higgs particle) receive masses around the PeV scale while the gauginos acquire masses at the TeV scale [58]. This model is attractive in its simplicity, and furthermore it is connected to the rich phenomenology associated with anomaly-mediated models which includes possibilities for the detection of dark matter via observations at the next generation of γ-ray telescopes [59, 60, 61] and characteristic

gluino decay signatures that could be observed at the LHC [62, 63].

The problem with getting Dirac leptogenesis to work in loop-split supersymmetry is that not only does the theory require $m_{3/2}$ to be around the PeV scale (which is in itself not particularly worrisome), but also mandates a particular relationship between $m_{3/2}$ and the LSP mass through equation (3.14) and the AMSB gravitino mass relation [58, 64]

$$m_{3/2}^2 = \frac{F_X^\dagger F_X}{M_P^2}. \tag{3.15}$$

Figure 3.2 indicates that Dirac leptogenesis prefers a splitting $m_{3/2}/m_{LSP}$ substantially larger than that dictated by equation 3.14, which means that Ω_{LSP}^{NT} will generally exceed the WMAP bound. Loop-split supersymmetry can still be made to work—for example in a situation where lepton number production is amplified by resonance effects—but tuning the M_{Φ_i} to this degree begs some sort of motivation or additional theoretical machinery. It should be emphasized, however, that the splitting between m_{LSP} and $m_{3/2}$ can be much larger [56, 65] in more general split supersymmetry scenarios, making Dirac leptogenesis far easier to realize.

3.1.2 Goldstone Bosons and Symmetry Breaking

Finally, in addition to the battery of constraints outlined above, Dirac leptogenesis must respect cosmological bounds associated with the production of light scalars. As was mentioned in chapter II, some new symmetry must be posited in order to construct the Dirac leptogenesis superpotential and forbid Majorana masses for the right-handed neutrinos. In Dirac leptogenesis, neutrino masses are the result of the scalar component of the χ superfield acquiring a VEV which breaks this new symmetry, producing a Goldstone boson or pseudo-Goldstone boson, depending on the way the symmetry is broken (which we have not yet specified). Let

us first examine the case where the breaking has an explicit component and the relevant scalar is a pseudo-Goldstone boson. Constraints on such particles arise from both BBN and cosmic microwave background (CMB) considerations [66] as well as from the detection of abnormalities in the neutrino flux associated with supernova events [67], and they can become problematic (depending on the mass of the Goldstone boson) when the symmetry-breaking VEV is less than around 1 GeV.

In the case where symmetry breaking is completely spontaneous, a true Goldstone boson will result, which these constraints seem to rule out. Of course this assumes that the Goldstone boson is a physical state: in the case where the additional symmetry which forbids neutrino Majorana masses is a gauge symmetry, the Goldstone boson is "eaten" by the gauge field and the relevant constraints become those associated with extensions of the Standard Model gauge structure. If it is an Abelian gauge symmetry, for example, one must take care that bounds associated with $U(1)$ mixing are not violated and that the gauge theory is free of anomalies (which would not be the case given the field content in table 2.1). We will discuss these requirements and investigate their implications further in section 5.3.

3.2 Neutrino Physics

3.2.1 Experimental Constraints

In addition to respecting constraints arising from cosmological considerations, in order to be phenomenologically viable, a given Dirac leptogenesis model must yield a neutrino spectrum that accords with current experimental constraints. The most stringent such constraints come from solar and atmospheric neutrino oscillation experiments [68, 69], and place limits both on

the mass splittings

$$\Delta m^2_{ab} \equiv m^2_{\nu_a} - m^2_{\nu_b}, \tag{3.16}$$

where the indices a and b label the different neutrino mass eigenstates, and on the mixing angles θ_{ab} between these eigenstates. The primary connection between the latter and observable physics occurs through the leptonic mixing matrix

$$U_{MNS} = U^{(\nu)} U^{(e)}, \tag{3.17}$$

where $U^{(\nu)}$ is the neutrino mixing matrix and $U^{(e)}$ is the charged lepton mixing matrix. In the basis where the charged lepton mass matrix is diagonal, U_{MNS} is the neutrino mixing matrix and may be expressed in terms of the neutrino mixing angles θ_{ab} as

$$U_{MNS} = \begin{pmatrix} c_{12}c_{13} & s_{12}c_{13} & s_{13}e^{i\delta_{CP}} \\ -s_{12}c_{23} - c_{12}s_{23}s_{13}e^{i\delta_{CP}} & c_{12}c_{23} - s_{12}s_{23}s_{13}e^{-i\delta_{CP}} & s_{23}c_{13} \\ s_{12}s_{23} - c_{12}c_{23}s_{13}e^{-i\delta_{CP}} & -c_{12}s_{23} - s_{12}c_{23}s_{13}e^{-i\delta_{CP}} & c_{23}c_{13} \end{pmatrix}, \tag{3.18}$$

where $c_{ab} = \cos\theta_{ab}$, $s_{ab} = \sin\theta_{ab}$, and δ_{CP} is a CP-violating phase. The present limits[2] on the Δm^2_{ab} and θ_{ab} are [70]

$$\begin{gathered} \sin^2\theta_{12} = 0.30^{+0.04}_{-0.05}, \quad \sin^2\theta_{23} = 0.50^{+0.14}_{-0.12}, \quad \sin^2\theta_{13} \leq 0.031, \\ \Delta m^2_{21} = \left(7.9^{+0.6}_{-0.6}\right) \times 10^{-5}\mathrm{eV}^2, \quad |\Delta m^2_{31}| = \left(2.2^{+0.7}_{-0.5}\right) \times 10^{-3}\mathrm{eV}^2. \end{gathered} \tag{3.19}$$

The smaller of the two mass splittings, Δm^2_{21}, is to be identified with the $\Delta m^2_{\odot}$ obtained from solar neutrino data (the MSW-LMA solution); the larger, Δm^2_{31}, with the Δm^2_A from atmospheric neutrino data. When we take these constraints and substitute them into the U_{MNS}

[2]We do not take into account the LSND result which would require an extra neutrino mass eigenstate. In the case that forthcoming data from experiments such as MiniBooNE corroborate the LSND signal, it will be necessary to extend the neutrino content of our model.

matrix, we arrive a set of bounds

$$|U_{MNS}| = \begin{pmatrix} .79 - .86 & .49 - .58 & 0 - .18 \\ .30 - .58 & .40 - .68 & .61 - .80 \\ .19 - .46 & .50 - .77 & .59 - .79 \end{pmatrix}, \tag{3.20}$$

However, the constraints in (3.19) say nothing about the sign of the largest mass squared difference Δm^2_{31}. As as result, we are left with two possibilities: the physical neutrino ν_3 can be either the heaviest of the three mass eigenstates, i.e. $m_1 < m_2 \ll m_3$ (a situation dubbed the "normal hierarchy") or the lightest, i.e. $m_3 \ll m_1 < m_2$ (the "inverted hierarchy").

The reason U_{MNS} is of particular importance is that in the basis where the charged lepton mass matrix is diagonal, it becomes the unitary matrix responsible for diagonalizing the squared neutrino mass matrix:

$$\left(m^2_\nu\right)_{diag} = \; U^\dagger_{MNS}\; m_\nu m^\dagger_\nu\; U_{MNS}. \tag{3.21}$$

We can therefore estimate [70] the generic form of the neutrino mass matrix squared, since it has to be diagonalized by U_{MNS}. In the normal hierarchy scenario, we find that

$$(m^2_\nu)_{norm} \sim \Delta m^2_{31} \begin{pmatrix} \xi & \xi & \xi \\ \xi & 1 & 1 \\ \xi & 1 & 1 \end{pmatrix}, \tag{3.22}$$

where the ξ are small compared to the $\mathcal{O}(1)$ entries and not necessarily the equal to one another. Similarly, in the inverted hierarchy scenario, we find

$$(m^2_\nu)_{inv} \sim \Delta m^2_{31} \begin{pmatrix} 1 & \xi & \xi \\ \xi & 1 & 1 \\ \xi & 1 & 1 \end{pmatrix}. \tag{3.23}$$

In either case, the ratio of the $\mathcal{O}(1)$ entries to the small ξ is constrained to be at least of order $\rho_{32} \equiv \Delta m^2_{31}/\Delta m^2_{21}$, which, according to (3.19), must respect the bounds

$$20.0 < \rho_{23} < 39.7 \ . \tag{3.24}$$

In order for Dirac leptogenesis to be phenomenologically viable leptogenesis model we need simultaneously to be able to satisfy the above constraints and reproduce the form of the neutrino mass matrix given in (3.22) or (3.23). Ideally, we should like to find a simple way of arriving at one of these matrix structures that is motivated by theoretical considerations as well as data pressures. Of course this solution must also be compatible with successful baryon number generation, the astrophysical constraints discussed in section 3.1, etc.

3.2.2 The Flavor Structure of the Trilinear Couplings

As we saw in chapter II, the neutrino mass-squared matrix in Dirac leptogenesis is given by

$$|m_\nu|^2_{\alpha\beta} = \Big(v\langle\chi\rangle \sin\beta\Big)^2 \sum_{i,j=1}^{2\ (or\ 3)} \sum_{\gamma=1}^{3} \lambda^*_{i\gamma}\lambda_{j\gamma}h^*_{i\alpha}h_{j\beta}\frac{1}{M^*_{\Phi_i}M_{\Phi_j}}. \tag{3.25}$$

As long as λ and h are completely generic and there are at least three sets of Φ and $\overline{\Phi}$, it is apparent that a matrix of this form can yield an arbitrary neutrino mass spectrum. On the one hand this is good, for it means that the theory is perfectly viable, in the sense that there exists some set of parameters that will satisfy the battery of constraints given in equation (3.19); on the other hand, this arbitrariness comes at the price of introducing many additional free parameters, whose relative values must be determined by some additional underlying physics. As a first step toward understanding what that additional physics ought to involve, let us examine the spectrum of a simplified model containing only a single pair of heavy fields Φ_1 and

$\overline{\Phi}_1$ of mass M_{Φ_1}, or alternatively, a theory in which $M_{\Phi_1} \ll M_{\Phi_i}$ for all $i > 1$. In such cases the mass-squared matrix is proportional to an outer product of the family-space vectors $\lambda_{1\alpha}$ and thus its eigenvalues are

$$m_{\nu_1} = 0 \quad m_{\nu_2} = 0 \quad m_{\nu_3} = \sum_{\alpha}^{3} \lambda_{1\alpha} h_{1\alpha}. \tag{3.26}$$

Here, two of the physical neutrinos are massless. For each additional set of Φ and $\overline{\Phi}$ with a mass similar to M_{Φ_1}, an additional neutrino acquires a nonzero mass. Thus in "short-suited" models where $M_{\Phi_1} \ll M_{\Phi_2}$ and $M_{\Phi_2} \ll M_{\Phi_i}$ for all $i > 2$ (i.e. where there are effectively only two sets of ϕ and $\overline{\phi}$ involved in determining the neutrino spectrum), one neutrino mass eigenstate is massless and a hierarchy will exist between the other two, determined by $\delta = M_{\Phi_1}/M_{\Phi_2}$. One can then arrange for the other two neutrino masses to take the experimentally observed values $m^2_{\nu_2} \approx \Delta m^2_{21}$ and $m^2_{\nu_3} \approx \Delta m^2_{31}$ by tinkering with δ and the structures of λ and h. Conveniently, leptogenesis in such models is well-approximated by the toy model considered in section II, in which there were only two sets of Φ and $\overline{\Phi}$.

Let us now examine the effect of λ and h on the neutrino spectrum in models with this sort of hierarchy among the heavy particle masses. It is apparent from equation (3.25) that the matrix structure of m^2_ν is primarily determined by h rather than λ. In the limit where $\delta \ll 1$, this matrix becomes

$$|m_\nu|^2 = \Big(v\langle\chi\rangle \sin\beta\Big)^2 \sum_{\gamma} |\lambda_{1\gamma}|^2 \frac{1}{M^2_{\Phi_1}} \begin{pmatrix} |h_{11}|^2 & h^*_{11}h_{12} & h^*_{11}h_{13} \\ h^*_{12}h_{11} & |h_{12}|^2 & h^*_{12}h_{13} \\ h^*_{13}h_{11} & h^*_{13}h_{12} & |h_{13}|^2 \end{pmatrix} + \mathcal{O}(\delta), . \tag{3.27}$$

If for some reason the off-diagonal elements of h are much smaller than the diagonal elements (i.e. h_{12}, $h_{13} \gg h_{11}$), this matrix will take form (3.22) that reproduces the normal hierarchy

solution. If h_{12} and h_{13} are roughly of the same order, so that $h_{12} \approx h_{13} \equiv \tilde{h}$, equation (3.27) becomes

$$|m_\nu|^2 \approx (v\langle\chi\rangle \sin\beta)^2 \sum_\gamma |\lambda_{1\gamma}|^2 \frac{|\tilde{h}|^2}{M_{\Phi_1}^2} \begin{pmatrix} \xi^2 & \xi & \xi \\ \xi & 1 & 1 \\ \xi & 1 & 1 \end{pmatrix} + \mathcal{O}(\delta), \tag{3.28}$$

where $\xi = h_{11}/\tilde{h}$. Here we have implicitly assumed that contributions of $\mathcal{O}(h_{11}/\tilde{h})$ dominate over the $\mathcal{O}(\delta)$ contributions. If this is not the case, and in particular if $h_{11} = 0$, the matrix structure becomes

$$(m_\nu^2) \propto \begin{pmatrix} \delta^2 & \delta & \delta \\ \delta & 1 & 1 \\ \delta & 1 & 1 \end{pmatrix}. \tag{3.29}$$

Again the generic structure yielding the normal hierarchy scenario is obtained, but in this case the value of δ fixes the ratio ρ_{23}. In any case, what is significant here is that imposing the two simple hierarchical requirements, $M_{\Phi_1} \ll M_{\Phi_{2,3}}$ and $h_{11} \ll h_{12} \sim h_{13}$ generically gives rise to the correct neutrino phenomenology.

These considerations suggest that we ought to look for some setup that will ensure that the diagonal element h_{11} is small compared to the off diagonal terms h_{12} and h_{13}. One particularly simple way to do this is to posit an antisymmetry condition on the matrix h, in which case the neutrino mass matrix will take the form given in (3.29), with small entries of $\mathcal{O}(\delta)$. This option is of particular interest because there is also a theoretical motivation for it: antisymmetric Yukawa matrices emerge quite naturally in certain grand unified theories and in models with non-Abelian flavor symmetries [71, 73, 74, 72]. We shall put off discussion of such matters until section 5.2, where we provide a theoretical motivation for the hierarchies among the M_{Φ_i} and

elements of λ and h.

3.2.3 Constrained Hierarchical Dirac Leptogenesis

Motivated by the preceding remarks, we now define a particular model that ought to be able to yield a phenomenologically acceptable neutrino spectrum. We define **constrained hierarchical Dirac leptogenesis (CHDL)** [38] as the setup in which:

1. The mass matrix (M_Φ) is real and diagonal.
2. The coupling matrices λ and h are antisymmetric
3. The large mixing angles in the neutrino sector are result from the smallness of $\delta = M_{\Phi_1}/M_{\Phi_2}$.

In this model, the antisymmetry of λ and h allows us to parameterize them in the manner

$$\lambda = f \begin{pmatrix} 0 & 1 & a_2 \\ -1 & 0 & a_3 \\ -a_2 & -a_3 & 0 \end{pmatrix} \qquad h = f \begin{pmatrix} 0 & b_1 & b_2 \\ -b_1 & 0 & b_3 \\ -b_2 & -b_3 & 0 \end{pmatrix}, \tag{3.30}$$

which is convenient when the a_i and b_i are all roughly $\mathcal{O}(1)$. Since the assumption of a hierarchy among the M_{Φ_i} leads to the neutrino mass-squared matrix of the form (3.22), we expect that a_3 and b_3, the effects of which show up only at the $\mathcal{O}(\delta)$ level, will be less tightly constrained than the rest of the a_i and b_i, which contribute to the leading term. This is in fact the case: if a_1, a_2, b_1, or b_2 deviates significantly from one, the neutrino spectrum cannot satisfy the constraints in (3.19). It is therefore appropriate, since the value of f is unimportant as far as this set of constrains are concerned (any rescaling of f can be compensated for by a similar rescaling of $\langle\chi\rangle$), to analyze constrained hierarchical models as functions of a_3 and b_3 alone.

In figure 3.4, we show the region of viability in $a_3 - b_3$ space for two different values of δ: in the left-hand panel, we set $\delta = m_e/m_\mu$ (and $M_{\Phi_2}/M_{\Phi_3} = m_\mu/m_\tau$) as required in the minimal version of CHDL discussed above; in the right-hand panel, we set $\delta = 10^{-1}$. We consider a given combination of a_3 and b_3 to be phenomenologically viable if there is any combination of the remaining a_i and b_i for which the combination simultaneously obeys all the neutrino oscillation constraints in (3.19). The entirety of the shaded region shown in each panel, including all differently-shaded bands, is permitted by these constraints: the bands represent of contours $\sin\theta_{13}$ the value of which will be measured or constrained in future neutrino experiments. This plot demonstrates two important features of the Yukawa matrices in CHDL: first, it is indeed possible to satisfy the neutrino oscillation constraints for $\delta = m_e/m_\mu$; second, while b_3, like most of the other a_i and b_i, is constrained to lie fairly close to 1, a_3 is permitted to be quite large when δ is small. In the same figure, we also show contours for the value of $\sin\theta_{13}$, the value of which will be measured or constrained in future neutrino experiments. It is seen that the value of $\sin\theta_{13}$ increases with increased a_3 until reaching its maximum experimental bound.

Let us now take a moment to address how these results affect leptogenesis. Since we are assuming that $M_{\Phi_3} \gg M_{\Phi_1}, M_{\Phi_2}$, the formula (2.8) for the decay asymmetry ϵ tells us that $\mathrm{Im}(\lambda^*_{1\alpha}\lambda_{2\alpha}h^*_{1\beta}h_{2\beta}M_{\Phi_1}M^*_{\Phi_2})$ will vanish (when it involves diagonal elements of λ or h) unless $\beta = \alpha = 3$. This means that

$$\epsilon \propto \mathrm{Im}\left(a_2^* a_3 b_2^* b_3\right) \frac{\delta}{1-\delta} \tag{3.31}$$

in CHDL; the two panels in figure 3.4 then show that for a given δ, the largest amount of left-handed lepton number L_L (and therefore the largest baryon asymmetry) will be obtained when $a_3 = a_3^{max}(\delta)$, where $a_3^{max}(\delta)$ is the maximum possible value of a_3 for a given δ consistent with

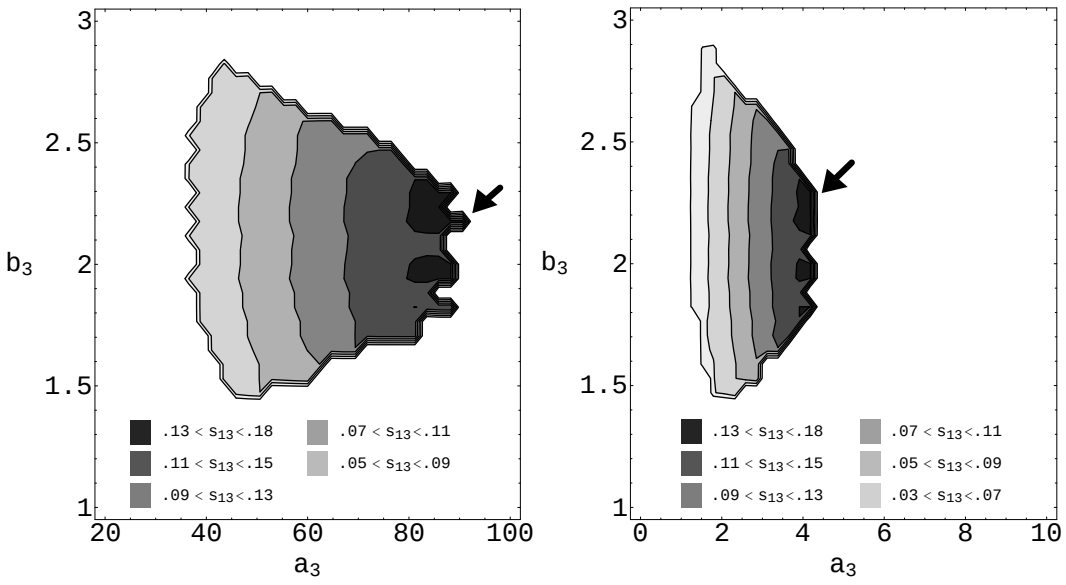

Figure 3.4: Here, the regions of $a_3 - b_3$ space (see equation (3.30) for a description of the Yukawa-matrix parametrization used) for which all constraints on neutrino masses and mixings (3.19) are simultaneously satisfied for some combination of the remaining a_i and b_i are shown for two different values of δ [38]. Additionally, contours depicting the ranges for $s_{13} = \sin\theta_{13}$ (which depends primarily on a_3, but varies slightly with the remaining a_i and b_i) are shown. In the right panel $\delta = 10^{-1}$; in the left panel, $\delta = m_e/m_\mu = 4.83 \times 10^{-3}$ The plots reveal that while b_3 is constrained, along with most of the other a_i and b_i, to lie reasonably near 1, $a_3^{max}(\delta)$ can be quite large and increases with decreasing $\delta = 10^{-1}$, making it easier to obtain a realistic baryon-to-photon ratio η. For $\delta = 10^{-1}$, $a_3^{max} \simeq 4.5$; for $\delta = 4.83 \times 10^{-3}$, $a_3^{max} \simeq 95$. In each panel, the configuration that yields the greatest decay asymmetry ϵ is marked with an arrow.

neutrino masses and mixings. It is interesting to note that since the maximum experimental value of $\sin\theta_{13}$ sets the value of a_3^{max}, then the maximum baryon asymmetry will be obtained when $\sin\theta_{13}$ acquires its maximal experimental value, which we take to be $\sin^2_{max}\theta_{13} = 0.031$. For $\delta = 10^{-1}$, the result is $a_3^{max}(1/10) \approx 4.5$, as indicated in the right panel of figure 3.4. It is also of note that $a_3^{max}(\delta)$ rises sharply as δ is decreased, as indicated by the result for $\delta = 4.83 \times 10^{-3}$ (a value which, as we shall see in section 5.2, is predicted by certain theoretically-

motivated extensions of CHDL) shown in the left panel, in which case $a_3^{max} \simeq 95$.

One of the assumptions we have been implicitly making here is that we have maximal CP violation in the decays of the fields Φ and $\overline{\Phi}$ (i.e. the overall phase in the product $a_2^* a_3 b_2^* b_3$ must be $\pi/2$). In this case one can obtain a value for the effective CP violation in the lepton sector. This can be defined in a phase invariant way in terms of the quantity $J = \mathrm{Im}(U_{12} U_{22}^* U_{23} U_{13}^*)$ [75, 76], where $U_{ij} \equiv (U_{MNS})_{ij}$. Taking for example the two points that will generate the most baryon number in the left and right handed panels of figure 3.4 (marked with an arrow) we find $J \simeq 0.034$ for the point in the left panel and $J \simeq 0.030$ for the point in the right panel (since the maximal value for J is $|U_{12} U_{22}^* U_{23} U_{13}^*|$, which for these points yields a value of $J \simeq .038$, the CP-violation here is close to maximal). It could be interesting to do a more detailed study of the issue of linking more generally the effective CP violation in the lepton sector to the CP violation in the interactions of the heavy fields Φ and $\overline{\Phi}$. Nevertheless, we will not pursue this issue further in the present work.

We have shown here that it is possible to construct Dirac leptogenesis scenarios that are capable of satisfying current constraints on the light neutrino spectrum. In CHDL, the set of parameters relevant to neutrino physics and to leptogenesis is quite small, given the anti-symmetry condition on the two coupling matrices λ and h: the leptogenesis scale M_{Φ_1}, the intermediate scale $\langle \chi \rangle$, the trilinear matrix entries a_3 and b_3, the mass ratio δ, and the overall coupling strength f are essentially the only free parameters in the model. In fact, even this represents an overcounting: equations (3.25) and (3.19) imply an additional constraint on these parameters. For example, take the case where $\delta = 10^{-1}$ and a_3 and b_3 have been set to the values most advantageous for baryogenesis, $a_3 = 4.5$ and $b_3 = 2.2$ (see figure 3.4). In this case,

the constraint becomes

$$\frac{f^2\langle\chi\rangle}{M_{\Phi_1}}\sin\beta = 1.009\times10^{-13}, \tag{3.32}$$

and the model contains only five free parameters (and that's including b_3, which is rather stringently constrained). We will generally use this constraint to eliminate $\langle\chi\rangle$ or f, depending on which is most convenient for the purpose at hand.

While we again emphasize that it is certainly not the only scenario for obtaining a realistic neutrino spectrum in Dirac leptogenesis, CHDL is a particularly simple and predictive model—and it will be the one on which we will focus our attentions from this point forward. It still remains to be seen whether CHDL (or indeed any Dirac leptogenesis model) can also simultaneously satisfy the constraints from gravitino physics and yield a realistic baryon number for the universe, however, though as we shall see in chapter IV, thermal Dirac leptogenesis will indeed turn out to be workable in a variety of models.

3.3 Soft Masses and Flavor Violation

3.3.1 Flavor Violation in Supersymmetric Models

Another requirement which Dirac leptogenesis must satisfy in order to be considered viable is that the theory must be compatible with present constraints on flavor violation in the lepton sector. The most stringent bounds come from measurements of the branching ratios for flavor-violating decays and conversions of heavy leptons, such as $\mu\to e\gamma$, $\tau\to\mu\gamma$, $\mu\to eee$ and $\mu A\to eA$. The current experimental limits on the 2-body decay processes are [77]

$$BR(\mu\to e\gamma) \;<\; 1.2\times10^{-11}, \tag{3.33}$$

$$BR(\tau\to\mu\gamma) \;<\; 1.1\times10^{-6}. \tag{3.34}$$

The MEG experiment [78] is expected to improve on bound on $\mu \to e\gamma$ by several orders of magnitude in the near future, bringing it to $\mathcal{O}(10^{-13} - 10^{-14})$ or lower. Other related projects, such as PRIME [79] (sensitive to $\mu A \to eA$ conversion), are expected to go online over the next few years, and projects have also been proposed [80] that would lower the bound on $BR(\tau \to \mu\gamma)$ to $\mathcal{O}(10^{-9})$.

Supersymmetric theories with generic soft parameters tend to result in unacceptable levels of flavor violation due to flavor misalignment between quark and lepton mass eigenstates on the one hand, and squark and slepton eigenstates on the other. There are a variety of ways to address this problem, the most common one being the assumption of soft mass universality. Here, one assumes that whatever mechanism gives rise to supersymmetry breaking at some high scale M (the Planck scale, the GUT scale, etc.) results in a set of squark and slepton soft mass-squared matrices that are flavor-blind and diagonal and A-terms proportional to the Standard Model Yukawa couplings, i.e. that

$$\begin{gathered}
\mathbf{m}_Q^2 = m_Q^2\mathbf{1}, \quad \mathbf{m}_L^2 = m_L^2\mathbf{1}, \quad \mathbf{m}_{\overline{u}}^2 = m_{\overline{u}}^2\mathbf{1}, \\
\mathbf{m}_{\overline{d}}^2 = m_{\overline{d}}^2\mathbf{1}, \quad \mathbf{m}_{\overline{e}}^2 = m_{\overline{e}}^2\mathbf{1}, \quad \mathbf{m}_{\overline{\nu}}^2 = m_{\overline{\nu}}^2\mathbf{1}, \\
\mathbf{a}_u = A_u\mathbf{y}_u, \quad \mathbf{a}_u = A_u\mathbf{y}_d, \quad \mathbf{a}_u = A_u\mathbf{y}_e, \quad \mathbf{a}_u = A_u\mathbf{y}_\nu,
\end{gathered} \tag{3.35}$$

then all squarks and sleptons become degenerate in mass and can be freely rotated into one another up to A-term-induced mixings, which will only be large for sfermions of the third generation. Flavor-violating effects would then be expected to be very small.

In Dirac leptogenesis, even if soft masses are universal at scale M, as they are run down from M to the leptogenesis scale M_{Φ_1} flavor-off-diagonal terms will be generated by quantum corrections, due to the nontrivial matrix structure of the trilinear coupling matrices λ and h.

It can be shown that, under assumption of universal supersymmetry breaking, this is not a damning problem for the MSSM (for a brief review, see [81]). However, since the lepton sector of the Dirac leptogenesis superpotential (2.1) is modified from that of the MSSM and includes new coupling matrices with nontrivial flavor structure, we must ensure that any off-diagonal contributions to the slepton mass matrices m^2_{LL}, m^2_{RR} and m^2_{LR} generated by these modifications do not result in an unacceptable level of flavor violation. The renormalization group evolution (RGE) equations for parameters appearing in a general superpotential soft supersymmetry breaking Lagrangian are well known [82], and the RGE equation for a soft mass is given by

$$\begin{aligned}\beta_{(m^2)^i_j} &= \frac{1}{16\pi^2}\left[\frac{1}{2}y^*_{ipq}y^{pqn}(m^2)^j_n + \frac{1}{2}y^{jpq}y^*_{pqn}(m^2)^n_i + 2y^*_{ipq}y^{jpr}(m^2)^q_r \right. \\ &\left. + a^*_{ipq}a^{jpq} - 8g^2_a C_a(i)|M_a|^2\delta^j_i + 2g^2_a(T^a)^j_i \mathrm{Tr}[T^a m^2]\right], \end{aligned} \tag{3.36}$$

where the a_{ijk} are soft A-terms, M_a are gaugino masses, y_{ijk} are trilinear couplings appearing in the superpotential, and a sum over gauge groups is implied. The $C_a(i)$ are quadratic Casimir group invariants, defined in terms of the generators T^a by the relation

$$C_a(i)\delta^j_i = (T^a T^a)^j_i. \tag{3.37}$$

Assuming the Universality condition at the high scale and that all soft A-terms are equal to the relevant Yukawa coupling multiplied by the universal soft supersymmetric mass m_s, one can simply estimate the flavor violating corrections to the mass matrix by integrating the RGE equations iteratively [83, 84], and using this method, one obtains off-diagonal contributions to the slepton masses δm^2_{LL} and δm^2_{RR}:

$$\delta m^2_{LL} \approx -\frac{1}{2\pi^2}\ln\left(\frac{M}{M_{\Phi_1}}\right) h^*_{i\alpha}h_{i\beta}m^2_s \tag{3.38}$$

$$\delta m^2_{RR} \approx -\frac{1}{2\pi^2}\ln\left(\frac{M}{M_{\Phi_1}}\right) \lambda^*_{i\alpha}\lambda_{i\beta}m^2_s. \tag{3.39}$$

Another off-diagonal scalar mass term arises from the effective A-term in (2.11) once electroweak symmetry breaking occurs in models where the F-term of χ acquires a VEV $\langle F_\chi \rangle \neq 0$ (a corollary in many mechanisms where its scalar component obtains its VEV). After electroweak symmetry breaking, this term results in a contribution

$$\delta m^2_{LR} = h^\dagger_{i\alpha} \lambda_{i\beta} \frac{\langle F_\chi \rangle}{M_{\Phi_1}} v \sin\beta \tag{3.40}$$

to the sneutrino mass matrix which mixes left-handed and right-handed sneutrinos[3].

In order to examine the effect of these mixings, the full mass matrices for both the charged sleptons and sneutrinos must be taken into account. For simplicity, we will continue to assume that the leading soft breaking sector is flavor diagonal and universal with a common scalar mass m_s. The resulting additional contributions to the slepton mass squared matrices, given by equations (3.38), (3.39), and (3.40), can thus be expressed in terms of the 3×3 submatrices δm^2_{LL}, δm^2_{RR}, and δm^2_{LR} as

$$\delta m^2_{\tilde{\ell}^\pm} = \left(\begin{array}{c|c} \delta m^2_{LL} & 0 \\ \hline 0 & 0 \end{array} \right) \qquad \delta m^2_{\tilde{\nu}} = \left(\begin{array}{c|c} \delta m^2_{LL} & \delta m^2_{LR} \\ \hline (\delta m^2_{LR})^\dagger & \delta m^2_{RR} \end{array} \right). \tag{3.41}$$

The only contribution to the charged slepton mass squared matrix comes from δm^2_{LL} (no off-diagonal terms will be generated radiatively in the RR part of charged slepton matrix $m^2_{\tilde{\ell}^\pm}$ since the Yukawa coupling matrix Y_e can always be chosen diagonal at the high scale), while the sneutrino mass squared matrix receives not only additional flavor mixings among left-handed and among right-handed sneutrinos, but also an effective A-term from δm^2_{LR} which intermixes left-handed and right-handed sneutrinos.

[3]The CP-violating phases in λ and h required for leptogenesis can induce new phases in the slepton mass matrices during the RGE running or through the mixing term of Eq. (3.40). We have checked that the effect of these phases is too small to reach the experimental bounds on lepton EDM's, within the region of parameter space considered here in which leptogenesis is successful. As for the rest of phases of the MSSM, they are assumed to be small enough to avoid violating these same experimental bounds.

In CHDL, where we have a specific flavor structure for the matrices λ, h and M_Φ, one has a specific prediction for flavor mixing among sleptons once the electroweak and hidden symmetries are broken. Using the neutrino mass constraint (3.32), we can express the overall dependence of the slepton mass terms in (3.38), (3.39), and (3.40) on the relevant mass scales in the theory:

$$\begin{aligned} \delta m^2_{LL} &\propto f^2 \propto \tfrac{M_{\Phi_1}}{\langle\chi\rangle} \\ \delta m^2_{RR} &\propto f^2 \propto \tfrac{M_{\Phi_1}}{\langle\chi\rangle} \\ \delta m^2_{LR} &\propto \tfrac{f^2}{M_{\Phi_1}} \propto \tfrac{1}{\langle\chi\rangle}. \end{aligned} \tag{3.42}$$

It should be noted here that the proportionality constants for the bottom two equations are not dimensionless: the ones associated with δm^2_{LL} and δm^2_{RR} each contain a factor of m_s^2 and have mass dimension $[m]^2$, while the one associated with δm^2_{LR} contains a factor of $\langle F_\chi\rangle v$ and has mass dimension $[m]^3$.

3.3.2 Lepton-Sector Flavor Violation in Dirac Leptogenesis

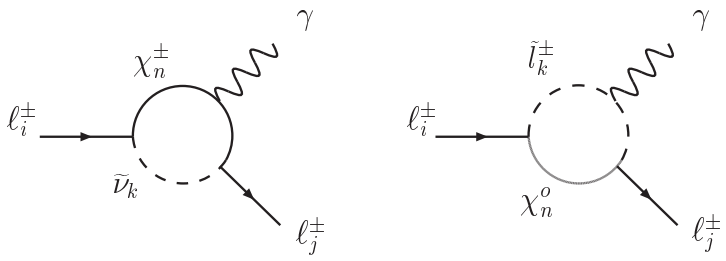

Figure 3.5: Feynman diagrams giving the two leading order contributions to the flavor-changing process $\ell_i^- \to \ell_j^-\gamma$ due to sneutrino (left diagram) and charged slepton (right diagram) mass mixings.

The effective interaction leading to lepton flavor violating decays of the form $\ell_i \to \ell_j\gamma$,

where ℓ_i and ℓ_j are charged leptons, can be written as

$$\mathcal{I} = i\,e\,m_{\ell_j}\,\bar{u}_i(q-p)\,\sigma_{\alpha\beta}\,q^\beta\left(A^L P_L + A^R P_R\right)u_j(p)\,\epsilon^*(q), \tag{3.43}$$

where q and p are the momenta of the photon and the outgoing lepton ℓ_j respectively, and m_{ℓ_j} is the outgoing lepton mass. The resulting decay rate is

$$\Gamma(l_j^- \to l_i^-\,\gamma) = \frac{e^2}{16\pi} m_{l_j}^5 (|A^L|^2 + |A^R|^2). \tag{3.44}$$

The leading contributions to the amplitudes A^L and A^R appear at one loop level and are shown in figure 3.5. They involve both a sneutrino (and chargino) mass eigenstate and charged slepton (and neutralino) mass eigenstate running in the loop. These amplitudes were computed in [83] for a general MSSM scenario and we have included the modified expressions which account for the presence of light right-handed neutrino and sneutrino fields in appendix A.

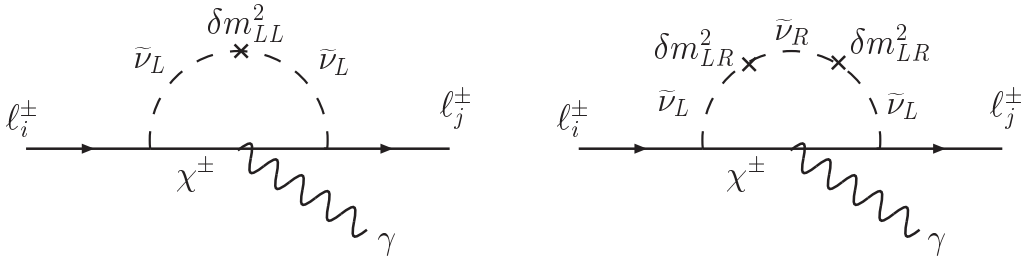

Figure 3.6: Feynman diagrams for the leading-order process involving δm^2_{LL} (left diagram), and for the leading process involving δm^2_{LR} (right diagram), with sneutrinos running in the loop in the mass-insertion approximation. Note that any process involving δm^2_{LR} necessarily involves two mass insertions, and any one involving δm^2_{RR} (given by the diagram on the right with an additional δm^2_{RR} insertion) necessarily involves three.

Since the relationship between the Dirac leptogenesis model parameters f, $\langle\chi\rangle$, and M_{Φ_1}, which enter into equation (3.44) via the masses and mixings defined in appendix A, and the

flavor-violation rates (3.44) is somewhat obscure, let us take a moment to make it a bit more transparent. Consider an exclusion contour in parameter space corresponding to the $\mu \to e\gamma$ bound (which will turn out to be the more stringent of the two) in equation (3.33). Along this bound, the branching ratio for $BR(\mu \to e\gamma)$ is by definition quite low and flavor-violating effects will be small. It is therefore valid to use the mass-insertion approximation there and treat δm^2_{LL}, δm^2_{LR}, and δm^2_{RR} as small corrections to the slepton propagators. Let us focus on corrections to the sneutrino propagator, which enters in the left diagram in figure 3.5, since it can receive corrections from all three of these. The leading contributions involving each of δm^2_{LL} (left panel) and δm^2_{LR} (right panel) are shown in figure 3.6 (the leading contribution to δm^2_{RR}, which would require three mass insertions, is the least important of the three, and is not shown). Since there is no coupling between leptons and right-handed sneutrinos, corrections from δm^2_{LR} and δm^2_{RR} only appear at second and third order in the mass insertion expansion, respectively. Therefore, if there is no substantial hierarchy among these three sets of mixing terms, mixings between left-handed sleptons provide the primary source of flavor violation. In the approximation that all slepton, chargino, and neutralino masses are roughly on the same scale m_{soft}, the branching ratio may be estimated as

$$BR(\mu \to e\gamma) \propto \frac{\alpha^3}{G_F^2} \frac{(\delta m^2_{LL})^2}{m_s^8}. \tag{3.45}$$

In interpreting this result, let us treat M_{Φ_1} and $\langle\chi\rangle$ as free parameters, treat δ, a_3 and b_3 as fixed, and eliminate f using the constraint (3.32). Equation (3.45) tells us that contours of branching ratio in the $M_{\Phi_1} - \langle\chi\rangle$ plane correspond to contours of δm^2_{LL}. According to equation (3.42), $\delta m^2_{LL} = c_1 M_{\Phi_1}/\langle\chi\rangle$, where c_1 is a dimensionless proportionality constant with dimension $[m]^2$,

so the exclusion contour associated with left-left mixing takes the form

$$\ln M_\Phi = \ln\langle\chi\rangle + C_{LL}, \tag{3.46}$$

where $C_{LL} = -\ln(\delta m^2_{LL}/c_1)$ is an as yet undetermined constant.

In the absence of any large hierarchy between δm^2_{LL}, δm^2_{LR}, and δm^2_{RR} the oblique contour defined by equation (3.46) is the only important one. However, there is no a priori reason why such a hierarchy should not exist. The δm^2_{LR} contribution (3.40) is proportional to $\langle F_\chi\rangle$, which has little relevance to baryogenesis other than that it serves to equilibrate the left- and right-handed sneutrino fields and is essentially unconstrained. As was pointed out in section 2.2, $\sqrt{\langle F\rangle}$ can potentially be quite large (10^6 GeV or higher), and if this is the case, contribution from δm^2_{LR} could be as important as those from δm^2_{LL}. Let us assume for a moment that this is the case and examine the constraints related to δm^2_{LR} and δm^2_{LR} together. In regions of parameter space where $\langle\chi\rangle$ is small, we now have

$$BR(\mu \to e\gamma) \propto \frac{\alpha^3}{G_F^2 m_S^8}\frac{(\delta m^2_{LR})^4}{m^4_{\tilde{\nu}_R}} = \text{constant} \tag{3.47}$$

along any exclusion contour. Equation (3.42) tells us that,

$$\delta m^2_{LR} = c_2\frac{1}{\chi}, \tag{3.48}$$

where c_2 has mass dimension $[m]^3$. The associated contour is therefore given by

$$\ln\langle\chi\rangle = C_{LR}, \tag{3.49}$$

where $C_{LR} = \ln(c_2/\delta m^2_{LR})$. As for δm^2_{RR}, equation (3.42) implies that it becomes important (and in fact the dominant contribution to the right-handed sneutrino mass) in regions of parameter space where $\langle\chi\rangle$ is small and M_{Φ_1} is large. In this regime the mass insertion

approximation can no longer be used, but we can use the approximation $m^2_{\tilde{\nu}_R} \simeq \delta m^2_{RR}$ in the sneutrino propagator in equation (3.47). The amplitude for the process in the left panel of 3.5 then implies

$$\frac{(\delta m^2_{LR})^2}{\delta m^2_{RR}} = c_3 \frac{1}{M_{\Phi_1}\langle\chi\rangle}, \tag{3.50}$$

where c_3 is a proportionality constant with mass dimension $[m]^4$. This implies yet another oblique exclusion contour corresponding to the line

$$\ln M_{\Phi_1} = -\ln\langle\chi\rangle + C_{RR}, \tag{3.51}$$

where

$$C_{RR} = \ln\left(c_3 \, \frac{\delta m^2_{RR}}{(\delta m^2_{LR})^2}\right). \tag{3.52}$$

This line runs parallel to the one from left-left mixing (3.46). As discussed above, it will generally be the case that the δ^2_{LL} contour provides a more stringent bound than δm^2_{RR}, and hence this contour can generally be ignored.

Taken together, the contours determined by equations (3.46) and (3.49) suggest that unacceptable amounts of flavor violation will occur in regions with large M_{Φ_1} and small χ. It is not yet obvious exactly how large M_{Φ_1} and how small χ must be before problems arise (or to put it another way, what the precise values of C_{LL} and C_{LR} are) in a given Dirac leptogenesis model, however, nor is it obvious that these constraints are compatible with those from gravitino cosmology, neutrino physics, etc. These issues will be addressed in the next chapter through a careful numerical calculation which takes into account the full formulae for the masses, mixings, et al. given in appendix A.

CHAPTER IV

EVOLUTION OF THE BARYON ASYMMETRY

4.1 Boltzmann Equations

Let us now turn to the numerical calculation of η and the solution of the full Boltzmann equations. This is slightly more complicated for Dirac than for Majorana leptogenesis because in the latter, it is only necessary to keep track of the overall lepton number. In contrast, the former involves the creation of several distinct stores of lepton number with different properties. The heavy fields aside, in Dirac leptogenesis there are six particle species charged under lepton number (ν_R, $\tilde{\nu}_R$, ℓ, $\tilde{\ell}$, and the right-handed charged lepton and slepton fields e_R and $\tilde{e}_R$), and thus six individual stores of lepton number to keep track of: L_ℓ, L_{ν_R}, $L_{\tilde{L}}$, $L_{\tilde{\nu}_R}$, L_{e_R}, and $L_{\tilde{e}_R}$. Some of these stores are positive and some negative, some of the particle species are involved in sphaleron interactions while others are not, and so forth, so it might appear necessary that we keep track of each field and each store individually. Including an equation for the overall baryon number of the universe B and accounting for the dynamics of the heavy fields in the Φ_1 and $\overline{\Phi}_1$ supermultiplets raises the total number of equations in the Boltzmann system to twenty-one. The situation can be greatly simplified, however, by noting that the fields ℓ, $\tilde{\ell}$,

e_R, and $\tilde{e}_R$ participate in $SU(2)$ and/or $U(1)_Y$ gauge interactions, which should be sufficiently rapid (compared to other processes relevant to leptogenesis) that these species will always be in chemical equilibrium with one another. As a result, any lepton number stored in any one of them will be rapidly distributed among L_ℓ, $L_{\tilde{\ell}}$, L_{e_R}, and $L_{\tilde{e}_R}$ in proportion to the relative number of degrees of freedom of each respective field. These fields then compose a distinct, "visible" sector of the theory with an aggregate lepton number L_{vis}.

As for the remaining two species charged under lepton number, there are two possible choices. While the ν_R, by construction, have no interactions with the visible sector and thus can be seen as forming a "hidden" sector which only equilibrates with the visible sector fields at late times through the effective neutrino Dirac Yukawa, no such requirement exists for the right-handed sneutrinos $\tilde{\nu}_R$. When $\langle F_\chi \rangle$ is large, the $\tilde{\nu}_R$ fields have additional, rapid interactions with the visible sector fields (and in particular $\tilde{\ell}$) through effective A-terms (2.11) and should thus be considered part of the visible sector. As shown in section 3.3.2, an F-term VEV of order $\langle F_\chi \rangle \sim 10^8$ GeV is still permitted by flavor violation constraints in theories with weak-scale slepton squared masses, and in split supersymmetry scenarios with much heavier sfermions, even this bound no longer applies, so rapid sneutrino equilibration is far from excluded. On the other hand, when $\langle F_\chi \rangle$ is small, the $\tilde{\nu}_R$ fields decouple and become part of the hidden sector. In either case, since none the hidden sector fields interacts via electroweak sphalerons, an aggregate lepton L_{hid} can be defined for the hidden sector, which is just the sum of the lepton numbers individually stored in each of its constituent fields. We will henceforth refer to these two situations as the large-$\langle F_\chi \rangle$ and small-$\langle F_\chi \rangle$ scenarios.

The definitions of L_{vis} and L_{hid} simplify our task considerably; in the limit of rapid equilibration within the visible sector, only three Boltzmann equations are required to describe the

evolution of lepton and baryon number asymmetries of the light fields in Dirac leptogenesis: one for L_{vis}, one for L_{hid}, and one for the overall baryon number B. In addition to these, it turns out (see appendix B) that only three additional equations are needed to describe the dynamics of the heavy fields: two to describe the evolution of the individual lepton numbers L_{ϕ_Φ} and $L_{\phi_{\overline{\Phi}}}$ stored respectively in ϕ_1 and $\overline{\phi}_1$, and one to track the abundance of one of the heavy fields (we choose $Y^c_{\phi_\Phi}$). Our Boltzmann system has now been reduced from twenty-one equations down to a far more manageable six.

In addition to the rapid gauge interactions that equilibrate the fields in L_{vis}, there are a variety of additional processes which we must take into account. First, we must include the decays and inverse decays of the fields in Φ_1 and $\overline{\Phi}_1$. This introduces a pair of rates $\Gamma_L = \Gamma(\phi \to \widetilde{\ell} + \chi)$ and $\Gamma_R = \Gamma(\phi \to \nu^c_R + \tilde{H}^c_u)$, which are related to the overall ϕ decay rate Γ_D given in (2.6) by the defining relation

$$\Gamma_D = \Gamma_L + \Gamma_R. \tag{4.1}$$

Second of all, we must include interactions involving virtual ϕ_i and $\overline{\phi}_i$ fields (and their fermionic superpartners) that can transfer lepton number between L_{vis} and L_{hid}. The dominant contribution to the transfer rate comes from $2 \leftrightarrow 2$ processes, and since this rate, which we will call $\Gamma_{2\leftrightarrow 2}$, will be suppressed by inverse factors of the leptogenesis scale for $T \ll M_{\Phi_1}$, these processes cannot be considered rapid compared to the gauge interactions. Third, since annihilation processes second-order in the heavy fields can serve to reduce the abundances of these particles during the leptogenesis epoch [85, 86], we should include them as well, with rate Γ_A. Fourth and finally, we must include sphaleron processes with rate Γ_{sph}, which will interconvert B and L_{vis}.

We are now ready to write the full set of Boltzmann equations governing the evolution of

baryon number B in the early universe, a full derivation for which is provided in appendix B, along with explicit definitions for all quantities used therein. Since these equations will differ slightly between the large-$\langle F_\chi \rangle$ and small-$\langle F_\chi \rangle$ scenarios, due to the differing constitution of L_{vis} and L_{hid}, they need to be written down separately for each case. We will concentrate on the large-$\langle F_\chi \rangle$ scenario, in which they are

$$\frac{dB}{dz} = \frac{z}{H(M_{\Phi_1})}\left[-\langle\Gamma_{sph}\rangle(B+\frac{8}{15}L_{vis})\right] \tag{4.2}$$

$$\begin{aligned}\frac{dL_{vis}}{dz} = \frac{z}{H(M_{\Phi_1})}\Big[&-2\epsilon\langle\Gamma_D\rangle(Y^c_{\phi_\Phi}-Y^{eq}_{\phi_\Phi})+\langle\Gamma_L\rangle(L_{\phi_\Phi}+L_{\phi_{\overline{\Phi}}}) \\ &+\langle\Gamma_R\rangle L_{\phi_{\overline{\Phi}}}-2L_{vis}\Big(\langle\Gamma_D\rangle_{ID}+\langle\Gamma_L\rangle_{ID}\Big) \\ &+(L_{hid}-\frac{1}{7}L_{vis})\langle\Gamma_{2\leftrightarrow 2}\rangle-\langle\Gamma_{sph}\rangle(B+\frac{8}{15}L_{vis})\Big]\end{aligned} \tag{4.3}$$

$$\begin{aligned}\frac{dL_{hid}}{dz} = \frac{z}{H(M_{\Phi_1})}\Big[&2\epsilon\langle\Gamma_D\rangle(Y^c_{\phi_\Phi}-Y^{eq}_{\phi_\Phi})+L_{\phi_\Phi}\langle\Gamma_R\rangle-2L_{hid}\langle\Gamma_R\rangle_{ID} \\ &-(L_{hid}-\frac{1}{7}L_{vis})\langle\Gamma_{2\leftrightarrow 2}\rangle\Big]\end{aligned} \tag{4.4}$$

$$\begin{aligned}\frac{dY^c_{\phi_\Phi}}{dz} = \frac{z}{H(M_{\Phi_1})}\Big[&-\langle\Gamma_D\rangle(Y^c_{\phi_\Phi}-Y^{eq}_{\phi_\Phi})+\frac{1}{2}L_{vis}\langle\Gamma_L\rangle_{ID}+\frac{1}{2}L_{hid}\ \langle\Gamma_R\rangle_{ID} \\ &-\langle\Gamma_A\rangle\left(\left(Y_{\phi^c_\Phi}/Y^{eq}_{\phi_\Phi}\right)^2-1\right)\Big]\end{aligned} \tag{4.5}$$

$$\frac{dL_{\phi_\Phi}}{dz} = \frac{z}{H(M_{\Phi_1})}\left[-\langle\Gamma_D\rangle L_{\phi_\Phi}+2L_{vis}\langle\Gamma_L\rangle_{ID}+2L_{hid}\langle\Gamma_R\rangle_{ID}\right] \tag{4.6}$$

$$\frac{dL_{\phi_{\overline{\Phi}}}}{dz} = \frac{z}{H(M_{\Phi_1})}\left[-\langle\Gamma_D\rangle L_{\phi_{\overline{\Phi}}}+2L_{vis}\langle\Gamma_D\rangle_{ID}\right] \tag{4.7}$$

in terms of the variable $z \equiv M_{\Phi_1}/T$. Here, the inverse decay rates $\langle\Gamma_D\rangle_{ID}$, $\langle\Gamma_L\rangle_{ID}$, and $\langle\Gamma_R\rangle_{ID}$

are defined by

$$\langle \Gamma_D \rangle_{ID} = \frac{1}{7} \frac{n_{\phi_\Phi}^{eq}}{n_\gamma} \left(\frac{K_1(z)}{K_2(z)} \right) \Gamma_D, \tag{4.8}$$

$$\langle \Gamma_L \rangle_{ID} = \frac{1}{7} \frac{n_{\phi_\Phi}^{eq}}{n_\gamma} \left(\frac{K_1(z)}{K_2(z)} \right) \Gamma_L, \quad \text{and} \tag{4.9}$$

$$\langle \Gamma_R \rangle_{ID} = \frac{n_{\phi_\Phi}^{eq}}{n_\gamma} \left(\frac{K_1(z)}{K_2(z)} \right) \Gamma_R, \tag{4.10}$$

where Γ_D is the total decay width of ϕ_1 given in equation (2.6), n_ϕ^{eq} is the equilibrium number density of ϕ_1 (and $\overline{\phi}_1$, etc.), and the quantities Γ_L and Γ_R represent the partial decay widths for $\phi \to \nu_R \tilde{H}$ (or $\overline{\phi} \to \tilde{\nu}_R H$) and $\overline{\phi} \to \ell \tilde{\chi}$ (or $\phi \to \tilde{\ell} \chi$). The ratio of modified Bessel functions $K_1(z)$ and $K_2(z)$ appearing in these rates is a result of averaging over time-dilation factors: see (B.23) in Appendix B. We will examine this scenario from this point forward.

4.2 Numerical Analysis of the Boltzmann System

4.2.1 Calculation of Rates

From this point forward we will focus our attention on the large-$\langle F_\chi \rangle$ case and proceed to solve the Boltzmann equations (4.2 - 4.7) numerically. In order to do this we must first calculate the relevant rates appearing in these equations in terms of the model parameters M_{Φ_1}, δ, a_3, b_3, and f (or alternatively $\langle \chi \rangle$). We already have expressions for Γ_{sph} (1.20) and Γ_D (2.6), from the latter of which Γ_L and Γ_R can be obtained trivially. This leaves only the rate $\Gamma_{2 \leftrightarrow 2}$ for processes that shuffle lepton number between L_{vis} and L_{hid} and the heavy field annihilation rate Γ_A. We now turn to address each of these in turn.

While there are a large number of $2 \leftrightarrow 2$ processes which shuffle lepton number between different particle species, only a few will transfer it between L_{vis} and L_{hid}. The rest, which

collectively serve to assist the rapid $SU(2) \times U(1)_Y$ gauge interactions in equilibrating lepton number among the fields in the L_{vis} sector, can be ignored. The relevant s-channel diagrams are pictured in figure 4.1. In addition to these, there are contributions from the t-channel transforms (two per diagram) of these diagrams. In order to evaluate diagrams containing virtual heavy fermions, we define the Dirac spinor

$$\Psi_{Di} = \begin{pmatrix} (\psi_{\Phi_i})_\alpha \\ (\psi_{\overline{\Phi}_i})^{\dagger\dot{\alpha}} \end{pmatrix}, \tag{4.11}$$

where $(\psi_{\Phi_i})_\alpha$ and $(\psi_{\overline{\Phi}_i})_\alpha$ are the Weyl spinor components of the Φ_i and $\overline{\Phi}_i$ superfields. Numerical calculation of the thermally averaged cross-sections for the diagram pictured on the left in the top row of figure 4.1, which involves two Yukawa-type couplings of a scalar to two fermions, yields $\langle \sigma v \rangle_{i\alpha\beta} \simeq \sigma_i^{(2Y)} |\lambda_{i\alpha}|^2 |\lambda_{i\beta}|^2$, where [38]

$$\sigma_i^{(2Y)} \equiv 10^{-2} \frac{T^2}{(M_{\Phi_i}^2 + T^2)^2}. \tag{4.12}$$

For the diagram on the right in the first row of figure 4.1, which includes one Yukawa-type coupling and one trilinear scalar coupling proportional to M_{Φ_i}, the result is very nearly temperature independent and well approximated by $\langle \sigma v \rangle_{i\alpha\beta} \simeq \sigma_i^{(1Y1S)} |\lambda_{i\alpha}|^2 |h_{i\beta}|^2$, where

$$\sigma_i^{(1Y1S)} \equiv 0.5 \times \frac{1}{M_{\Phi_i}^2}. \tag{4.13}$$

The contribution from each of the two diagrams in the second row of figure 4.1, which involve two Yukawa couplings and a mass insertion from the heavy fermions, is equal to that in (4.13). These interactions dominate among $2 \leftrightarrow 2$ processes. The diagram in the bottom row of figure 4.1, which involves a trilinear scalar coupling to the down-type Higgs, may be approximated by $\langle \sigma v \rangle_{i\alpha\beta} \simeq \sigma_i^{(Hd)} |\lambda_{i\alpha}|^2 |\lambda_{i\beta}|^2$, where

$$\sigma_i^{(Hd)} \propto \frac{\mu}{M_{\Phi_i}^3}. \tag{4.14}$$

The constant of proportionality in this equation is $\mathcal{O}(1)$, and is thus suppressed relative to the rate given in (4.13) by μ/M_{Φ_i}. Here, we will assume that μ is several orders of magnitude smaller than all the M_{Φ_i}, and therefore the effect of these processes can be neglected.

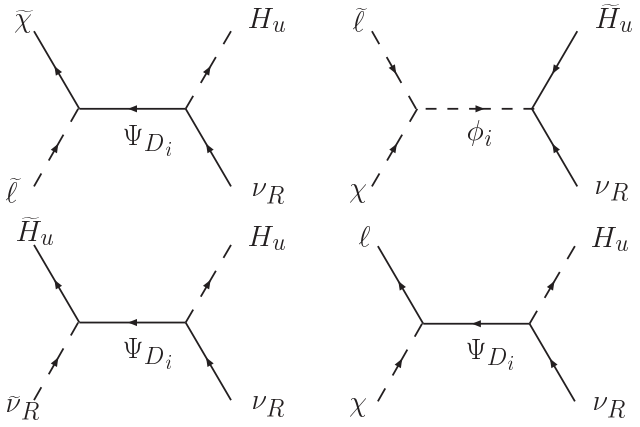

Figure 4.1: Diagrams for $2 \leftrightarrow 2$ s-channel processes which transfer lepton number between L_{aggVis} (the aggregate lepton number in the sector comprising the fields ℓ, $\tilde{\ell}$, $\tilde{\nu}_R$, e_R, and $\tilde{e}_R$, which are assumed to be in chemical equilibrium with one another due to rapid gauge and $\langle F_\chi \rangle$-term equilibration interactions); and L_{hid} (the lepton number stored in right handed neutrinos). The two t-channel interactions associated with each diagram appearing above must also be included in calculating the full thermally averaged cross-section.

Taking into account contributions involving virtual fields in the Φ_2 and $\overline{\Phi}_2$ supermultiplets, as well as those in Φ_1 and $\overline{\Phi}_1$, we find the total interconversion rate between L_{vis} and L_{hid} in the large-$\langle F_\chi \rangle$ scenario to be

$$\begin{aligned}
\Gamma_{2\leftrightarrow 2} &\simeq 3n_\gamma \sum_\alpha \sum_\beta \left(\sigma_1^{(2Y)} |\lambda_{1\alpha}|^2 |\lambda_{1\beta}|^2 + \sigma_2^{(2Y)} |\lambda_{2\alpha}|^2 |\lambda_{2\beta}|^2 \right) \\
&+ 9n_\gamma \sum_\alpha \sum_\beta \left(\sigma_1^{(1Y1S)} |\lambda_{1\alpha}|^2 |h_{1\beta}|^2 + \sigma_2^{(1Y1S)} |\lambda_{2\alpha}|^2 |h_{2\beta}|^2 \right) \\
&+ 3n_\gamma \sum_\alpha \sum_\beta \left(\sigma_1^{(Hd)} |\lambda_{1\alpha}|^2 |\lambda_{1\beta}|^2 + \sigma_2^{(Hd)} |\lambda_{2\alpha}|^2 |\lambda_{2\beta}|^2 \right), \qquad (4.15)
\end{aligned}$$

where we have assumed an equilibrium number density for all non-leptonic light species (e.g.

H_u, χ) involved.

The annihilation rate for the heavy fields Γ_A, which is associated with second order processes of the form $\phi_1\phi_1^c \to ij$ and $\phi_1\overline{\phi}_1^c \to ij$ (and miscellaneous supersymmetrizations thereof), is most readily expressed in terms of the reaction density, given by the general expression

$$\gamma \equiv \frac{T}{64\pi^4}\int_{s_{min}}^{\infty} s^{1/2}K_1\left(\frac{\sqrt{s}}{T}\right)\hat{\sigma}(s), \tag{4.16}$$

where T is temperature, s is the usual Mandelstam variable, and $\hat{\sigma}(s)$ is the total reduced cross section for annihilations of $\phi_1\phi_1^c$, $\phi_1\overline{\phi}_1^c$, etc. into light fields. This is defined by the formula

$$\hat{\sigma}(s) = \frac{1}{8\pi s}\int_{t_-}^{t_+}\sum_i |\mathcal{M}_i(t)|^2 dt, \tag{4.17}$$

where both t and s denote the Mandelstam variables. The limits of integration are given by $t_\pm = M_{\Phi_1}^2 - s(1\mp r)/2$, with r defined below. The relationship between the reaction density for the annihilation of two particles i and j with number densities n_i and n_j, the thermally-averaged cross-section $\langle\sigma|v|\rangle$ for annihilation, and the annihilation rate Γ via

$$\gamma = n_i n_j\langle\sigma|v|\rangle = \frac{n_i n_j}{n_\gamma}\Gamma. \tag{4.18}$$

Hence, in the case under consideration here, the annihilation reaction densityγ_A between ϕ_1 and ϕ_1^c is given by

$$\gamma_A \simeq \frac{s^2}{n_\gamma}Y_{\phi_\Phi^c}^2\,\Gamma_A \tag{4.19}$$

in the (very good) approximation than $L_{\phi_\Phi} \ll Y_{\phi_\Phi^c}$.

In supersymmetric Dirac leptogenesis, the total reduced cross-section γ_A, including all rel-

evant decay processes, is [43]

$$\begin{aligned}\hat{\sigma}^{tot}_{SUSY} &= \frac{1}{16\pi}\left[6g_Y^2g_2^2\left(\left(-7+\frac{4}{x}\right)r+\left(\frac{8}{x^2}-\frac{4}{x}+9\right)\ln\left(\frac{1+r}{1-r}\right)\right)\right. \\ &\quad +g_2^4\left(\left(32+\frac{66}{x}\right)r+3\left(-\frac{16}{x^2}-\frac{16}{x}+9\right)\ln\left(\frac{1+r}{1-r}\right)\right) \\ &\quad \left.+\,g_Y^4\left(\left(19-\frac{36}{x}\right)r+\left(\frac{16}{x^2}-\frac{8}{x}+17\right)\ln\left(\frac{1+r}{1-r}\right)\right)\right], \qquad (4.20)\end{aligned}$$

where $x \equiv s/M_{\Phi_1}^2$, $r = \sqrt{1-4/x}$, and g_2 and g_Y are the $SU(2)$ and $U(1)_Y$ coupling constants. The effect of such second order annihilation processes on the parameter space of Dirac leptogenesis is shown in figure 4.2, where, for comparison, we show two sets of leptogenesis exclusion contours: one representing no second-order processes and one representing annihilation in a supersymmetric model. It is evident from this graph that second order processes do indeed lower the upper exclusion contour, though the effect is not a dramatic one.

4.2.2 Numerical Results

Now that we have calculated the requisite rates, we proceed to a numerical evaluation of the Boltzmann system. As discussed above, CHDL contains five free parameters, so in presenting our results, we will begin by selecting a particular value of δ small enough to be consistent with the neutrino physics constraints in (3.19) (we choose $\delta = 10^{-1}$) and tune a_3 and b_3 to the values most advantageous for leptogenesis (in this case $a_3 = 4.5$ and $b_3 = 2.2$). Treating the reparameterized coupling strength f, the overall scaling factor in both λ and h in the parametrization defined in equation (3.30), as a free parameter, we display the results corresponding to several different choices of M_{Φ_1} in $f-\delta$ parameter space in the right panel of figure 4.3. Here, the regions of $f-\delta$ parameter space in which the final value of η generated falls within the WMAP-allowed range given in (1.1), appear as thin 'ribbons' corresponding

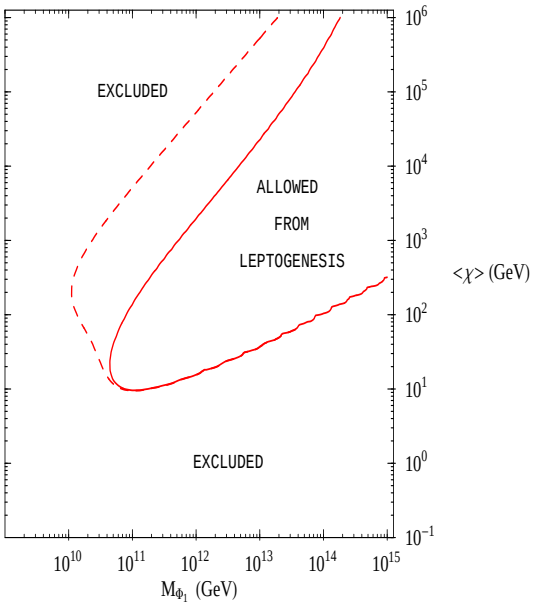

Figure 4.2: This figure, taken from [43], illustrates the effect of second-order processes of the form $\phi_1\phi_1 \to ij$ and $\tilde{\phi}_1\phi_1 \to ij$ on the exclusion contours from leptogenesis. Contours are displayed for the case without annihilation (dashed line) and with annihilation (solid line).

to each value of M_{Φ_1}. We should reemphasize that δ specifies the values of a_3 and b_3 and hence the results displayed are precisely valid only for points lying along the grey, vertical line corresponding to the specific value of δ chosen. To illustrate the effect of changing δ on the shape of the ribbons, we have included a second plot for which $\delta = 4.83 \times 10^{-3}$ in the left panel of figure 4.3. The motivation for selecting this particular value of δ for contrast will be made apparent in section 5.2.

In figure 4.3, the effects of the processes detailed in section 4.2.1 are apparent, and certainly nontrivial. Physically, these effects can be interpreted as follows: increasing the strength of the neutrino-sector couplings (here parameterized by f) increases Γ_D, which in turn increases

the initial value of B; however, from equation (4.15), increasing f also increases the rates for the $2 \leftrightarrow 2$ processes which shuffle lepton number back and forth between L_{vis} and L_{hid}. Furthermore, it increases the rate for inverse decays. This allows two possibilities for generating a realistic final value for B. In the first case, where f is small, the initial baryon number produced by ϕ and $\overline{\phi}$ decays is approximately within the range allowed by WMAP, and $2 \leftrightarrow 2$ and inverse decay processes are so slow as to be negligible; this is the "drift-and-decay limit" of equation (2.16). In the second case, where f is large, a surfeit of baryon number will initially be produced, but these processes, which occur more rapidly for larger f, subsequently reduce B to a phenomenologically acceptable level; this we refer to as the "strong-washout regime". These two possibilities are shown in the two panels of figure 4.4, in which the dynamical evolution of B, L_{vis} and other relevant quantities has been plotted, for $\delta = 4.83 \times 10^{-3}$ and $M_\Phi = 10^{12}$ GeV. In figure 4.3, the two regimes are represented respectively by the lower and upper portions of each ribbon—or more properly, by the two points at which these two portions of the ribbon intersect the grey line corresponding to the chosen value of δ in each graph. In the $\delta = 10^{-1}$ case, the strong washout corresponds to $f = 8.3 \times 10^{-2}$ and the drift-and-decay limit corresponds to $f = 1.5 \times 10^{-3}$. Alternatively, one can use equation (3.32) to express things in terms of $\langle\chi\rangle$ once M_{Φ_1} is specified: for $M_{\Phi_1} = 10^{12}$ GeV, $\langle\chi\rangle \sim 5$ GeV in the strong washout case and $\langle\chi\rangle \sim 50$ TeV in the drift-and-decay limit; for $M_{\Phi_1} = 10^{10}$ GeV the two cases converge and $\langle\chi\rangle \sim 1$ TeV.

Having discussed the general effects of the washout processes described above as a group, it is also important to address their characteristics relative to one another. Inverse decays dominate over $2 \leftrightarrow 2$ processes only for a brief period, where $1 \lesssim z \lesssim 50$, but during this period they are extremely effective in reducing lepton number, and in fact are the primary factor in determining

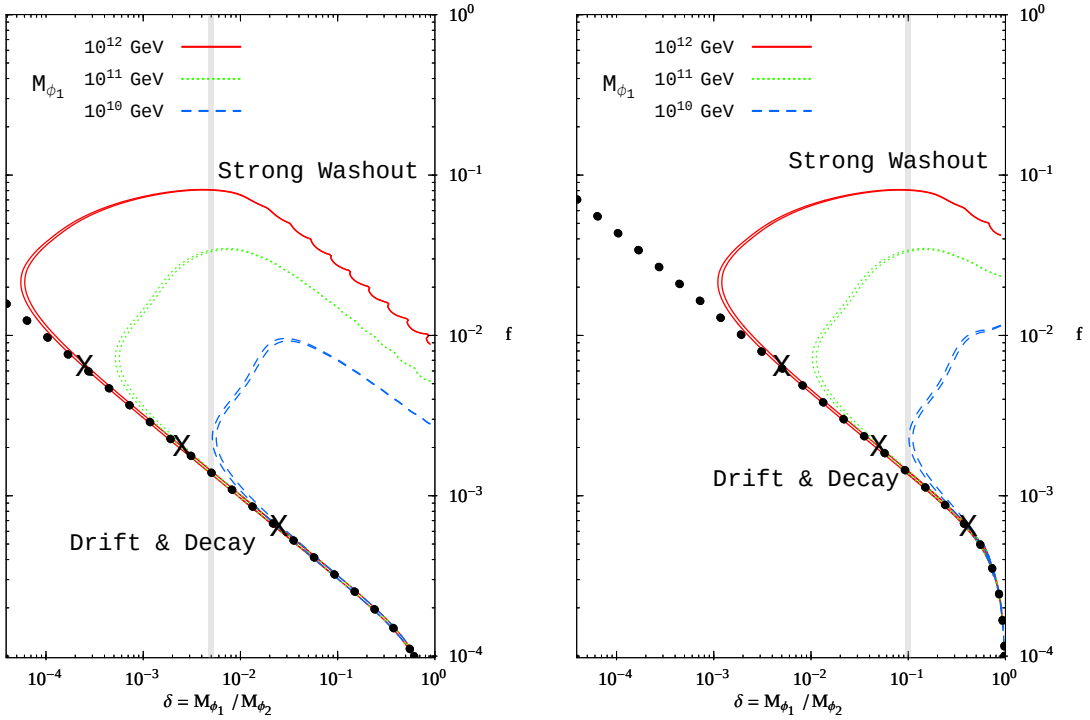

Figure 4.3: Bands in $f-\delta$ parameter space for which the final baryon number B_f falls within the range permitted by WMAP, for different choices of M_{Φ_1} [38]. Here f parameterizes the couplings of the Φ_i fields (see eq. (3.30)). The configuration of the left (right) panel is the one marked with a dot in the left (right) panel of figure 3.4, in which $a_3 = 95$ ($a_3 = 4.5$). The shaded vertical lines show the constraint on the value of δ coming from neutrino mixings and masses ($\delta = m_e/m_\mu \approx 4.83 \times 10^{-3}$ in the left and $\delta = 10^{-1}$ in the right). Note that there are two points that yield a realistic value of B_f for a given δ (the points at which the grey vertical line intersects a given ribbon). When f is small enough, the initial baryon number generated is just enough to be consistent with WMAP, while the washout effect of inverse decays and $2 \leftrightarrow 2$ processes is negligible. In this situation the baryon number generated is independent of M_Φ and its the final value is proportional to the CP violating parameter ϵ (see eq. (2.16)). The dark dotted curve shows the band of consistent baryon number calculated in this "drift and decay" limit. Each "X" marks the point in which $\Gamma_D/H = 1$ for each different M_{Φ_1}. At these points, the "strong washout" regime starts. The now active washout processes reduce an initial surfeit of baryon number (due to a larger f) down to an acceptable level (see figure 4.4).

the final value of η. For larger z, until they freeze out, the $2 \leftrightarrow 2$ interactions dominate and further reduce L_{vis} and L_{hid} (and consequently B). It should be noted, however, that the total

$B - L_{tot}$ number of the universe is manifestly conserved by the Boltzmann equations (4.2) - (4.7) (the sum of the rates for the various lepton numbers involved is zero), and since we began with $B - L_{tot} = 0$, we end up with $B - L_{tot} = 0$ in any case, as expected.

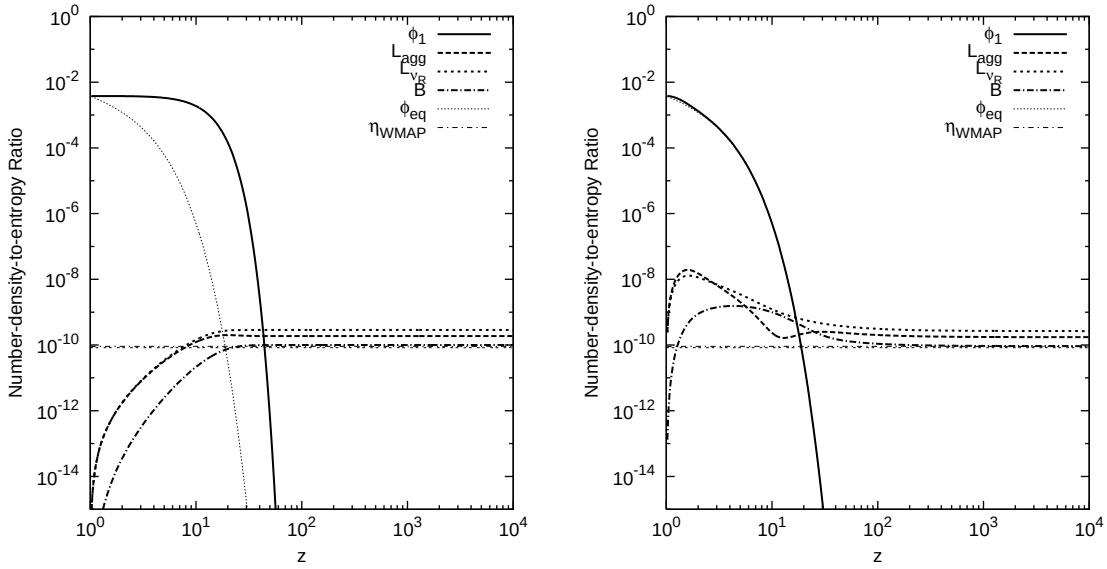

Figure 4.4: These two plots, originally appearing in [38], show the evolution of baryon number B for $M_{\Phi_1} = 10^{12}$ GeV and $\delta = m_e/m_\mu = 4.83 \times 10^{-3}$, in the two different regimes that produce a realistic value for the final baryon number of the universe, B_F. For the rescaled coupling strength $f = \sqrt{\lambda_{23} h_{23}} = 1.5 \times 10^{-3}$, as shown in the left panel, the effects of $2 \leftrightarrow 2$ lepton-number-changing processes are negligible and the final baryon-to-entropy ratio is the same as that initially produced by ϕ and $\overline{\phi}$ decays. For stronger coupling $f = 3.8 \times 10^{-2}$, as shown in the right panel, baryon number is initially overproduced, but $2 \leftrightarrow 2$ processes, which are stronger for stronger coupling, reduce B to an acceptable level by the time they freeze out. The left and right panels correspond respectively to the lower and upper parts of the 'ribbon' in figure 4.3.

The upshot of figure 4.3 is that Dirac leptogenesis can work even when the constraints from chapter III are taken into consideration, but that these constraints have important implications for the theory. Combined constraints from baryogenesis and neutrino physics make it extremely difficult simultaneously to obtain a realistic neutrino spectrum and obtain the correct baryon

number when $M_{\Phi_1} < 10^{10}$ GeV, which in turn requires a reheating temperature $T_R \gtrsim 10^{10}$ GeV. This means that the constraints from gravitino cosmology discussed in section 3.1, and especially the particularly stringent BBN constraints that arise when $m_{3/2} \lesssim 10^5$ GeV, are of genuine concern. Even for heavier heavy gravitino masses 10^5 GeV $\lesssim m_{3/2} \lesssim 10^8$ GeV, we must require either that m_{LSP} is light enough that the naive reheating temperature bound permits a reheating temperature above 10^{10} GeV (see figure 3.1), or else that the ratio $m_{3/2}/m_{LSP}$ be large enough that LSP annihilations are effective (figure 3.2). Barring some auxiliary mechanism (such as resonant leptogenesis) for increasing baryon number generation, then Dirac leptogenesis indeed appears to require heavy gravitinos. However, when $m_{3/2}$ is sufficiently large that $M_{\Phi_1} > 10^{10}$ GeV is permitted, CHDL succeeds in providing an explanation for the origin of the observed baryon asymmetry and neutrino mixings.

4.3 Satisfying the Flavor Constraints

The results in the previous section are enough to support the claim that Dirac leptogenesis works in theories with a heavy gravitino and sfermion masses heavy enough to evade the flavor violation constraints in 3.33. We now expand our analysis to the case where the sparticle spectrum is light. Doing so greatly increases the number of parameters in our theory, however: the flavor violation rates in (3.44) depend not only on the CHDL model parameters but also on the gaugino masses M_1 and M_2, the Higgs mass parameter μ, the ratio of Higgs VEVs $\tan\beta$, and the soft masses for the sleptons in the manner discussed in appendix A. In order to obtain precise predictions for the rates, these need to be specified. In our analysis, we choose the values $M_1 = 160$ GeV, $M_2 = 220$ GeV, $\mu = 260$ GeV, and $\tan\beta = 10$. As for the slepton soft

masses we will assume a common scale $m_s = 200$ GeV for them. We will also examine what effect varying m_s and $\tan\beta$ from these chosen values has on $BR(\mu \to e\gamma)$ and $BR(\tau \to \mu\gamma)$. We will assume that the high scale at which soft masses are universal is $M = 2 \times 10^{16}$ GeV, though the results are not particularly sensitive to this choice. We will continue to work in the large-$\langle F_\chi \rangle$ regime, and since the flavor violation rate is sensitive to $\langle F_\chi \rangle$, through the left-right slepton mixing term (3.40) (whereas baryon number is not), we need to specify it explicitly; we choose $\sqrt{\langle F_\chi \rangle} = 10^7$ GeV.

The results of our calculation are displayed in figure 4.5. In the left panel, we show exclusion contours in M_{Φ_1}-$\langle \chi \rangle$ space for $m_s = 200$ GeV. The areas below and to the right of the lower contour (the white region) are excluded by the experimental bound from $\mu \to e\gamma$. The contours associated with $\tau \to \mu\gamma$ are far weaker and do not eliminate any otherwise acceptable region of parameter space, and as such we do not display them here. We also include contours demarcating the region wherein baryogenesis can succeed. The exclusion contours take the form anticipated by equations (3.46) and (3.49), and things become problematic when M_{Φ_1} is large and when $\langle \chi \rangle$ is small, as predicted. As discussed in section 3.3.2, the lower contour represents the result of left-right sneutrino mixing contributions δm^2_{LR} and is primarily controlled by $\langle F_\chi \rangle$. When $\langle F_\chi \rangle$ is increased, the lower contour in figure 4.5 is raised, and we find that when $\sqrt{\langle F_\chi \rangle} \gtrsim 10^9$ GeV, the entirety of parameter space is excluded.

In the right panel, we also show how varying the universal scalar mass affects the branching ratio for $\mu \to e\gamma$, which reaches a maximum when m_s is around the weak scale. This is to be expected: when m_s is much larger than the weak scale both the slepton mass-squared eigenvalues and the flavor-violating terms scale like m_s^2 and the sneutrino and charged slepton mixing matrices asymptote to a constant value, while the branching ratio is still suppressed by

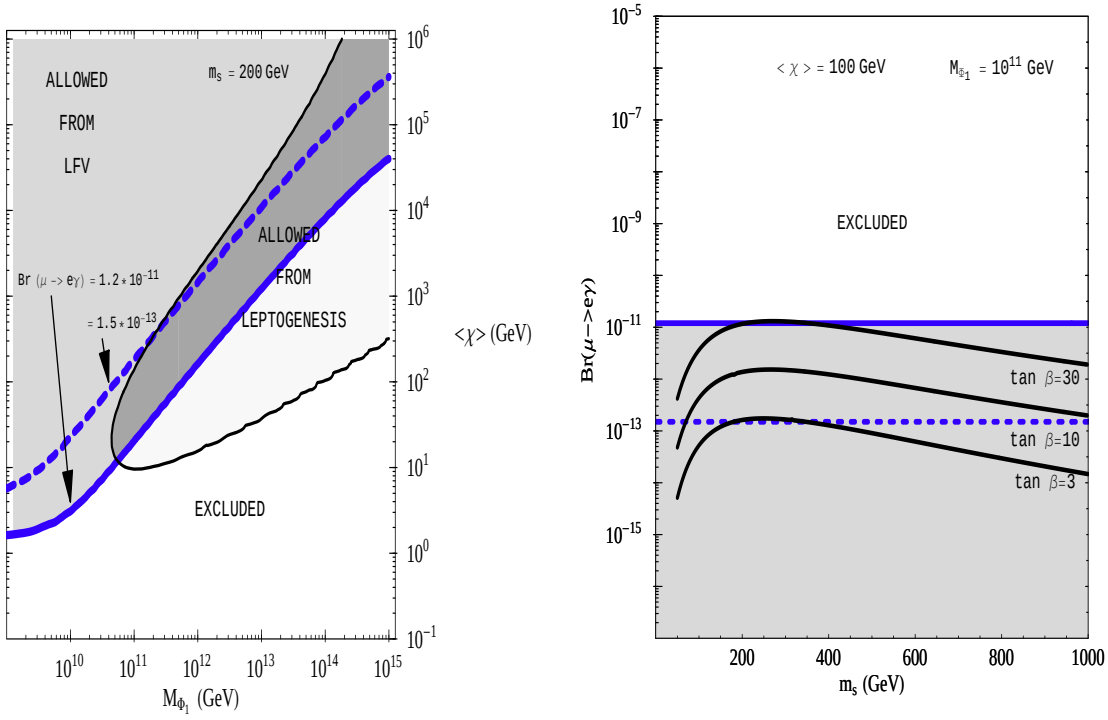

Figure 4.5: Exclusion plots [43] combining constraints from both leptogenesis and flavor violation in the process $\mu \to e\gamma$. The left-hand panel shows exclusion contours in M_{Φ_1}-$\langle\chi\rangle$ space for a universal scalar soft mass $m_s = 200$ GeV, with $\tan\beta = 10$; the right hand panel shows the variation of the branching ratio $BR(\mu \to e\gamma)$ with respect to m_s using $\tan\beta = 3, 10$ and 30. In both plots, we have taken $M_1 = 160$ GeV, $M_2 = 220$ GeV, and $\mu = 260$ GeV. We have also assigned the χ superfield an F-term VEV $\sqrt{\langle F_\chi\rangle} = 10^7$ GeV. Such a large VEV results in large trilinear couplings between Higgs fields and sneutrinos and therefore induces potentially sizeable mixings between left-handed and right-handed sneutrinos after electroweak symmetry breaking. In each plot, the thick solid contours represent the current experimental bound on the branching fraction (3.33); the dashed lines represent the expected future experimental bound of 1.5×10^{-13} from MEG. The thin solid contour in the left-hand panel delimits the region allowed by leptogenesis constraints.

the masses running in the loop; as m_s decreases below the weak scale, δm^2_{LL} and δm^2_{LL} go to zero and the slepton masses are dominated by flavor diagonal electroweak contributions. We also observe that, as in the supersymmetric see-saw case [83, 84], the flavor violation rate is quite sensitive to $\tan\beta$. The lepton-flavor-violating processes depicted in figure 3.5 involve a

$\tan\beta$-dependent chirality flip, and hence are augmented when $\tan\beta$ is large.

The important result we learn from figure 4.5 is that Dirac leptogenesis and the satisfaction of flavor violation constraints associated with weak-scale soft masses are indeed compatible—a conclusion that would not have been obvious a priori. There is substantial overlap between the region of parameter space within which CHDL is capable of reproducing the observed baryon asymmetry of the universe and the region in which lepton-sector flavor violation accords with experimental bounds. The improvement of these bounds from the next generation of lepton flavor-violation experiments will either confirm that some beyond-the-standard-model source of flavor violation exists or else rule out a substantial amount of the available parameter space. Thus these experiments will serve as an important check on Dirac leptogenesis models with slepton masses near the weak scale. We again emphasize that these tensions can be relaxed by elevating the universal sfermion mass parameter m_s. In theories like split supersymmetry where m_s is extremely large, flavor violation constraints can be ignored entirely.

4.4 The Resonant Escape

It is clear at this point that the primary model tension in Dirac leptogenesis is a conflict between the ceiling gravitino cosmology places on the reheating temperature after inflation and the condition that baryogenesis reproduce the WMAP η. In CHDL, this tension is overcome by arranging a large hierarchy among the Yukawa couplings to different sets of Φ and $\overline{\Phi}$. Couplings to the second lightest set, which are crucial to baryogenesis but otherwise have little physical effect, are large enough to produce substantial baryon number while couplings to the first remain small so as to avoid violating the out-of-equilibrium condition (2.13), which forces $\lambda_{1\alpha}$ and $h_{1\alpha}$ down when M_{Φ_1} is itself required to be small. There is, however, a second

possibility for avoiding this bound. It can be seen from the definition of the decay asymmetry ϵ in equation (2.7) that if $M_{\Phi_1} \approx M_{\Phi_2}$ (in other words, if $\delta \approx 1$), a resonance condition in is obtained. The perturbation theory we have used in calculating equation (2.7) is good as long as the separation of M_{Φ_1} and M_{Φ_2} is substantially greater than the value of the off-diagonal elements M_{ij} in the $\Phi - \overline{\Phi}$ mass mixing matrix induced at the one-loop level:

$$M_{ij} \sim g^* g' (M_{\Phi_1} + M_{\Phi_1}) I_{ij}, \tag{4.21}$$

where g_i and g'_j represent the appropriate λ and h, summed over the fermion family index, and I_{ij} is a numerical factor on the order of $1/16\pi^2$ from the loop integral. Thus for small λ and h, δ can be set very close to one and M_{ϕ_1} and M_{ϕ_2} may be very nearly degenerate. This allows for the possibility of resonant leptogenesis, as has been done in the Majorana leptogenesis case [40, 87, 88, 89], which can be invoked to generate a large baryon number in cases where the bounds on T_R are more severe. This possibility could potentially allow Dirac leptogenesis to work in scenarios such as PeV-scale supersymmetry, where is is otherwise all but ruled out.

CHAPTER V

EXTENSIONS OF THE MODEL

Thus far, we have shown that Dirac leptogenesis is a self-consistent model and that there exists a simple version of that model, CHDL, which can simultaneously reproduce both the observed baryon asymmetry of the universe and the observed neutrino spectrum without violating any additional constraints from astrophysical observations, flavor-violation experiments, etc. At this point, we turn to outline some of the theoretical motivations for CHDL and to examine some interesting possible extensions of the model, including a potential connection between the Dirac leptogenesis superpotential and the origin of the Higgs μ-term, a method for canceling $U(1)_N$ anomalies, and the possibility for right-handed sneutrino dark matter.

5.1 Origin of the μ-term

One of the advantages of Dirac leptogenesis is that unlike in Majorana leptogenesis, where they are essentially determined by the leptogenesis scale, neutrino masses are set not only by the masses M_{Φ_i} of the heavy fields, but also by the scalar VEV $\langle\chi\rangle$. This leaves us more freedom to choose the mass scale of the heavy fields, but can also be thought of as a drawback since we have

lost some predictiveness. For this reason, it would be interesting if some of these additional intermediate scales could be tied to other intermediate scales that arise in supersymmetric models. One interesting possibility involves making use of the $U(1)_N$ symmetry to link the dynamics of the χ field to the origin of the supersymmetric Higgs mass parameter μ. A simple way of doing this is to posit an interaction coupling the up- and down-type Higgs fields with χ and modifying equation (2.9) to

$$\mathcal{W}_{eff} \ni \frac{\lambda_{i\alpha} h^*_{i\beta}}{M_{\Phi_i}} \chi L_\beta H_u N_\alpha + Y_\chi \ \chi H_u H_d, \tag{5.1}$$

where Y_χ is an $\mathcal{O}(1)$ coupling constant. The Higgs superfields are now necessarily charged under the new hidden sector symmetry, and therefore the charge assignments given in table 2.1 must be revised. Furthermore, the rest of the standard model quark and lepton fields which couple to the Higgs fields must also be assigned nontrivial charges under this symmetry. This makes the task of arranging anomaly cancelation, arranging for gauge couplings to unify at some high scale, etc. vastly more difficult. In this situation, we have $\mu = Y_\chi \langle \chi \rangle$ and any observation or limits on Higgsino dark matter would directly constrain the VEV $\langle \chi \rangle$. (Split) supersymmetry might also give us some ideas as to how to relate the heavy fields Φ to the SUSY breaking scale.

5.2 Theoretical Motivations for CHDL

While the combination of small δ and antisymmetric h and λ which constitutes CHDL may yield the correct neutrino phenomenology, we have not offered any explanation of how such a situation might arise. Ideally, we would like to have a theoretical framework that would provide both the form of the superpotential required for Dirac leptogenesis (2.1) and the necessary flavor structure. We would like to take a moment and indicate one interesting possibility in which

simple assumptions enable us to reproduce the needed conditions, while at the same time reducing the number of new free parameters that must be introduced.

In many grand unified theories and models with non-Abelian flavor symmetries, the Yukawa matrices (and in general the flavor interactions) can be symmetric, antisymmetric, or both (see for example [71, 73, 74] and references therein). Operating in this paradigm, let us assume that the SM left-handed leptons have the same flavor charge as the heavy fields $\bar{\Phi}$, and the SM right-handed charged leptons have same flavor charge as the fields Φ. Upon breaking of the flavor symmetry, let us assume that the charged lepton Yukawa matrix is symmetric due to a symmetric flavon VEV configuration $\langle S_{\alpha\beta}\rangle$. The corresponding effective superpotential is

$$W \supset Y_l \ \frac{\langle S_{\alpha\beta}\rangle}{M_F} H_d L_\alpha e_\beta + Y_\Phi \ \langle S_{\alpha\beta}\rangle \bar{\Phi}_\alpha \Phi_\beta + \text{h.c.} \tag{5.2}$$

where Y_l and Y_Φ are dimensionless couplings, and α and β are flavor indices. The charged lepton Yukawa matrix $(y_l)_{\alpha\beta}$ and the mass matrix $(M_\Phi)_{\alpha\beta}$ of the heavy fields Φ would be both symmetric and proportional

$$(M_\Phi)_{\alpha\beta} = M_F \frac{Y_\Phi}{Y_l} \ (y_l)_{\alpha\beta} \tag{5.3}$$

This specific structure predicts exactly the mass spectrum for the ϕ fields in terms of the flavor scale M_F, which is at the origin of the intermediate scale required for successful thermal leptogenesis.

$$M_{\Phi_1} = m_e \frac{M_F}{v}, \quad M_{\Phi_2} = m_\mu \frac{M_F}{v} \ \text{ and } \ M_{\Phi_3} = m_\tau \frac{M_F}{v} \tag{5.4}$$

If the flavor scale is of the order of some GUT scale $M_F \sim 10^{16}$ GeV, we would then expect $M_{\Phi_1} \sim 10^{11}$ GeV, with $\delta = M_{\Phi_1}/M_{\Phi_2} = m_e/m_\mu = 4.83 \times 10^{-3}$ being a small parameter. Because this ratio is quite small and ϵ is approximately proportional to δ for small δ, one

might worry that this might doom baryogenesis. However, as indicated in the left panel of figure 3.4, $a_3^{max}(m_e/m_\mu) \approx 95$, so that a hierarchy between couplings to different sets of Φ and $\overline{\Phi}$ is permitted, and the result is that ϵ is only suppressed by an $\mathcal{O}(1)$ numerical factor. This is corroborated by the results of our numerical analysis, displayed in the left panel of figure 4.3 and explains why we chose to examine the $\delta = 4.83 \times 10^{-3}$ case.

Another related possibility that can help reduce the proliferation of scales (M_{Φ_1}, M_F, etc.) in the model is to link the supersymmetry-breaking scale M_{SUSY} to other physical scales in the theory by coupling the spurion field X responsible for supersymmetry breaking to the Φ_i and $\overline{\Phi}_i$ fields. If the spurion field is charged under the same symmetry (e.g. the $U(1)_N$ introduced in section 2.1), responsible for dictating the form of the superpotential in (2.1), one could arrange that

$$W \supset \frac{S_{\alpha\beta}}{M_F}\left(Y_l\ H_d L_\alpha e_\beta + Y_\Phi\ X\ \bar{\Phi}_\alpha \Phi_\beta\right) + \text{h.c.} \tag{5.5}$$

where again Y_l and Y_Φ are dimensionless couplings. Supersymmetry breaking effects can provide the field X with a VEV $\langle A_X \rangle \sim \left(m_{3/2} M_{Pl}\right)^{1/2}$, and upon flavor symmetry breaking we could get the effective superpotential

$$W_{eff} \supset (y_l)_{\alpha\beta}\ \left(H_d L_\alpha e_\beta + \sqrt{m_{3/2} M_{Pl}}\ \bar{\Phi}_\alpha \Phi_\beta\right) + \text{h.c.} \tag{5.6}$$

where we have assumed that the original constants $Y_l \sim Y_\Phi$. In this situation, for example with $m_{3/2} \sim 10^{10}$ GeV (a value sufficiently high as to avoid any model tensions associated with gravitino cosmology), the mass of the lightest Φ field would be $M_{\Phi_1} \sim 10^{11}$ GeV.

Now, let us also assume that the flavon VEV $\langle S_{\alpha\beta} \rangle$ is symmetric and that the coupling $\bar{\Phi} L \chi$ becomes antisymmetric upon flavor breaking, i.e. the superpotential can be written as

$$W \supset (y_l)^{sym}_{\alpha\beta} H_d L_\alpha e_\beta\ + (M_\Phi)^{sym}_{\alpha\beta} \bar{\Phi}_\alpha \Phi_\beta\ + \lambda_{\alpha\beta} N_\alpha \Phi_\beta H_u + h^{antisym}_{\alpha\beta} \bar{\Phi}_\alpha L_\beta \chi \tag{5.7}$$

where we have $\lambda_{\alpha\beta} \equiv \langle A^N_{\alpha\beta} \rangle$ and $h^{anti}_{\alpha\beta} \equiv \langle A^\chi_{\alpha\beta} \rangle$, with the flavon A^N acquiring an antisymmetric VEV configuration and with the VEV configuration of A^χ being arbitrary in flavor space. As alluded to above, this assumption is well-motivated from GUT considerations. While the flavor structure of A^χ is not important for our present purposes, in a specific model of flavor it would likely end up being some linear combination of symmetric and antisymmetric VEV configurations.

Let us see what the implications of these ingredients are for our model. In general, the charged lepton Yukawa matrix $(y_l)_{\alpha\beta}$ can be diagonalized by a biunitary transformation of the type

$$U^\dagger y_l V = y_l^{(diag)}, \tag{5.8}$$

but when y_l is symmetric, this biunitary transformation takes the simpler form

$$U^T y_l U = y_l^{(diag)}. \tag{5.9}$$

If $(M_\Phi) \propto (y_l)$, as in the setup described above (see equation (5.3)), then (M_Φ) will be diagonalized by the same transformation. When the mass matrices for the charged leptons and the $\phi - \overline{\phi}$ system are simultaneously diagonalized (that is, when we go to the charged lepton basis), λ and h transform as

$$\lambda' = U^T \lambda U \qquad h'^{\,anti} = U^T h^{anti} U. \tag{5.10}$$

Transformations of this type preserve the antisymmetry of h (and λ if also antisymmetric); thus in the charged lepton basis the matrix h remains antisymmetric and (M_Φ) is real and diagonal; this reproduces the neutrino mass matrix structure given in (3.29), in which the diagonal elements of h are zero and it is the smallness of δ that is responsible for the large mixing angles observed in the lepton mixing matrix U_{MNS}.

From a purely structural point of view, it will be noted that any matrix of the form

$$(M_\Phi) = Ay_l + BI_{3\times 3}, \tag{5.11}$$

where A and B are arbitrary constants and $I_{3\times 3}$ it the 3×3 identity matrix, can be diagonalized along with y_l. Thus $(M_\Phi) \propto y_l$ is not required for the transformation rules in (5.10) to hold. It follows from this that M_Φ may receive arbitrary diagonal contributions and $\delta = M_{\Phi_1}/M_{\Phi_2} = m_e/m_\mu$ is not required: δ can in principle take any value (as long as it is consistent with the observational bounds on the neutrino spectrum). This gives us a great deal more freedom to adjust model parameters without sacrificing the theoretical motivations we have developed here.

5.3 Sneutrino Dark Matter

5.3.1 Dark Matter in Dirac Leptogenesis

In order to be a viable dark matter candidate, the LSP must be stable (which follows automatically from R-parity conservation) and interact only weakly with the standard model fields. The most obvious choice is the lightest neutralino, $\tilde{N}_1$, and this choice is perfectly compatible with Dirac leptogenesis. The choice of model parameters outlined in section 4.3, for example, yields a stable, predominately bino LSP with a mass of around 160 GeV. In the context of PeV-scale supersymmetry or split supersymmetry, little changes except for that the LSP mass may be quite large, potentially facilitating the detection of energetic photons from cold dark matter annihilation at the galactic center by the next generation of Cherenkhov telescopes [90, 59, 60, 61]. We explore this possibility further in chapter VI.

Dirac leptogenesis does, however, offer a new potential candidate for LSP: the lightest right-handed sneutrino $\tilde{\nu_{R_1}}$. Unlike in Majorana leptogenesis scenarios, where right-handed sneutrino masses receive a supersymmetry-respecting contribution on the order of the leptogenesis scale, here they acquire mass only through soft terms, and since the $\tilde{\nu_R}$ are still singlets under the Standard Model $SU(3) \times SU(2) \times U(1)_Y$ gauge group, it is certainly possible that their soft masses are significantly smaller than—and perhaps of a different origin entirely from—those of the SM squarks and sleptons. Obtaining the observed value of Ω_{CDM} (3.4) with a pure right-handed sneutrino LSP is somewhat difficult, however, owing to the fact that the particle's interactions are so weak that annihilations are insufficient in reducing its relic density to the appropriate level. One solution to this problem is to make the LSP a mixture of left- and right-handed sneutrinos [91, 92] with mixing angle θ. The $SU(2)$ gauge interactions of the $\tilde{\nu}_L$ then permit the particles to annihilate efficiently enough to reduce Ω_{LSP} to an acceptable level, but (since the annihilation rate is suppressed by $\sin^4\theta$) not too efficiently. Here we will take another approach: we will gauge the global $U(1)_N$ symmetry we introduced in order to forbid Majorana masses for neutrinos and allow $\tilde{\nu_{R_1}}$ to annihilate down to an acceptable level via their interactions with $U(1)_N$ gauge bosons and gauginos.

Since neutralino dark matter still works in the context of Dirac leptogenesis, investigating the viability of another, more exotic CDM candidate might appear a somewhat frivolous endeavor. However, there is a compelling reason why sneutrino dark matter is of particular interest. It is a puzzling but well-documented fact about our universe that the dark matter abundance Ω_{CDM} (3.4) and the abundance of baryonic matter Ω_b (1.2) are roughly the same order, and in the standard picture of neutralino dark matter there is no known reason why this should be the case. However, in situations where an asymmetry develops in some globally

conserved quantum number under which the LSP is charged [93], it is possible to link these two quantities. Consider for a moment an effective theory containing both visible and hidden sectors, coupled only by dynamics at some high scale whose precise nature is unimportant. As the universe evolves down from the scale of the unifying dynamics, an asymmetry in this conserved quantum number develops between the two sectors. Suppose the hidden sector contains a number of light fields charged under the relevant global symmetry, each with charge Q_i and number density n_i, and their antiparticles, with charge $-Q_i$ and number density $\overline{n}_i$. The respective particle asymmetries A_{vis} and A_{hid} in the visible and hidden sectors, normalized with respect to the entropy density of the universe s, are then

$$A_{hid} = \sum_i \frac{Q_i(n_i - \overline{n}_i)}{s} = -A_{vis}. \tag{5.12}$$

If the hidden sector contains a massive, stable (or at least extraordinarily long-lived) particle a with mass m_a, this particle becomes a potential dark matter candidate. Let us assume that it also carries a sizeable fraction of this asymmetry $A_a = \alpha A_{hid}$ at the time of the freeze-out epoch and consider the limit where annihilation processes are efficient and conserve A_a. In this case, a and its conjugate a^* will annihilate rapidly with each other until only one or the other remains (even if the annihilation rate is quite large, a and a^* cannot annihilate further via such processes once either a or a^* is entirely depleted). The particles left over, having no conjugates with which to annihilate, become the dark matter, with a relic abundance

$$\Omega_{CDM} = \frac{m_a|A_a|s_0}{\rho_{crit,0}} = 2.236 \times 10^{10} m_a|A_a| \tag{5.13}$$

proportional to the asymmetry. An asymmetry on the order $|A_a| \sim 10^{-12} - 10^{-10}$ (depending on m_a) will thus replicate adequately the observed dark matter abundance. Since Majorana neutralinos are their own antiparticles, they must have vanishing $U(1)$ charge, and thus cannot

be used to link Ω_b and Ω_{CDM} in this manner. In contrast, when effective A-terms mixing left- and right-handed sneutrinos (such as those engendered by $\langle F_\chi \rangle$) are small, a right-handed sneutrino LSP in Dirac leptogenesis fits the bill perfectly: it is stable; it resides in a hidden sector essentially decoupled from the visible sector fields until well after the freeze-out epoch; and it is charged under the globally conserved quantum number $B-L$, under which the visible sector fields are also charged. The $B-L$ asymmetry between the hidden and visible sectors created during the decay of the heavy Φ_1 and $\overline{\Phi}_1$ superfields will also determine the relic density of $\tilde{\nu}_{R_1}$, and consequently the mechanism responsible for baryogenesis will also be responsible for generating Ω_{CDM}.

The simplified scenario resulting in (5.13) is somewhat difficult to realize in practice, however, due the fact that it simultaneously requires the net rate $\Gamma(a^*a \to X)$ (where X represents some unspecified final state comprising light, hidden-sector particles) for A_a-conserving annihilation processes to be efficient in reducing the dark matter abundance to a cosmologically acceptable level and the rate $\Gamma(aa \to X)$ for A_a-violating processes[1] to be negligibly small. The correct hierarchy of rates can be achieved in certain circumstances—in the presence of large s-channel contributions to $\Gamma(a^*a \to X)$ that have no t-channel equivalent, for example—and we will discuss these possibilities when we solve the Boltzmann equations for a right-handed sneutrino LSP. Before we do this, however, we turn briefly to address the modifications necessary for gauging the $U(1)_N$ symmetry, as this is the simplest and most convenient method of making L-conserving sneutrino annihilations efficient.

[1]We assume that CP-violation can be neglected and that the rates for the conjugate processes $aa \to X$ and $a^*a^* \to X^*$ are equivalent, hence $\Gamma_{aa} = \Gamma_{a^*a^*}$.

5.3.2 Extending the Hidden Sector

In order for our theory to be consistent, we must require that our new $U(1)_N$ symmetry is non-anomalous. With the field content listed in table 2.1, we find that there are no mixed $SU(2)_L^2\,U(1)_N$, $U(1)_Y^2 U(1)_N$ or $U(1)_Y\,U(1)_N^2$ anomalies, but that

$$(grav.)^2 U(1)_N: \quad 3(+1) + 3(-1) + 3(+1) + (-1) = 2 \tag{5.14}$$

$$U(1)_N^3: \quad 3(-1)^3 + 3(-1)^3 + 3(+1)^3 + (-1)^3 = 2 \tag{5.15}$$

are non-vanishing. It has been shown [94] that in the case where the only non-vanishing anomalies for a hidden sector $U(1)$ are $U(1)^3$ and $(grav.)^2 U(1)$ (i.e. mixed anomalies vanish), it is possible to cancel those anomalies by introducing new fields charged only under that $U(1)$. We therefore look for an appropriate expansion of the field content in the hidden sector that will cancel the above anomalies. The simplest way to cancel these anomalies would be to introduce two additional fields with the same charges as χ, but mixing between the fermionic components of these fields will ensure that at least one linear combination of them will be massless. Since these fields are necessarily odd under R-parity, this choice is problematic for dark matter and therefore must be excluded. The next simplest option[2] requires four new fields ξ_a $(a = 1, 2)$, φ, and ρ, the charge assignments for which are recorded in table 5.1 (the reason for the R-parity assignments therein will become evident in a moment). Adding these fields permits us to write down two new superpotential terms

$$W \supset \tilde{\mu}\,\chi\,\rho + \zeta_a\,\chi\,\xi_a\,\varphi, \tag{5.16}$$

where $\tilde{\mu}$ is a supersymmetric mass term and ζ_a $(a = 1, 2)$ are dimensionless couplings.

[2]Here we have assumed that all new superfields Ξ_i have $U(1)_N$ charges (not necessarily integral) $Q_i < 20$.

Field	$U(1)_L$	$U(1)_N$	$SU(2)$	$U(1)_Y$	P_M
ξ_a	0	-4	**1**	0	+1
φ	0	5	**1**	0	+1
ρ	0	1	**1**	0	+1

Table 5.1: This table shows the charge assignments for minimal set of additional superfields necessary to cancel the $U(1)_N^3$ and $(grav.)^2U(1)_N$ anomalies of the fields in table 2.1.

Since our aim is to arrange for $\tilde{\nu}_{R_1}$ to be the LSP, we must make sure that none of the new R-parity-odd fields in the hidden sector ends up massless and that the scalar component of χ can still acquire a VEV on the appropriate order to yield a realistic set of neutrino masses.

The scalar potential in the hidden sector, which contains both an F-term contribution from (5.16)

$$\begin{aligned} V_F &= |\tilde{\mu}\rho + \zeta_a\xi_a\varphi|^2 + |\tilde{\mu}\chi|^2 + |\zeta_a\chi\xi_a|^2 + (|\zeta_1|^2 + |\zeta_2|^2)|\chi\varphi|^2 \\ &= |\tilde{\mu}|^2|\rho|^2 + |\tilde{\mu}|^2|\chi|^2 + (\tilde{\mu}^*\zeta_a\xi_a\varphi\rho^* + h.c.) \\ &\quad + |\zeta_a|^2|\xi_a\varphi|^2 + |\zeta_a|^2|\xi_a\chi|^2 + (|\zeta_1|^2 + |\zeta_2|^2)|\chi\varphi|^2 \end{aligned} \tag{5.17}$$

and a D-term contribution from the new $U(1)_N$ gauge interaction given by

$$V_D = \frac{g^2}{2}\left(|\tilde{n}|^2 - |\tilde{\chi}|^2 + |\rho|^2 - 4|\xi_1|^2 - 4|\xi_2|^2 + 5|\varphi|^2\right)^2, \tag{5.18}$$

both of which serve to stabilize the fields. In addition, a contribution V_S will arise from soft supersymmetry-breaking Lagrangian. As for the fermions (which, as they are singlets under the Standard Model $SU(3) \times SU(2) \times U(1)_Y$, will be referred to as "neutralinos" from this point forward), their mass matrix, in the $\{\tilde{Z}', \tilde{\chi}, \tilde{\rho}, \tilde{\xi}_1, \tilde{\xi}_2, \tilde{\varphi}\}$ basis, is

$$\mathcal{M} = \begin{pmatrix} M' & -\sqrt{2}g\,\langle\chi\rangle & \sqrt{2}g\,\langle\rho\rangle & -4\sqrt{2}g\,\langle\xi_1\rangle & -4\sqrt{2}g\,\langle\xi_2\rangle & 5\sqrt{2}g\,\langle\varphi\rangle \\ \cdot & 0 & \tilde{\mu} & \zeta_1\langle\varphi\rangle & \zeta_2\langle\varphi\rangle & \zeta_1\langle\xi_1\rangle + \zeta_2\langle\xi_2\rangle \\ \cdot & \cdot & 0 & 0 & 0 & 0 \\ \cdot & \cdot & \cdot & 0 & 0 & \zeta_1\langle\chi\rangle \\ \cdot & \cdot & \cdot & \cdot & 0 & \zeta_2\langle\chi\rangle \\ \cdot & \cdot & \cdot & \cdot & \cdot & 0 \end{pmatrix}. \tag{5.19}$$

As long as the scalar components of χ and ξ_1 receive nonzero VEVs, all the physical mass eigenstates resulting from this matrix will be massive, as desired. This can be engineered by introducing tachyonic soft squared-masses for these fields in V_S. Assuming the other scalars ξ_2, φ, and ρ receive large, positive squared-masses the effective (tree-level) potential for the remaining fields becomes

$$V = (|\tilde{\mu}|^2 + m_\chi^2)|\chi|^2 + (|\tilde{\mu}|^2 + m_{\xi_1}^2)|\xi_1|^2 + |\zeta_1|^2|\xi_1|^2|\chi|^2 + \frac{g^2}{2}\left(|\chi|^2 + 4|\xi_1|^2\right)^2. \tag{5.20}$$

It should be noted that since the $U(1)_N$ charges of χ and ξ_1 are of the same sign, there are no problems with D-flat directions.

Minimizing the potential in equation (5.20), we find that in terms of the quantities

$$\tilde{m}_\chi^2 \equiv -(|\tilde{\mu}|^2 + m_\chi^2), \qquad \tilde{m}_{\xi_1}^2 \equiv -(|\tilde{\mu}|^2 + m_{\xi_1}^2), \tag{5.21}$$

the expectation values for ξ_1 and χ are given by

$$\begin{aligned} \left\langle |\xi_1|^2 \right\rangle &= \frac{(4\,\tilde{m}_\chi^2 - \tilde{m}_{\xi_1}^2)}{3|\zeta_1|^2} \\ \left\langle |\chi|^2 \right\rangle &= \frac{1}{g^2}\left[\tilde{m}_\chi^2 - \frac{(g^2 + |\zeta_1|^2)}{3|\zeta_1|^2}(4\,\tilde{m}_\chi^2 - \tilde{m}_{\xi_1}^2)\right]. \end{aligned} \tag{5.22}$$

Equation 5.21 implies that in order to avoid having to introduce fine-tunings among the hidden sector mass parameters $\tilde{\mu}$, m_χ, and m_{ξ_1}, these parameters ought to be of roughly the same magnitude as the physical scales $\langle\chi\rangle$ and $\langle\xi_1\rangle$ (if $\tilde{\mu}$ were small or vanishing, some of the hidden-sector neutralinos would be too light). In order for both VEVs to be positive, we must have

$$\left(\frac{4\alpha - 1}{\alpha}\right) \;<\; \frac{\tilde{m}_{\xi_1}^2}{\tilde{m}_\chi^2} \;<\; 4, \tag{5.23}$$

where $\alpha = (g^2 + |\zeta_1|^2)/3|\zeta_1|^2 \geq 1/3$. Both of these inequalities must be satisfied in order for ξ_1

and χ to receive VEVs.[3] As for Z' vector boson associated with the gauged $U(1)_N$ symmetry, when the symmetry is broken by the VEVs of ξ_1 and χ, it acquires a mass

$$M_{Z'}^2 = 2g^2 \left(\langle \chi \rangle^2 + 16 \langle \xi_1 \rangle^2 \right). \tag{5.24}$$

Thus all fields in the hidden sector acquire masses on the order of the scales $\langle \chi \rangle$ and $\langle \xi_a \rangle$ or larger, and the lightest right-handed sneutrino remains a viable LSP candidate. In fact, it should be pointed out that gauging $U(1)_N$ introduces new D-term contributions to the physical mass of the right-handed sneutrino which serve to drive down $m_{\tilde{\nu}_R}^2$. The total result, including soft terms, but assuming that left-right mixing through effective A-terms is negligible, is

$$m_{\tilde{\nu}_R}^2 = m_{\tilde{\nu}_R,soft}^2 - g^2 \left(\left\langle |\chi|^2 \right\rangle + 4 \left\langle |\xi_1|^2 \right\rangle + 4 \left\langle |\xi_2|^2 \right\rangle - \left\langle |\rho|^2 \right\rangle - 5 \left\langle |\varphi|^2 \right\rangle \right), \tag{5.25}$$

and since $m_{\tilde{\nu}_R,soft}^2$ is essentially a free parameter, it can be tuned freely so that the mass of the lightest right-handed sneutrino is small, as desired. It should also be pointed out that this setup results in a VEV for the scalar field χ without necessarily producing an F-term VEV $\langle \chi \rangle$, and hence the right-handed fields are indeed part of the hidden sector, as is required for relating Ω_{CDM} and Ω_b in the manner discussed above.

5.3.3 Evolution of the Dark Matter Abundance

In order to ascertain the dark matter abundance in any nontrivial model, it is necessary to solve the coupled system of Boltzmann equations that govern the evolution of $\tilde{\nu}_{R_1}$ and $\tilde{\nu}_{R_1}^*$ during the freeze-out epoch. The two-to-two processes which yield the leading contribution to

[3] Equation (5.23) also indicates why the matter parity assignments given in table 5.1 were chosen as they were. If ξ_1 and φ were taken to be odd under matter parity, the coupling constant ζ_1 in (5.16) would vanish, sending $\alpha \to \infty$.

dark matter annihilation include both processes of the form $\tilde{\nu}_{R_1}\tilde{\nu}^*_{R_1} \to X$, which contribute to washout of the dark matter density but do not alter $L_{\tilde{\nu}_R}$ (which is equivalent to $(B-L)_{\tilde{\nu}_R}$, since electroweak sphalerons do not affect the fields in the hidden sector and hence B and L are separately conserved there), and those of the form $\tilde{\nu}_{R_1}\tilde{\nu}_{R_1} \to X$, which contribute to the depletion of both Ω_{CDM} and $(B-L)_{\tilde{\nu}_R}$. Let us call the net rate for the former processes $\Gamma_{\tilde{\nu}\tilde{\nu}^*}$ and the rate for the latter $\Gamma_{\tilde{\nu}\tilde{\nu}}$. The Boltzmann equations can be written either in terms of $\tilde{\nu}_{R_1}$ and $\tilde{\nu}^*_{R_1}$ or, equivalently, for the dark matter abundance $Y_{DM} = Y_{\tilde{\nu}_R} + Y_{\tilde{\nu}^*_R}$ and the lepton number asymmetry $L_{\tilde{\nu}_R}$. We find these equations to be

$$\frac{dL_{\tilde{\nu}_R}}{dz} = -\frac{2z}{H(m_{\tilde{\nu}_R})s}\Gamma_{aa}\left(L_{\tilde{\nu}_R}Y_{DM} - \frac{g_{*s}}{2}(L_{hid} - L_{\tilde{\nu}_R})Y^{eq^2}_{DM}\right) \tag{5.26}$$

$$\frac{dY_{DM}}{dz} = \frac{z}{2H(m_{\tilde{\nu}_R})s}\left[\Gamma^{(+)}\left(Y^{eq\ 2}_{DM} - Y^2_{DM}\right) + \Gamma^{(-)}\ L^2_{\tilde{\nu}_R}\right], \tag{5.27}$$

where $z \equiv m_{\tilde{\nu}_R}/T$, and $H(m_{\nu_R})$ is the Hubble parameter at scale $T = m_{\tilde{\nu}_R}$. The effective rates

$$\Gamma_{\tilde{\nu}\tilde{\nu}} = \gamma_{\tilde{\nu}\tilde{\nu}}/Y^{eq^2}_{DM} \qquad \text{and} \qquad \Gamma^{\pm} = \Gamma_{\tilde{\nu}\tilde{\nu}^*} \pm 2\Gamma_{\tilde{\nu}\tilde{\nu}} = 4(\gamma_{\tilde{\nu}\tilde{\nu}^*} \pm \gamma_{\tilde{\nu}\tilde{\nu}})/Y^{eq^2}_{DM} \tag{5.28}$$

are determined from the reaction densities $\gamma_{\tilde{\nu}\tilde{\nu}}$ and $\gamma_{\tilde{\nu}\tilde{\nu}^*}$, defined as in (4.16), which are in turn determined from the reduced cross sections $\hat{\sigma}(\tilde{\nu}\tilde{\nu})$ and $\hat{\sigma}(\tilde{\nu}\tilde{\nu}^*)$, a calculation of which is included in appendix D. Given in terms of $r = \sqrt{1 - 4m^2_{\tilde{\nu}_R}/s}$, $x_{\chi_1} = s/m^2_{\chi_1}$, $x_n = s/m^2_{\tilde{\nu}_R}$, and $A = (2x_n^{-1} - 2x_\chi^{-1} - 1)$, the results are

$$\hat{\sigma}(\tilde{\nu}\tilde{\nu}) = \frac{g^4}{\pi}\frac{1}{x_\chi}\left(\frac{1}{A}\ln\left(\frac{A+r}{A-r}\right)^2 - 4\frac{r}{r^2-A^2}\right) \tag{5.29}$$

$$\begin{aligned}\hat{\sigma}(\tilde{\nu}\tilde{\nu}^*) = {} & \frac{g^4}{12\pi}\left(\frac{s}{s-M_Z^2}\right)^2 r^3 + \frac{g^4}{4\pi}\left(-4r + A\ln\left(\frac{A+r}{A-r}\right)^2\right) \\ & + \frac{g^4}{8\pi}\left(\frac{s}{s-M_Z^2}\right)\left(2Ar + \frac{(r^2-A^2)}{2}\ln\left(\frac{A+r}{A-r}\right)^2\right).\end{aligned} \tag{5.30}$$

We note that the equations (5.26 - 5.27) are actually quite general and can be applied in a variety of scenarios in which an asymmetry in some globally conserved quantum number between visible and hidden sectors (or between a pair of distinct hidden sectors) develops during the evolution of the universe and the dark matter particle is located in the hidden sector and charged under that quantum number.[4] Any model-dependent aspects of the Boltzmann evolution enter only in the relevant annihilation rates, in the mass of the dark matter particle, and in the input value for L_{hid}.

Before we move on to address the Boltzmann system (5.26 - 5.27) numerically, we note that in certain limiting cases it reduces to a particularly simple form. One of these cases is the trivial case, where $L_{\tilde{\nu}_R} = 0$ and we are left with the single equation

$$\frac{dY_{DM}}{dt} = \frac{1}{2s}\Gamma^{(+)} \left({Y_{DM}^{eq}}^2 - Y_{DM}^2 \right) \tag{5.31}$$

whose solution is the standard one for a dark matter abundance. Perhaps more interesting is the case where $\Gamma_{RR} \simeq 0$ and $L_{\tilde{\nu}_R} \neq 0$. In this case, $L_{\tilde{\nu}_R}$ is fixed and the equation for the dark matter abundance becomes

$$\frac{dY_{DM}}{dt} = \frac{1}{2s}\Gamma_{RR^c} \left[\left({Y_{DM}^{eq}}^2 - Y_{DM}^2 \right) + L_{\tilde{\nu}_R}^2 \right]. \tag{5.32}$$

This represents the case described in [93]. As mentioned above, this situation is somewhat difficult to engineer for a right-handed sneutrino in Dirac leptogenesis, but in the next section we will provide one or two possible schemes in which it can be realized.

5.3.4 Numerical Results and Discussion

[4] In special cases, such as that of a nearly-degenerate LSP-NLSP pair in supersymmetric models, the Boltzmann equations must be modified [95], but we do not consider such exceptions here.

We are now ready to solve the Boltzmann system given in (5.26) - (5.27) for right-handed sneutrino dark matter in supersymmetric Dirac leptogenesis. Obtaining the correct dark matter abundance in this scenario is not difficult, provided the $U(1)_N$ gauge coupling constant is on the appropriate order, but generating Ω_{CDM} via the mechanism described in equation (5.13) and thereby forging a link between this quantity the observed baryon asymmetry of the universe is not. The reason for this is that the $L_{\tilde{\nu}}$–conserving and $L_{\tilde{\nu}}$–violating rates determined respectively by (5.29) and (5.30) are naturally on the same order unless a hierarchy exists among the masses of the virtual particles exchanged. The Z' mass given in (5.24) depends primarily on the hidden-sector gauge coupling g, the soft squared masses m_χ^2 and $m_{\xi_1}^2$, and the supersymmetric mass parameter $\tilde{\mu}$ (which ought to be of roughly the same order as the aforementioned soft masses if we wish to avoid fine-tuning); while the neutralino mass and $U(1)_N$ gaugino content depend primarily on M'. Thus unless a hierarchy between scalar and gaugino masses emerges naturally from supersymmetry breaking in which gaugino masses are far heavier than scalar masses, $\hat{\sigma}(\tilde{\nu}\tilde{\nu})$ and $\hat{\sigma}(\tilde{\nu}\tilde{\nu}^*)$ will be of roughly the same order.

This leads us to choose between the two less-than-ideal outcomes depicted in figure 5.1. Here, we show the evolution of Y_{DM} and $L_{\tilde{\nu}_R}$ in two representative regimes: one in which the $U(1)_N$ gauge coupling g is comparatively strong ($g = 9.5 \times 10^{-2}$), and one in which it is weaker ($g = 5 \times 10^{-4}$). In each case, we have maintained the relations $g\langle\chi\rangle = 200$ GeV, $g\langle\xi_1\rangle = 100$ GeV, $\tilde{\mu} = 500$ GeV, and $\zeta_1/g = \zeta_2/g = 1$ and set $M' = 200$ GeV. By examining figure 4.5, one can verify that these parameter choices are both compatible with successful leptogenesis, given an appropriate choice of M_{Φ_1}. The mass of the lightest right-handed sneutrino is taken to be $m_{\tilde{\nu}_R} = 150$ GeV, which makes it the LSP. In the strong coupling case presented in the left panel, $\Gamma(\tilde{\nu}\tilde{\nu})$ and $\Gamma(\tilde{\nu}\tilde{\nu}^*)$ are large enough to reduce the sneutrino abundance to a level in accord

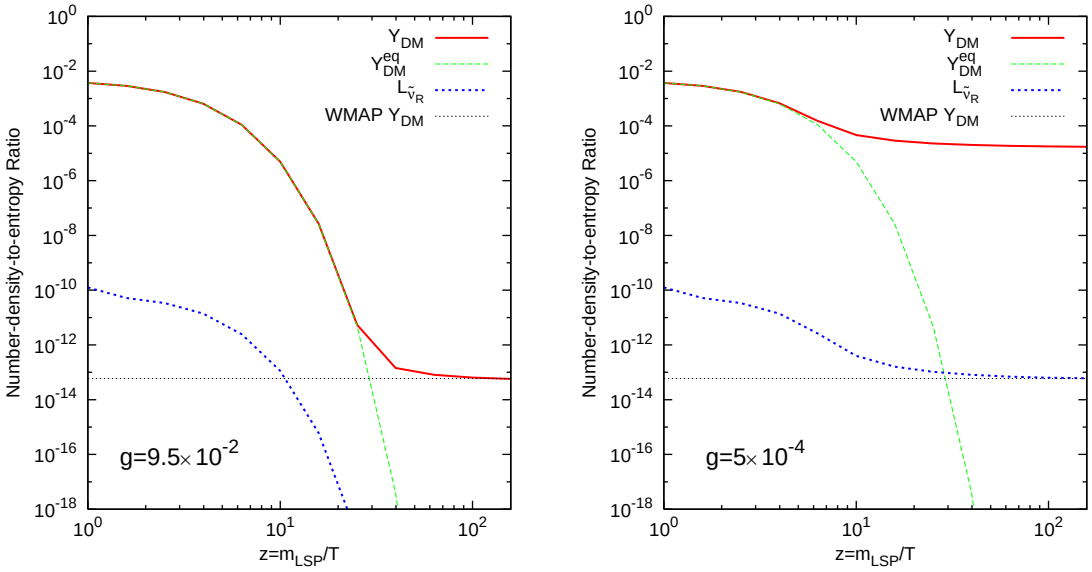

Figure 5.1: Here, we illustrate the two representative cases for sneutrino dark matter in Dirac neutrinogenesis. In each case, we have set $M' = 200$ GeV and $m_{\tilde{\nu}_R} = 150$ GeV and maintained the relations $g\langle\chi\rangle = 200$ GeV, $g\langle\xi_1\rangle = 100$ GeV, $\tilde{\mu} = 500$ GeV, and $\zeta_1/g = \zeta_2/g = 1$. The left panel depicts the situation where the $U(1)_N$ gauge coupling is reasonably strong ($g = 9.5\times10^{-}2$). As the universe evolves, T decreases and $z \to \infty$. Here, the number-density-to-entropy-density ratio Y_{DM} of a right-handed sneutrino LSP reproduces the WMAP prediction (the horizontal dashed line), but the lepton number $L_{\tilde{\nu}_R}$ stored in right-handed sneutrinos is washed out almost entirely and all connection between the dark matter abundance and the observed baryon number of the universe is lost. The right panel shows the situation where the gauge coupling is small $g = 5 \times 10^{-4}$. Here, washout is insignificant and $L_{\tilde{\nu}_R}$ persists essentially unchanged from its initial value until present time, but sneutrino annihilations are inefficient in reducing the dark matter abundance to an acceptable level. The equilibrium right-handed sneutrino abundance Y^{eq}_{DM} is also shown in each panel for reference. It should be emphasized that in the left panel, the correct dark matter relic density is obtained, and that while Ω_{CDM} and Ω_b are not tied to one another, there is no problem for cosmology, whereas the situation depicted in the right panel is cosmologically unacceptable, since dark matter is overproduced.

with the WMAP bound, but $\Gamma(\tilde{\nu}\tilde{\nu})$ is so large that L_{ν_R} is washed out rapidly and essentially completely. Here, the model is successful in yielding the correct dark matter abundance, but

all connection between L_{ν_R} (and therefore B) and Ω_{CDM} is lost, and the evolution of Y_{DM} reduces to the standard situation described in equation (5.31). In the right panel, for weak gauge coupling, things go even more awry: $\Gamma(\tilde{\nu}\tilde{\nu})$ is small enough to prevent the washout of L_{ν_R}, but since $\Gamma(\tilde{\nu}\tilde{\nu}^*)$ is likewise small, sneutrino annihilations are inefficient in reducing the right-handed sneutrino abundance to an acceptable level—in essence, we recover (literally, in the $g \to 0$ limit) the situation we had before gauging the $U(1)_N$ symmetry. The message here is that the right-handed sneutrino in Dirac leptogenesis is a viable dark matter candidate, but that a relationship between Ω_{CDM} and Ω_b does not emerge naturally from the Dirac leptogenesis framework, as least in the simple model presented here.

Arranging a hierarchy between $\Gamma_{\tilde{\nu}\tilde{\nu}^*}$ and $\Gamma_{\tilde{\nu}\tilde{\nu}}$, though difficult, is not altogether impossible, however. As mentioned previously, one way this could occur is if a hierarchy between gaugino and scalar masses, in which the former were much higher than the latter, emerged naturally from the supersymmetry-breaking mechanism, but this is not easy to achieve. The most promising model would appear to be gaugino mediation [96, 97, 98, 99], in which the supersymmetry-braking sector is confined to a "source" brane parallel to our own, visible brane in a five-dimensional bulk. The matter fields of the theory (the MSSM fields, right-handed neutrino superfields, etc.) are confined to the visible brane, while gauge supermultiplets are allowed to propagate in the bulk. As a result, one can arrange for a loop-splitting between gaugino and scalar soft masses, but it is difficult to arrange for this splitting to be as pronounced as we require. We thus turn to alternative methods for engineering a scale-separation between $\Gamma_{\tilde{\nu}\tilde{\nu}^c}$ and $\Gamma_{\tilde{\nu}\tilde{\nu}}$.

A second way of arranging a hierarchy between these rates is to further expand the field content of the theory and introduce additional light scalars into which the $\tilde{\nu}_{R_1}$ can decay. This

can be arranged by introducing pairs of vector-like superfields ω_i and $\overline{\omega}_i$ that are even under matter parity (so $\tilde{\nu}_{R_1}$ is still the LSP) and charged only under $U(1)_N$. Charges Q_i are assigned them so that the form of the Dirac leptogenesis superpotential (2.1) and its hidden sector extension (5.16) are unchanged,[5] save for the addition of mass terms

$$W \supset M_{\omega_i} \omega_i \overline{\omega}_i. \tag{5.33}$$

Since the new superfields come in vector-like pairs, they will not spoil anomaly cancelation. The soft Lagrangian will also contain new soft mass terms for the scalar fields in ω_i and $\overline{\omega}_i$, and a partial cancelation between a tachyonic soft squared mass and the contribution $M_{\omega_i}^2$ from the superpotential can arrange for the scalar components of ω_i and $\overline{\omega}_i$ (also denoted ω_i and $\overline{\omega}_i$) to remain light compared to $\tilde{\nu}_{R_1}$, while their fermionic superpartner $\tilde{\omega}_i$ and $\tilde{\overline{\omega}}_i$ acquire masses $M_{\omega_i} \geq m_{\nu_R}$. In this case, an additional s-channel contribution to the right-handed sneutrino annihilation cross-section via the diagrams in figure 5.2 will arise, which has no t-channel equivalent. The contribution to $\hat{\sigma}(\tilde{\nu}\tilde{\nu}^*)$ from each pair of ω_i and $\overline{\omega}_i$ is

$$\Delta\hat{\sigma}(\tilde{\nu}\tilde{\nu}^*) = \frac{g^4 Q_i^2}{8\pi} \left(\frac{s}{s - M_{Z'}^2} \right)^2 r, \tag{5.34}$$

where r is defined as above equation (5.29), and if the number of additional scalars is large (or the charges assigned them are large), the L_{ν_R}–conserving rate can be increased without simultaneously increasing the L_{ν_R}–violating one.

While this idea seems promising, it turns out to be difficult to realize in practice. The reason is that the reduced cross-section (5.34) for sneutrino annihilations, like the usual expressions (5.29) and (5.30), is proportional to g^4, and g must be kept small in order to prevent $L_{\tilde{\nu}_R}$

[5] This is trivial and can be easily accomplished, for example, by giving assigning fractional charges to all the ω_i and $\overline{\omega}_i$.

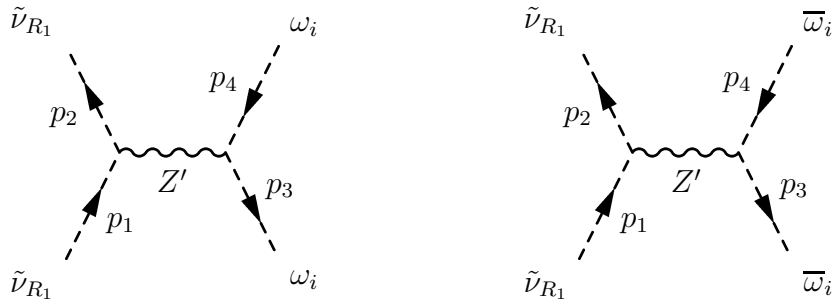

Figure 5.2: The additional contribution to $\hat{\sigma}(\tilde{\nu}\tilde{\nu}^*)$ that arises in the right-handed sneutrino dark matter scenario in the presence of additional light scalars ω_i and $\overline{\omega}_j$ charged under the $U(1)_N$ gauge group.

from being washed out. This substantially hinders the effectiveness of this new contribution at reducing Y_{DM}: one must either add a very large number N_ω of vector-like superfield pairs to the theory—or else make the charges Q_i of the new superfields inordinately large—in order to achieve the desired hierarchy between $\Gamma_{\tilde{\nu}\tilde{\nu}}$ and $\Gamma_{\tilde{\nu}\tilde{\nu}^*}$. In figure 5.3, we show the effect on Y_{DM} of adding light scalars to the theory. Here, we have chosen the (quite large) value $|Q| = 20$ for the magnitude of the charge assigned to all $\omega_i - \overline{\omega}_i$ pairs and set $g = 1.5 \times 10^{-3}$ (the input values for all other relevant model parameters are the same as in figure 5.1). To compensate for the smallness of the $g^4 \sim 10^{-12}$ prefactor in (5.34), an additional $N_\omega \sim 10^5$ field pairs are needed. This is highly unmotivated, to say nothing of the havoc such fields would wreak on the RGE running of the $U(1)_N$ coupling in terms of the prospects for gauge coupling unification, etc., and therefore not a particularly compelling solution to the rate correlation problem.

The possibility that Dirac leptogenesis presents for right-handed sneutrino dark matter is indeed an interesting one, and as the left panel of figure 5.1, one that can reproduce the observed value of Ω_{CDM}. The disappointment is that it it a challenge to tie the size of the observed dark matter matter abundance to the baryon number of the universe through their mutual connection

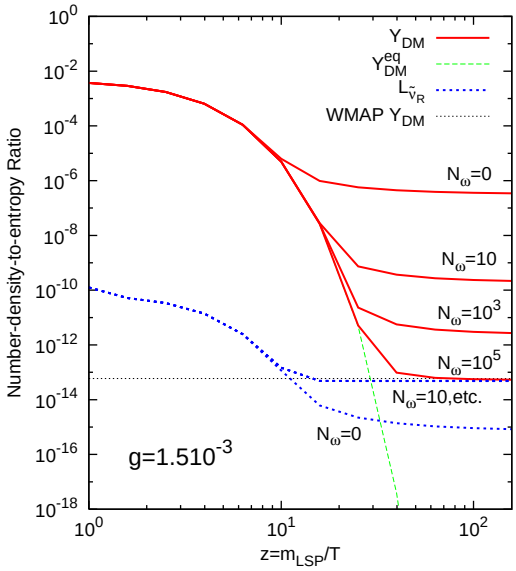

Figure 5.3: The effect on the dark matter number-density-to-entropy-density ratio Y_{DM} of adding a number N_ω of vector-like pairs of light scalars to the theory. Here, all such scalars have $U(1)_N$ have charge magnitude $|Q| = 20$, and results are shown for $N_\omega = 10,\ 10^3$, and 10^5, as well as for the unmodified case $N_\omega = 0$. As in the right panel of figure 5.1, $M' = 200$ GeV and $m_{\tilde{\nu}_R} = 150$ GeV and maintained the relations $g\langle\chi\rangle = 200$ GeV, $g\langle\xi_1\rangle = 100$ GeV, $\tilde{\mu} = 500$ GeV, $\zeta_1/g = \zeta_2/g = 1$, and $g = 1.5 \times 10^{-3}$. The addition of light scalars does not affect the lepton number $L_{\tilde{\nu}_R}$ stored in right-handed sneutrinos appreciably for $N_\omega \geq 10$. Because g is small, an inordinately large number of light fields are required in order to achieve a situation in which $L_{\tilde{\nu}_R}$ dictates the size of Y_{DM}. When N_ω is large enough, L_{ν_R} creates an effective "floor" for the dark matter abundance (corresponding to a dark matter abundance consisting only of $\tilde{\nu_R}$ and none of its antiparticle $\tilde{\nu_R}^*$).

to L_{ν_R} in a way where the former is driven automatically driven by the latter to the correct value. It should again be emphasized that the link between L_{ν_R} the baryon number B of the universe is forged at the leptogenesis scale $M_{\Phi_1} \gtrsim 10^{10}$ GeV. The two asymmetries do not communicate with one another during the CDM freeze-out epoch, and the the rate $\Gamma_{\tilde{\nu}\tilde{\nu}}$ does not alter the total lepton number L_{hid} stored in the hidden sector, but rather transfers the portion of that asymmetry L_{ν_R} stored in right-handed sneutrinos to right-handed neutrinos

(or perhaps light scalars). Thus the dynamics associated with $\Gamma_{\tilde{\nu}\tilde{\nu}}$ have no effect on B, and baryogenesis proceeds unhindered no matter to what degree L_{ν_R} is washed out. Thus sneutrino dark matter is perfectly compatible with baryogenesis in Dirac leptogenesis scenarios. However, it is generally not feasible to forge a connection between Ω_{CDM} and the relic abundance Ω_b of baryonic matter through a mutual connection to $L_{\tilde{\nu}}$: a correlation between the the rates $\Gamma^*_{\tilde{\nu}\tilde{\nu}}$ and $\Gamma_{\tilde{\nu}\tilde{\nu}}$ for $L_{\tilde{\nu}}$–conserving and $L_{\tilde{\nu}}$–violating processes makes it difficult simultaneously to preserve $L_{\tilde{\nu}}$ while reducing $Y_{\tilde{\nu}}$ to an acceptable level.

CHAPTER VI

INDIRECT DARK MATTER DETECTION

6.1 Detecting Heavy Neutralino Annihilations

In section 5.3, it was mentioned that Dirac leptogenesis is compatible with neutralino dark matter. Furthermore, it strongly prefers a heavy gravitino and hence is quite naturally compatible with split supersymmetry, which is associated with a particular, characteristic type of neutralino dark matter. In theories where anomaly mediation is responsible for the generation of gaugino masses M_1, M_2, and M_3 (as is the case in split supersymmetry), the neutralino spectrum is dictated by the β-functions of the Standard Model gauge groups by equation (3.14). In the MSSM, to lowest order, the relationship is

$$M_3 \simeq 3M_1 \simeq 9M_2, \tag{6.1}$$

which implies that if a neutralino is in fact the LSP, it will be predominately either Wino or (depending on the value of μ), Higgsino. We now turn to investigate the possibility for detecting such an LSP experimentally.

In section 3.1, we discussed the relic abundance of such an LSP, which had both a thermal component Ω_{LSP}^{Th} given by equation (3.5) or (3.6) for a majority Wino or Higgsino LSP, re-

spectively, and in theories with a heavy gravitino, an additional, nonthermal component Ω_{LSP}^{NT}, given by equations (3.9) - (3.11), resulting from gravitino decay. As is evident from figure 3.1, the thermal component places an upper bound on m_{LSP}, which turns out in each case to be [61]

$$m_{LSP} \leq 2.5 \text{ TeV} \quad \text{(for Wino)} \tag{6.2}$$

$$m_{LSP} \leq 1.2 \text{ TeV} \quad \text{(for Higgsino)}. \tag{6.3}$$

The direct detection of a heavy Wino or Higgsino LSP with a mass $m_{LSP} \gg M_W$ GeV is all but precluded at present and planned facilities [59] for all but the most unnaturally peaked halo models, and the cross-section for the annihilation of such an LSP into positrons is too small to yield a detectable signal. The only promising detection method available is to search for high-energy photons resulting from LSP annihilation processes in the galactic halo, and in particular $\tilde{N}_1\tilde{N}_1 \to \gamma\gamma$ and $\tilde{N}_1\tilde{N}_1 \to \gamma Z$. Expressions for the cross-sections for these processes have been computed [100], and in the limit where m_{LSP} is much larger than the weak scale, $\sigma v(\tilde{N}_1\tilde{N}_1 \to \gamma\gamma)$ and $\sigma v(\tilde{N}_1\tilde{N}_1 \to Z\gamma)$ take the asymptotic forms

$$\sigma v(\tilde{W}\tilde{W} \to \gamma\gamma) \simeq 4.0 \times 10^{-27} \text{ cm}^3\text{s}^{-1} \tag{6.4}$$

$$\sigma v(\tilde{W}\tilde{W} \to Z\gamma) \simeq 9.0 \times 10^{-27} \text{ cm}^3\text{s}^{-1}, \tag{6.5}$$

for a Wino LSP, and

$$\sigma v(\tilde{H}\tilde{H} \to \gamma\gamma) \simeq 9.0 \times 10^{-29} \text{ cm}^3\text{s}^{-1} \tag{6.6}$$

$$\sigma v(\tilde{H}\tilde{H} \to Z\gamma) \simeq 2.0 \times 10^{-29} \text{ cm}^3\text{s}^{-1}. \tag{6.7}$$

for a Higgsino LSP. The reason these processes are of particular interest is that the photons produced thereby are effectively monoenergetic, with respective energies

$$E_\gamma = m_{LSP} \qquad \text{and} \qquad E_\gamma = m_{LSP}\left(1 - \frac{m_Z^2}{4m_{LSP}^2}\right). \tag{6.8}$$

The detection of either signal would be compelling evidence for heavy Wino or Higgsino dark matter, since effectively monoenergetic signals at TeV-scale energies tend to originate in particle physics processes (rather than astrophysical ones); taken together, they would serve as a distinctive signal—were it possible to resolve them. Our aim here is to analyze the prospects for the detection of this signal at present and future γ-ray telescopes.

Calculation of the observed integral flux Φ of γ-rays from the galactic center is complicated somewhat by our ignorance of the precise density distribution profile $\rho(\psi, s)$ of dark matter in the galactic halo (expressed here as a function of line-of-sight distance s and the angle ψ away from the galactic center). The density profile enters into the integral flux (usually expressed in $\mathrm{cm}^{-2}s^{-1}$) through the expression

$$\Phi = [\sigma v(\tilde{N}_1\tilde{N}_1 \to X)] \times N_\gamma(X)\frac{1}{4\pi m_{LSP}^2}\int_L \rho^2(\psi, s)\, ds. \tag{6.9}$$

where $N_\gamma(X)$ is the number of photons in the final state X, and the integral is evaluated along the line of sight. It should be noted that $\rho(\psi, s)$ is proportional to the LSP mass and the asymptotic expressions for $\sigma v(\tilde{N}_1\tilde{N}_1 \to X)$ given in (6.4 - 6.7) are independent of m_{LSP}, so Φ is actually insensitive to m_{LSP} when $m_{LSP} \gg M_W$. Since the density integral is essentially independent of the particle physics, it is common practice to abstract it by defining the quantity

$$J(\psi) \equiv \frac{1}{8.5\ \mathrm{kpc}}\left(\frac{1}{0.3\ \mathrm{GeV}}\right)^2 \int_L \rho^2(\psi, s) ds. \tag{6.10}$$

While for an ideal detector, one would be interested only in $J(0)$, the value for the line passing directly through the galactic center, a real detector will receive incoming photons originating over some finite slice of solid angle. The relevant quantity is angular acceptance $\Delta\Omega$, the solid angle from which the detector actively receives light, which for a given detector may be adjusted as desired over a window ranging from a detector's angular resolution to its field of view. Thus

	α	β	γ	R
Isothermal profiles	2.0	2.0	0	3.5
NFW	1.0	3.0	1.0	20.0
Moore et al.	1.5	3.5	1.5	28.0

Table 6.1: The defining parameters α, β, γ and R (see equation 6.11) for the halo models we examine. R is given in kpc.

instead of $J(0)$, the quantity of interest is $\langle J(\psi)\rangle_{\Delta\Omega}$, the average of $J(\psi)$ over $\Delta\Omega$.

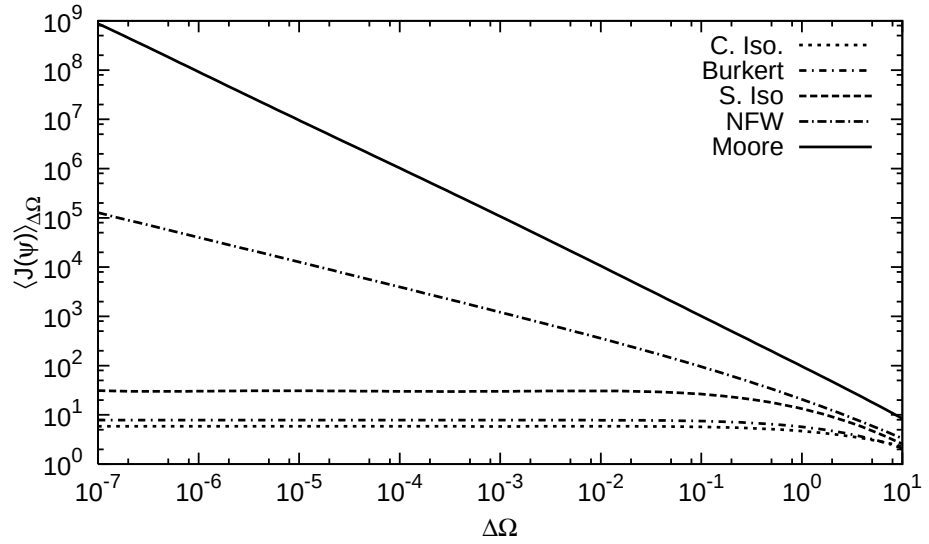

Figure 6.1: $\langle J(\psi)\rangle_{\Delta\Omega}$ (the line-of-sight integral through the halo density squared, averaged over the angular acceptance $\Delta\Omega$) vs. $\Delta\Omega$ for several halo profiles: smooth isothermal, clumpy isothermal, Burkert, NFW, and Moore et al. Taken from [61].

We have yet to discuss the dark matter density profile itself, and since its precise shape is not well known, we will survey a representative sample of profiles rather than focussing on any single model. In general, these profiles are derived from numerical simulations [101], and most take the form

$$\rho(r) = \frac{\rho_0}{(r/R)^\gamma(1+(r/R)^\alpha)^{(\beta-\gamma)/\alpha}}, \tag{6.11}$$

where the density function ρ has been expressed in terms of the radius r away from the galactic

center and spherical symmetry is assumed. The three power-law indices α, β, and γ, along with the characteristic radius R, serve to define a given model. The models we examine here include the relatively cuspy Moore et al. profile [102], the widely used Navarro-Frenk-White profile [103], and a pair of isothermal models [104], one with a smooth density distribution, the other with a greater level of dark matter clumping.[1] We list the α, β, γ, and R assignments which define each of these models in table 6.1. We also include in our survey one model in which the dark matter profile is not defined by equation (6.11), but by the relation

$$\rho(r) = \frac{\rho_0 r_0^3}{(r + r_0)(r^2 + r_0^2)}, \tag{6.12}$$

where r_0 and ρ_0 are fiducial distance and density parameters, respecively (for our galaxy, $r_0 \approx 11.7$ kpc and $\rho_0 \approx 0.34$ GeV cm^{-3} [105]). This model was originally proposed by Burkert et al. [106] and is also in use. Figure 6.1 shows the relationship between $\langle J(\psi) \rangle_{\Delta\Omega}$ and $\Delta\Omega$ that results from plugging each of the distributions we consider into equation (6.10). As one would expect, the more sharply peaked distributions (the Moore and Burkert profiles), in which the dark matter is concentrated near the galactic center, yield a higher value of $\langle J(\psi) \rangle_{\Delta\Omega}$ for a given $\Delta\Omega$, and therefore to a higher γ-ray flux.[2] It should be noted that different profiles can lead to drastically different values for Φ. The situation is further complicated by the possibility that the presence of a massive black hole at the center of the galaxy could significantly modify the dark matter abundance near the galactic center and lead to a pronounced density spike [108],

[1] The dark matter density given by the Moore et al. profile is divergent for $r \ll R$ and is assumed to be truncated at some small radius r_t. Here, we choose $r_t = 10^{-5}$ kpc.

[2] It is worth noting that the models surveyed here assume a spherically symmetric halo, and it has been observed [107] that triaxial models provide a better fit to the cosmological density profiles obtained in cosmological simulations than do spherical ones. The corrections introduced by taking such considerations into account would amount to an $\mathcal{O}(1)$ factor in the overall result, and since it will soon become evident that detection prospects will be an issue of orders of magnitude rather than numerical prefactors, such prefactors do not significantly compromise our results.

though there is some debate over the precise effect such a black hole would have, and for this reason we will not consider such modifications here.

6.2 Outlook at Present and Planned Facilities

Now that we have calculated Φ (up to considerations involving the shape of the dark matter profile), let us turn to a discussion of the performance of present and future γ-ray telescopes. These can be divided into two main types: satellite facilities, which detect incoming photons directly, and atmospheric Cherenkhov detectors (ACTs), which operate by observing showers of Cherenkhov light that result when high-energy γ-rays enter the Earth's upper atmosphere. In assessing performance and the ability to register a discovery at the 5σ level, the relevant detector attributes to consider are angular acceptance $\Delta\Omega$, energy resolution $\Delta E/E$, and effective collection area A_{eff}. In table 6.2, we provide a list of these performance specifics for a variety of present and planned experiments, including both satellite facilities and ACTs, as well as those for two hypothetical facilities (one a satellite detector, one an ACT) slightly more advanced than any currently planned facility of its kind, which we will use when examining the potential for observation of heavy Wino or Higgsino dark matter annihilation at the next generation of γ-ray experiments.

The advantage of satellite facilities, examples of which include EGRET and the soon-to-be-launched pair-production telescope GLAST [113], is that they can have excellent angular resolution and energy resolution. The field of view for GLAST, for example, will be on the order of a steradian, its angular resolution in the TeV range will be $\sim 0.1^\circ$, and its energy resolution will be on the order of 4%. The background seen by such facilities is—as one might expect—

Facility	$A_{\rm eff}$ (cm^2)	$\Delta E/E$	$\Delta\Omega_{\rm min}$ (sr)	$\epsilon_{\rm had}$
WHIPPLE (Arizona)	3.5×10^8	30%	1.88×10^{-5}	1.0
GRANITE II (Arizona)	5×10^8	20%	9.56×10^{-6}	1.0
HESS (Namibia)	7×10^8	15%	9.56×10^{-6}	0.25
VERITAS (Arizona)	1×10^9	15%	3.83×10^{-7}	0.25
EGRET (Satellite)	1×10^4	15%	3.22×10^{-2}	-
GLAST (Satellite)	1.5×10^4	4%	9.56×10^{-6}	-
Next generation ACT	1.5×10^9	10%	1.00×10^{-7}	0.25
Next generation PPT	2×10^4	1%	1.00×10^{-7}	-

Table 6.2: The performance parameters [109, 110] for current and planned γ-ray telescopes, including both ACTs (WHIPPLE, GRANITE II, HESS [111], and VERITAS [112]) and space telescopes (EGRET and GLAST [113]). Also included are the parameters corresponding to the hypothetical "next generation" atmospheric Cerenkhov telescope (ACT) and space-based pair production telescope (PPT) we have used in our analysis.

the actual diffuse gamma-ray background, which is not currently well known for energies in the TeV range. The best that can currently be done is to make the assumption that the power law spectrum from EGRET data (good up to ~ 100 GeV) can be extrapolated to higher energies [114, 115, 116]. In doing this, one obtains a power-law of the form

$$\frac{dn_{\rm BG}}{d\Omega dE} = N_0 \left(\frac{E}{1\ {\rm GeV}}\right)^{-\alpha} {\rm cm}^{-2}{\rm s}^{-1}{\rm GeV}^{-1}{\rm sr}^{-1}, \tag{6.13}$$

with a numerical prefactor N_0 on the order of 10^{-6} cm^2 and an exponent α somewhere between 2.0 and 2.5 (following [115], we take α to be 2.1 and N_0 to be 7.32×10^6). Since GLAST will provide a great deal of information about the diffuse γ-ray background at high energies, we can expect the uncertainties in α and N_0 to be dramatically reduced once it begins taking data. In figure 6.2, we plot the γ-ray flux that a satellite detector would observe as a function of angular acceptance along with the γ-ray background flux (for several different values of $\Delta E/E$) determined from equation (6.2). It should be noted that while the signal contours are largely

independent of m_{LSP}, the background contours are not: the power-law relation (6.13) indicates that with positive α, background flux will decrease with increasing m_{LSP}. Thus the results given for m_{LSP} near the bounds (6.2) - (6.3) represent the best-case scenario. One can see that for the sharply peaked Moore et al. and NFW profiles, the signal exceeds the background significantly when $\Delta\Omega$ is small.

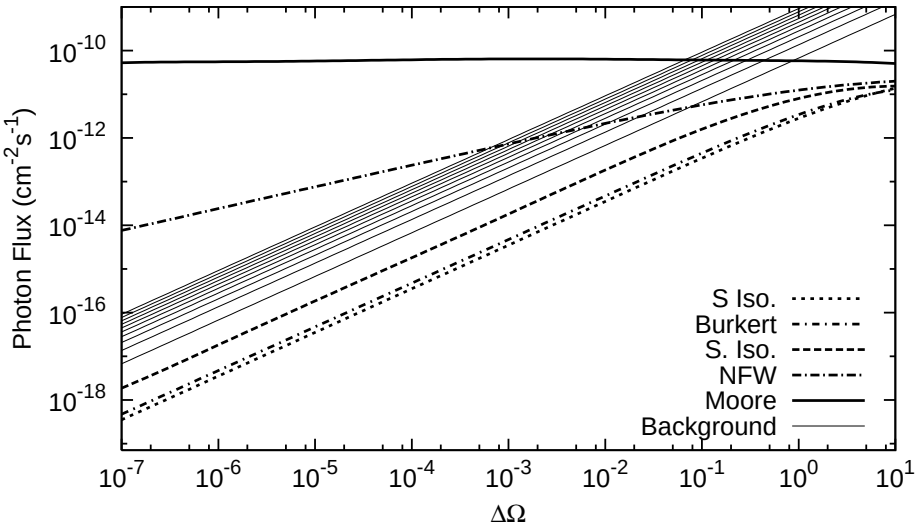

Figure 6.2: The expected flux from the annihilation of a heavy Wino LSP, as a function of $\Delta\Omega$, that would be detected by a satellite detector aimed at the galactic center [61]. Also included is the anticipated background flux for a 2.3 TeV Wino at such a detector for different values of detector energy resolution, ranging from $\Delta E/E = 50\%$ (top line) to $\Delta E/E = 5\%$ (bottom line). It should be noted that the spread in the signal is smaller than the width of the energy bin. From this, it is apparent that for the NFW and Moore et al. profiles, the prospects for detection increase with better angular resolution (decreasing $\Delta\Omega$). For a Higgsino LSP, the resulting curves are similar, but the signal is two orders of magnitude lower. The background flux for a 1.1 TeV Higgsino also is increased by a factor of ~ 10 over the 2.3 TeV Wino case, owing to the lower energy of the signal photons.

Satellite detectors do have a major drawback, however, which is that they are limited by collection area constraints. In order for the signal registered at any detector to be interpreted

as a discovery, not only must the significance level (the ratio of N_S, the total number of signal photons registered, to $\sqrt{N_{\rm BG}}$, where $N_{\rm BG}$ is the total number of background photons registered) exceed 5σ, but the total number of detected photons must exceed 25, the threshold below which Poisson statistics give an equivalent confidence limit[3]. These requirements, when written explicitly in terms of $A_{\rm eff}$, $\Delta E/E$, $\Delta\Omega$, and observation time, are

$$(.68)^2 \left(\frac{\Phi(\Delta\Omega)\sqrt{A_{\rm eff} t}}{\sqrt{\Phi_{\rm BG}(\Delta\Omega, \Delta E/E, \epsilon_{\rm had})}} \right) \geq 5 \tag{6.14}$$

$$\Phi(\Delta\Omega) A_{\rm eff} t \geq 25. \tag{6.15}$$

Since the effective collection area is constrained by the size of the telescope itself, present satellite facilities tend to have an $A_{\rm eff}$ on the order of 10^4 cm^2, and dramatic (i.e. order of magnitude) improvements on this in the future are unlikely. The consequences of this are shown in figure 6.3. Here, contours of total event count at an advanced, hypothetical space telescope (the "Next generation PPT" from table 6.2) are presented alongside significance plots corresponding to each of the halo models discussed above for both a Wino and Higgsino LSP, assuming an exposure time of 10^7 s. While obtaining the necessary $N_S/\sqrt{N_{\rm BG}}$ to claim a discovery is difficult in itself (and only achieved for the Moore et al. profile), the most troublesome issue is that none of the halo profiles surveyed yield enough events to register a 5σ discovery. Space telescopes are thus "event-count-limited," and as a result, the prospects for detecting monoenergetic photons from heavy LSP decay at such facilities (including GLAST) are quite dim.

For ACTs, the situation is quite different. This class of detector (examples of which include the HESS [111] and VERITAS [112] arrays) operates by observing showers of Cherenkhov light

[3]While the likelihood of random statistical fluctuations at the 5σ level increases with improved energy resolution, these can be differentiated from a true signal by requiring the signal to be consistent over multiple trials.

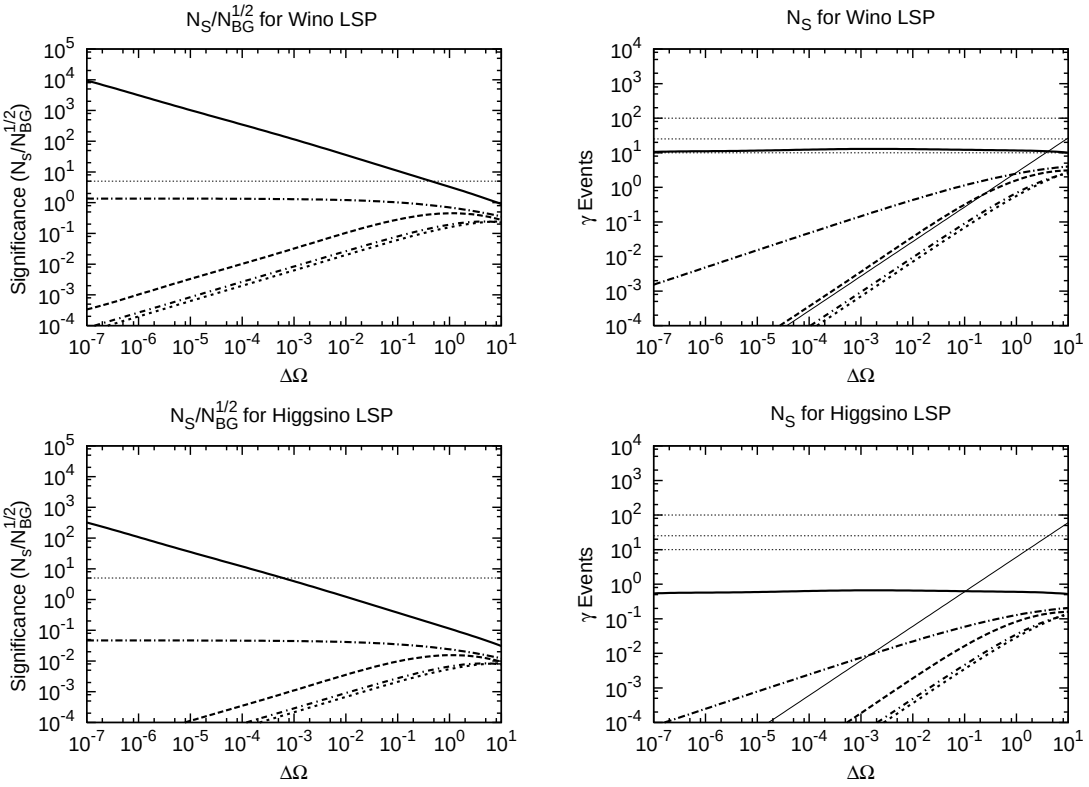

Figure 6.3: The ratio of $N_{\text{signal}}/\sqrt{N_{\text{background}}}$ (left panels) and total number of photons (right panels) collected by a generic space telescope with an effective area of 2×10^4 cm^2 and an energy resolution of 1%, over a range of $\Delta\Omega$, after 10^7 s (about 1/3 of an active year) of viewing time, and for both Wino (top panels) and Higgsino LSP (bottom panels) [61]. See figure 6.4 caption for the halo model key. The threshold for 5σ discovery has been included for reference in the significance graphs, and contours corresponding to 10, 25, and 100 events have been included in the event count graphs. It can be seen here that for such a space telescope, no halo profile is capable of producing the 25 events necessary for detection, and that only for the Moore et al. profile is the significance criterion even achieved.

produced by the incidence of high-energy γ-rays on the Earth's upper atmosphere. The general scale of the effective area associated with an ACT is determined by the area of the Cherenkhov light pool on the ground, which is $\sim 5 \times 10^8$ cm^2. Compared to the aforementioned A_{eff} scale associated with satellite facilities, this is enormous. The trade-off is that uncertainties in

reconstructing the energy of the primary photon from the properties of the radiation shower place limits on the energy resolution, which is generally quite poor: a single imaging detector can achieve $\Delta E/E \simeq 30 - 40\%$; an array of parallel detectors, $10 - 15\%$). Furthermore, the background "seen" by an ACT is not simply the diffuse γ-ray background. Any event that precipitates a similar Cherenkhov cascade is a source of background, and the primary background at such detectors actually comes from cosmic-ray protons, electrons, etc., which dominate over the diffuse gamma-ray background by an order or two of magnitude. It is possible to discriminate between hadronic showers and those initiated by γ-rays to a degree due to the shape of the cascade and to the time spread of the light pulse, but showers initiated by leptons (predominately electrons) are indistinguishable from γ-ray cascades. These backgrounds are higher than those seen by satellite detectors, though their spectra are reliably known up to 5 TeV . The power-law behavior [117] for hadronic and leptonic background events is given by

$$\frac{dN_{\rm had}}{dEd\Omega} = 1.0 \cdot 10^{-2} \epsilon_{\rm had} \left(\frac{E_0}{1\ {\rm GeV}} \right)^{-2.7}\ {\rm cm}^{-2}{\rm s}^{-1}\ {\rm GeV}^{-1}{\rm sr}^{-1} \tag{6.16}$$

$$\frac{dN_{\rm e^-}}{dEd\Omega} = 6.9 \cdot 10^{-2} \left(\frac{E_0}{1\ {\rm GeV}} \right)^{-3.3}\ {\rm cm}^{-2}{\rm s}^{-1}\ {\rm GeV}^{-1}{\rm sr}^{-1}, \tag{6.17}$$

where we have replaced N_0 and the power-law index α with their explicit numerical values. Here, $\epsilon_{\rm had}$ is a dimensionless coefficient which represents the detector's ability to reject hadronic events based on the criteria discussed above, normalized to the performance of the WHIPPLE telescope (for which $\epsilon_{\rm had} = 1$).[4] The total observed background is the sum of the hadronic and leptonic backgrounds given in equations (6.16) and (6.17). Improvements in hadronic rejection techniques have since lowered $\epsilon_{\rm had}$ to around 0.25 at instruments such as HESS and VERITAS. Once again, both hardonic and leptonic contributions to the overall Cherenkhov background

[4]In other words, $\epsilon_{\rm had} = 0.5$ indicates a hadronic rejection twice as good as WHIPPLE's and $\epsilon_{\rm had} = 0$ indicates perfect hadronic rejection and a background consisting purely of leptonic and photonic events.

scale with photon energy by a power law with a negative index; hence the best-case scenario will involve an LSP mass near the upper bounds given in equations (6.2) - (6.3).

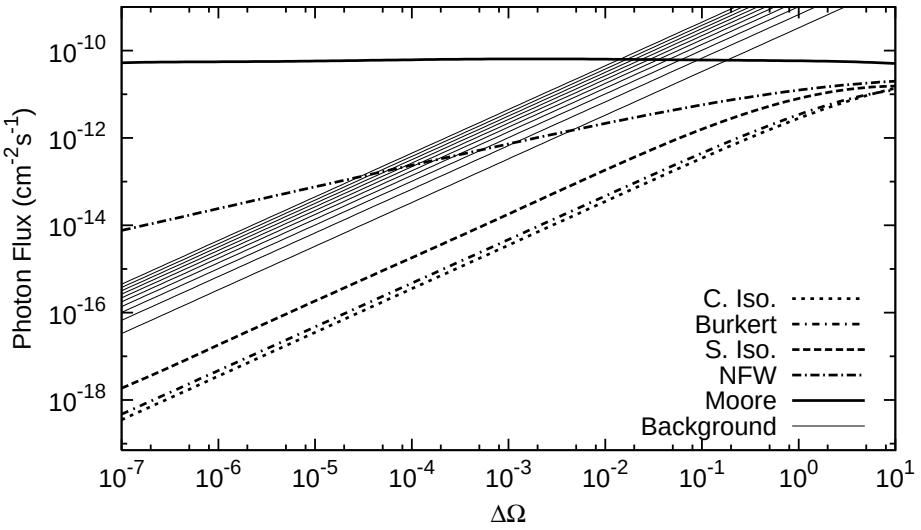

Figure 6.4: The expected flux from the annihilation of a heavy Wino LSP, as a function of $\Delta\Omega$, that would be detected by a Cherenkhov detector aimed at the galactic center [61]. Also included is the anticipated background flux from a 2.3 TeV Wino at such a detector for different values of detector energy resolution, ranging from $\Delta E/E = 50\%$ (top line) to $\Delta E/E = 5\%$ (bottom line). It should be noted that the spread in the signal is smaller than the width of the energy bin. From this, it is apparent that for the NFW and Moore et al. profiles, the prospects for detection increase with better angular resolution (decreasing $\Delta\Omega$). For a 1.1 TeV Higgsino LSP, the resulting curves are similar, but the signal is two orders of magnitude lower. The background flux is also increased by a factor of ~ 10 over the 2.3 TeV Wino case, owing to the lower energy of the signal photons

In figure 6.4, we plot the γ-ray flux observed at an ACT a function of angular acceptance for the different halo profiles surveyed along with background flux contours corresponding to different values of $\Delta E/E$. The background is larger than in the space telescope case (compare figure 6.2) by about a factor of ten. In figure 6.5, we plot both the signal significance and total number of signal photons recorded at an advanced, hypothetical Cherenkhov array (the "Next

generation ACT" from table 6.2) for a range of $\Delta\Omega$ and an exposure time of 10^7 s, in both the Wino and Higgsino LSP cases. It is evident from this plot that despite the larger background flux and poorer energy resolution, ACTs are far more likely to detect a statistically significant γ-ray signal from heavy LSP annihilation than are satellite detectors, due to their far greater effective area (on the order of $10^8 - 10^9$ cm^2). Since HESS and VERITAS have an angular resolution (and hence minimum $\Delta\Omega$) on the order of 10^{-7} steradians, detection would not be difficult if the dark matter density conformed to one of the more cuspy profiles. However, since the field of view (and hence maximum $\Delta\Omega$) for an ACT is generally around 10^{-3} steradians, the less sharply peaked dark matter distributions (the Burkert profile and the two isothermal models) will still be out of reach. It is an interesting coincidence that the NFW profile nearly demarcates the line between detection and non-detection for presently operational facilities: if the actual dark matter distribution is cuspier than that given by the NFW profile, the γ-ray signature of Wino dark matter in PeV-scale split supersymmetry should be detectable at the next generation of ACTs; if the actual profile is much less sharply peaked, it is unlikely that such a signal would ever be detectable at an ACT.

As mentioned previously, the energy resolution for ACTs is limited by considerations related to event reconstruction from the Cherenkhov cascade [109], and hence comparatively poor—around $10 - 15\%$. Due to this intrinsic limitation, it is unlikely that future facilities will offer significant (i.e. order of magnitude) improvements in $\Delta E/E$ over present facilities. Since the splitting between the $\gamma\gamma$ and $Z\gamma$ lines (6.8) requires $\Delta E/E = 0.8\%$ when $m_{LSP} = 500$ GeV, and even more precision for LSP masses near the upper bound (6.2) - (6.3) from thermal generation, the prospects for differentiating these lines at an ACT are effectively nil. Still, even if these lines cannot be resolved, the detection of any effectively monoenergetic photon signal in the

TeV range would serve as provocative evidence for heavy neutralino dark matter.

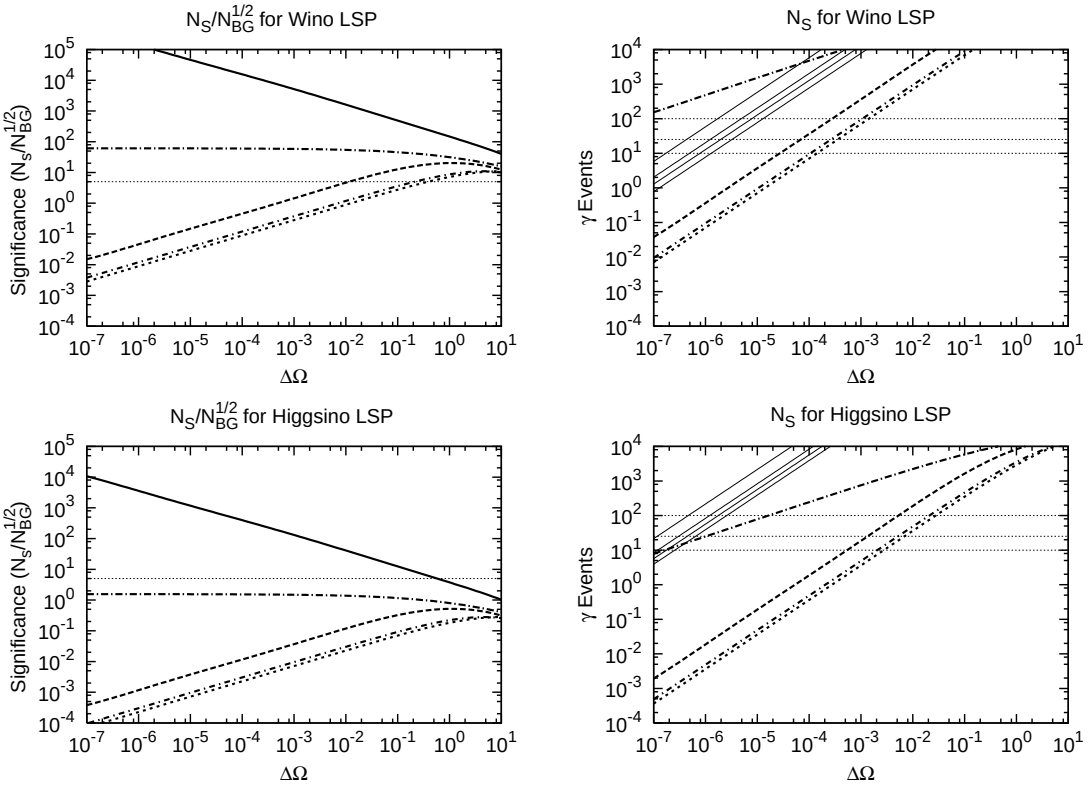

Figure 6.5: The ratio of $N_{\text{signal}}/\sqrt{N_{\text{background}}}$ (left panels) and total number of photons (right panels) collected by a generic Cherenkhov array with an effective area of 1.5×10^9 cm^2 and an energy resolution of 10%, over a range of $\Delta\Omega$, after 10^7 s (about 1/3 of an active year) of viewing time, and for both a heavy Wino (top panels) and Higgsino LSP (bottom panels) [61]. See figure 6.4 caption for the halo model key. The threshold for 5σ discovery has been included for reference in the significance graphs, and contours corresponding to 10, 25, and 100 events have been included in the event count graphs. It can be seen here that there are real prospects for detection with such a Cherenkhov detector, provided that the galactic CDM halo density resembles the NFW or Moore et al. profiles.

Thus far, we have examined the potential for detecting energetic photons from heavy neutralino annihilation at current and planned facilities (or hypothetical ones only slightly more advanced than these), but it is also interesting to take a slightly different point of view and ask

exactly what attributes would a detector need in order to conclusively register a discovery. We have seen that the effective area A_{eff} and angular acceptance $\Delta\Omega$ (which may be tuned to any value between the detector's angular resolution and its field of view) are the most important of the detector attributes in the detection of the LSP annihilation signal, so these variables will become our primary focus. In figure 6.6, we plot contours from both the significance constraint (6.14) and the event count constraint (6.15) in A_{eff}-$\Delta\Omega$ space. Since the significance contours are slightly different for space telescopes and ACTs, which "see" different backgrounds, we present a separate plot for each case (an ACT in the top left panel; a space telescope in the bottom left). The results shown are for 10^7 s of viewing time, and the $\Delta E/E$ values used in computing the significance limits are those given in table 6.2 for the GLAST telescope and the VERITAS array. The horizontal bars correspond to GLAST and VERITAS themselves, and the endpoints thereof are given by each detector's respective angular resolution and field of view. The criterion for discovery at either of these facilities is that for a given halo model, both the 5σ and $N_s \geq 25$ contours for that model lie below the corresponding bar. From this figure, it is once again evident that GLAST, primarily due to its small effective area, would be unable to detect CDM from PeV-scale split supersymmetry at all, while VERITAS would have far better hopes for detection.

Perhaps more importantly, however, it is also evident from figure 6.6 what improvements in detector area, angular resolution, and field of view would be necessary in order to detect a signal in even the least sharply peaked of halo models surveyed. A space telescope would need about a factor of 5 increase in A_{eff} in order to register the requisite number of signal events to claim a discovery even in the Moore et al. profile case, and this would require significant feats of engineering. The best way to increase the effective area of an ACT is to add further telescopes

to the detector array, but the increase in A_{eff} from each such addition is merely additive. We see from figure 6.6 that in order to register a discovery when the dark matter profile is one of the those included in our survey less sharply peaked than the NFW profile (the Burkert profile and the two isothermals), a factor of ten increase in A_{eff} is required (one could theoretically also widen the field of view by several orders of magnitude, but in practice this is even more difficult). This is in principle possible, of course, if one adds enough telescopes to a given array, but this is an expensive and somewhat impractical proposition.

In addition to the discrete lines arising from to $\tilde{N}_1\tilde{N}_1 \rightarrow \gamma\gamma$ and $\tilde{N}_1\tilde{N}_1 \rightarrow \gamma Z$, the γ-ray spectrum from heavy neutralino annihilation has a continuum component which arises primarily from pion decay. The requirement that this continuum contribution not exceed the flux observed by EGRET [115] provides another phenomenological check on the model. It was shown in [90] that the continuum photon flux produced by the decay of a heavy Wino or Higgsino LSP will be low enough that no conflict arises between the predictions of the dark matter scenario model and EGRET data. This is one advantage of heavy Wino or Higgsino dark matter in AMSB scenarios: this constraint is not a trivial one, and may be relevant in many models with a lighter LSP.

So far we have considered only the contribution to the γ-ray flux arising from annihilations in our own galactic halo, but it is also interesting to consider the effects of dark matter annihilation in other galaxies to the total observed photon background. The γ-ray flux arising from extragalactic WIMP annihilation has been investigated by several authors [118, 119, 120, 121]. The results depend significantly on the choice of halo profile and on other astrophysical inputs about which there is substantial uncertainty, including the number density distribution (often also called the cosmological mass function) $\frac{dn}{dM}(M, z)$ of halos in the universe as a function of

halo mass M and redshift z and the correlation between halo mass and dark matter concentration. The situation is further complicated by the possibility that a nontrivial fraction of dark matter could be bound in small subhalos within larger, virialized halos [122, 123], for in this case the contribution to the γ-ray flux from extragalactic dark matter annihilation can be substantially increased. Owing to these uncertainties, the best way to proceed is to choose a reasonable astrophysical model that is not too conservative (in terms of the resulting γ-ray flux) and ascertain whether the continuum spectrum from LSP annihilation is consistent with EGRET data. Results corresponding to the choice of a Press-Schechter [124] cosmological mass function, an NFW halo profile without subhalos, and a Wino or Higgsino LSP with a mass of 180 GeV were derived in [118]. It was shown that for the relatively cuspy NFW profile, the continuum component of this flux was not large enough to conflict with EGRET data, and one would expect a heavier LSP of the same sort would also be compatible with the observed γ-ray spectrum at energies $E_\gamma \lesssim 100$ GeV. For a cuspier distribution, such as the Moore et. al profile, or a model where a substantial fraction of the dark matter is concentrated in subhalos, however, the continuum flux could potentially come into conflict with these measurements.

In addition to the continuum flux, the extragalactic photon spectrum from LSP annihilation also has a "discrete" component—the $\tilde{N}_1\tilde{N}_1 \to \gamma\gamma$ and $\tilde{N}_1\tilde{N}_1 \to \gamma Z$ lines, which will be smeared out somewhat due to absorption and redshifting effects. If the diffuse γ-ray background in the TeV range indeed obeys the same power-law relation (6.13) that it does at lower energies, the $\gamma\gamma$ and $Z\gamma$ peaks will likely be difficult to detect in particle physics models of this sort. However, if the contribution to the γ-ray spectrum from all other sources drops significantly when $E_\gamma \gtrsim 100$ GeV, as is the case in certain models where blazar emissions dominate this spectrum at high energies [118], these peaks could dominate over the rest of the background

by several orders of magnitude. In practice, however, it is unlikely that the signal from the extragalactic annihilation of a TeV-scale Wino or Higgsino LSP offers much in the way of additional prospects for indirect detection. It was illustrated in figure 6.6 that GLAST, like all space telescopes, is hindered in its ability to meet the event count requirement (6.15) necessary for signal detection by its small effective area. Even when $\Delta\Omega$ is adjusted to near the telescope's field of view, the extragalactic photon flux from LSP annihilation will likely be insufficient to meet this requirement, and hence there is good reason to think that GLAST will fare little better in detecting extragalactic LSP annihilation than it will in detecting LSP annihilation at the center of our own galaxy, no matter what the shape of the diffuse photon background is at high energies. ACTs are also unlikely to detect this signal, since the background they see (6.16) - (6.17) is an order of magnitude larger than that seen by space telescopes and does not depend on the shape of the diffuse γ-ray background.

The message here is that while the γ-ray spectrum from extragalactic LSP annihilation is interesting both because it provides a consistency check on a given particle physics model (that the continuum spectrum does not conflict with EGRET data) and because it contains distinctive structures (the "monoenergetic" peaks) at energies as yet unprobed, the former consideration is not damning for the case of heavy Wino or Higgsino dark matter, and the latter is not likely to yield any new possibilities for indirect detection. As with the case with the signal from LSP annihilations in our own galactic halo, the difficulty in detecting the signal from extragalactic LSP annihilation stems from the limitations of satellite detectors due to their small collection areas.

To summarize the results of this chapter, although energy resolution considerations rule out discrimination between the $\gamma\gamma$ and $Z\gamma$ lines from heavy LSP decay, the detection of a single

monoenergetic photon "line" is still a possibility at atmospheric Cherenkhov detectors like HESS and VERITAS, which have a large enough effective collection area to register a statistically significant discovery. Space telescopes like GLAST, on the other hand, have far smaller effective areas and hence will be unlikely ever to observe the signal in question. Detection at Cherenkhov facilities is far from guaranteed, however, and prospects for it depend significantly on the dark matter distribution in our galaxy. Continuum photons are also produced during LSP annihilations, both in our galactic halo and in the halos of other galaxies, but these are not likely to run afoul of current experimental constraints on the γ-ray background unless the universal dark matter profile is extremely cuspy or involves substantial substructure.

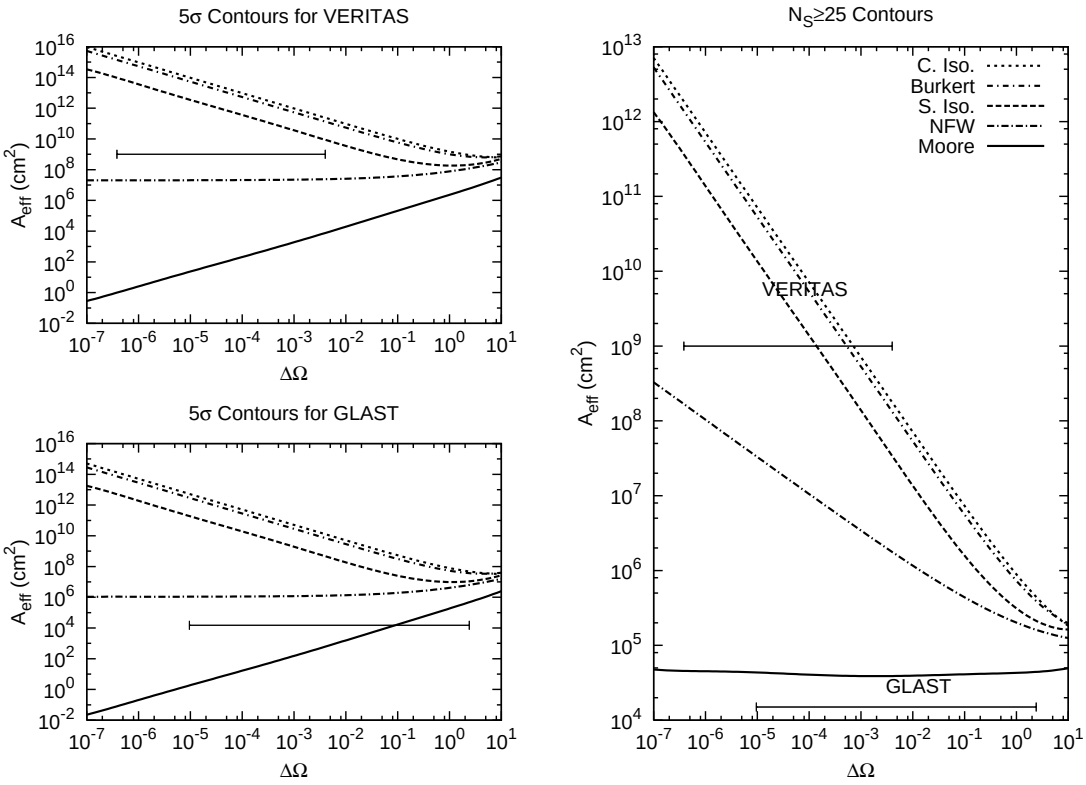

Figure 6.6: Detection boundary contours in $A_{\text{eff}} - \Delta\Omega$ parameter space for the γ-ray signature of a 2.3 TeV Wino, based on the 5σ significance requirement from equation 6.14 for VERITAS (top left panel), with $A_{\text{eff}} = 1 \times 10^9$ cm^2 and $\Delta E/E$, and GLAST (bottom left panel), with $A_{\text{eff}} = 1.5 \times 10^4$ cm^2; and based on the $N_S \geq 25$ event count requirement from equation 6.15 (right panel), for a variety of halo profiles. Bars showing the range of angular acceptances that can be chosen at VERITAS and GLAST have also been included. In order to register a discovery at either of these facilities for a given halo model, *both* the 5σ and $N_s \geq 25$ contours for that model must lie below the bar corresponding to that facility [61].

CHAPTER VII

CONCLUSIONS

Leptogenesis is an attractive model, and the prospect that its ability to relate the smallness of neutrino masses to the mechanism responsible for baryogenesis could be realized in a scenario where neutrinos are purely Dirac is an interesting one for many reasons. We have shown that thermal Dirac leptogenesis is not only an intriguing theoretical curiosity, but also a genuinely viable phenomenological model. Not only is it capable of producing a baryon-to-photon ratio η for the universe that matches that observed by WMAP, but it can also satisfy all relevant constraints from cosmology, flavor physics, etc. while reproducing the observed neutrino spectrum.

Specifically, from the research presented in this work and that originally presented in the publications [38, 43, 61] and reviewed herein, the following results and conclusions were obtained:

- **There is a particularly simple, theoretically-motivated realization of Dirac leptogenesis, constrained hierarchical Dirac leptogenesis (CHDL), which reproduces the observed neutrino spectrum.**

In its most general form, the Dirac leptogenesis superpotential (2.1) contains a large number of new free parameters, including the heavy particle masses M_{Φ_i}, the scalar VEV χ and the elements of the general, complex trilinear coupling matrices λ and h. It is thus not terribly surprising that some configuration of parameters is capable of satisfying all experimental bounds on neutrino masses and mixings, but it is of interest that this set of constraints can be satisfied in a simple, theoretically-motivated model that contains only five free parameters (four, if one does not include the highly constrained coupling matrix entry b_3). In [38], it was shown that a particularly simple model of Dirac leptogenesis, which was dubbed constrained hierarchical Dirac leptogenesis (CHDL), in which the trilinear coupling matrices λ and h are antisymmetric, the mass matrix M_Φ is real and diagonal, and the small ratio $\delta = M_{\Phi_1}/M_{\Phi_1}$ dictates the textures of the neutrino mass matrix, the experimental constraints are readily satisfied. The model is simple, robust and well-motivated by flavon physics (see section 5.2). Furthermore, as was shown in [38] and reviewed in chapter 4.2, this model is compatible with the additional constraints arising from baryogenesis, astrophysics, and cosmology.

- **Dirac leptogenesis strongly prefers a heavy gravitino with $m_{3/2} \gtrsim 10^5$ GeV and is compatible with split supersymmetry.**

  Dirac leptogenesis must respect a battery of astrophysical constraints in order to be considered a phenomenologically viable theory, and the most stringent of these are related to gravitino cosmology. The connection between this subject and leptogenesis occurs through the reheating temperature T_R. On the one hand, $T_R \lesssim M_{\Phi_1}$ is required for thermal leptogenesis; on the other, for certain values of the gravitino mass $m_{3/2}$, considerations related to BBN and nonthermal LSP production place stringent limits on T_R. In [38], it was

shown that baryogenesis considerations require $M_{\Phi_1} \gtrsim 10^{10}$ GeV, unless some additional mechanism—such as resonant leptogenesis—is invoked. Thus, when $m_{3/2} \lesssim 10^5$ GeV, nucleosynthesis bounds on T_R from late gravitino decay render Dirac leptogenesis in its simplest form essentially unworkable; when 10^5 GeV $\lesssim m_{3/2} \lesssim 10^8$ GeV things are better, but constraints related to nonthermal LSP creation also cause problems when the splitting between $m_{3/2}$ and m_{LSP} is small. These results are summarized in table 7.1. For this reason, Dirac leptogenesis strongly prefers a heavy gravitino with $m_{3/2} \gtrsim 10^5$ GeV. Since this is a natural consequence of split supersymmetry, this scenario becomes one possible context for Dirac leptogenesis. This scenario has the added advantage of keeping squark and slepton masses heavy to alleviate flavor-violation concerns, while keeping gauginos light to provide a (characteristic) dark matter candidate.

- **Dirac leptogenesis can succeed in models with light ($m_s = 200$ GeV) scalar masses.**

  In any model where supersymmetric scalar particles are light and where the mass eigenstates of these particles are not diagonal in the flavor basis of the Standard Model quarks and leptons, loop diagrams involving such particles can potentially give rise to unacceptable levels of flavor violation. In Dirac leptogenesis, the renormalization group running of slepton soft masses will tend to generate off-diagonal terms in the sneutrino and charged slepton mass matrices. It was shown in [43] that flavor violation constraints do not rule out CHDL: the model is successful for a universal scalar mass m_s as low as 200 GeV, respecting all lepton-flavor-violation constraints from processes such as $\mu \to e\gamma$ and $\tau \to \mu\gamma$. Dirac leptogenesis therefore does not require split supersymmetry and will be phenomenologically viable in a wide range of contexts. More general AMSB [58, 64]

models, for example, can yield a splitting between $m_{3/2}$ and m_{LSP} large enough to permit a gravitino with a mass slightly above the BBN bound ($m_{3/2} \lesssim 10^5$ GeV) and sparticle masses of $\mathcal{O}(200$ TeV) without running afoul of any of the late gravitino decay constraints.

- **Obtaining the appropriate superpotential for Dirac leptogenesis can be arranged in a consistent, anomaly-free manner through the introduction of a hidden sector $U(1)_N$ symmetry.**

  The Dirac leptogenesis superpotential requires some additional symmetry to forbid tree-level Dirac and Majorana masses for right-handed neutrinos. It was shown in section 5.3 that this can be accomplished in a simple, consistent, anomaly-free manner by enlarging the hidden sector of the model. It was shown that the necessary VEVs are obtained to yield small but nonzero masses and to ensure that all R-parity odd fields in the hidden sector become massive after supersymmetry is broken.

- **Right-handed sneutrino dark matter is a viable possibility in Dirac leptogenesis.**

  Unlike in Majorana leptogenesis, in Dirac leptogenesis the lightest right-handed sneutrino $\tilde{\nu}_{R_1}$ can be light, and as it is neutral under the Standard Model gauge group, it is a potential dark matter candidate if it is the LSP. Since the interactions of this particle are extremely weak (as they are suppressed by the powers of the effective neutrino Yukawa coupling), its relic abundance will in general be far larger than the upper bound (3.4) on Ω_{CDM} obtained from WMAP data. However, Dirac leptogenesis comes equipped with a mechanism for alleviating this problem: the theory requires an additional symmetry (to forbid Majorana masses for neutrinos) under which $\tilde{\nu}_{R_1}$ is necessarily charged. In

section 5.3, it was shown that if this symmetry is a gauged $U(1)$, annihilations through the gauge bosons and gauginos associated with this additional symmetry can reduce the right-handed sneutrino abundance to an appropriate level.

- **Linking Ω_{CDM} to Ω_b via an asymmetry in some conserved quantum number is generally quite difficult, at least in supersymmetric theories, and requires a hierarchy among annihilation rates.**

  The possibility that the cold dark matter abundance Ω_{CDM} and the relic density Ω_b of baryonic matter in the universe, which are of roughly the same order, might be linked is an intriguing one. One way of arranging this is the method of [93], in which the association is forged by charging a hidden-sector dark matter candidate under a globally conserved quantum number. Then dark matter particles annihilate with their antiparticles until only the excess given by the asymmetry is left, and this excess becomes the dark matter abundance. This cannot work in the usual neutralino dark matter scenario, since Majorana neutralinos cannot develop a charge asymmetry, but a right-handed sneutrino LSP in Dirac leptogenesis, which carries lepton number charge, has the right properties to allow this mechanism to work. Unfortunately, linking the right-handed sneutrino abundance to the lepton number L_{ν_R} stored in $\tilde{\nu}_{R_1}$ in this manner proves difficult in practice. It was shown in section 5.3 that this required the L_{ν_R}–violating rate $\Gamma_{\tilde{\nu}\tilde{\nu}}$ to be small, so as to preserve the lepton number asymmetry at the appropriate level, whereas it required the L_{ν_R}–conserving rate $\Gamma_{\tilde{\nu}\tilde{\nu}^*}$ to be several orders of magnitude larger, so that right-handed sneutrinos could annihilate efficiently and dark matter would not consequently be overproduced. However, in a supersymmetric model, s-channel diagrams in which a dark matter particle and its antiparticle annihilate through some virtual Z' are accompanied

by t-channel diagrams (with Majorana gaugino intermediaries) that violate L_{ν_R}. It is worth restating that the evolution of L_{ν_R} during the CDM freeze-out epoch will not affect the baryon number B of the universe whatsoever (the effect of $\Gamma_{\tilde{\nu}\tilde{\nu}}$ is simply to shuffle lepton number from $\tilde{\nu}_{R_1}$ to ν_R and other light hidden sector fields, and not to change L_{hid}), and so right-handed sneutrino dark matter is perfectly compatible with baryogenesis in Dirac leptogenesis scenarios. However, it was shown in section 5.3 that while it is possible to obtain the correct Ω_{CDM} with a right-handed sneutrino, the inherent tension between $\Gamma_{\tilde{\nu}\tilde{\nu}}$ and $\Gamma^*_{\tilde{\nu}\tilde{\nu}}$ makes it very difficult simultaneously to prevent L_{ν_R} from being washed out to the extent where it will have no bearing on the dark matter abundance. It was shown that there are ways of overcoming this hurdle, such as adding a large number of light scalars to the theory, but these methods are somewhat contrived. The prospects may be brighter for linking Ω_{CDM} and Ω_b in other situations where a dark matter candidate is charged under some conserved quantum number, but since it is the supersymmetrization of annihilation processes that lies at the root of the problem, the issue is a general one—especially since supersymmetric models naturally provide a compelling solution to the dark matter problem, in the form of the LSP, when R-parity is conserved.

- **The prospects for detecting the monoenergetic photon signal of heavy Wino or Higgsino dark matter reasonably good at atmospheric Chernenkhov telescopes (ACTs) like HESS and VERITAS, but slim at space-based facilities like GLAST.**

  Since split supersymmetry emerges as one promising context for CHDL, it is relevant to the study of Dirac leptogenesis, and of more general interest as well, to examine the discovery potential for the dark matter candidate that naturally emerges from this scenario:

a predominately Wino or Higgsino LSP with a mass around 1 TeV. The direct detection prospects for such a particle are somewhat dim, and the easiest way of discovering such a particle is through the observation of the effectively monoenergetic photon signal produced by its annihilations at the galactic center. In [61], we show that space telescopes such as GLAST are highly unlikely to record the necessary number of signal events to claim a statistically significant discovery, due to their small effective collection area A_{Eff}. Ground-based Cherenkhov arrays, however, have far larger effective areas and hence far better prospects for the discovery of a heavy Wino or Higgsino LSP.

Gravitino Mass Range (GeV)	Maximum M_{Φ_1} (GeV)	Workability of CHDL?	Comments
$m_{3/2} \lesssim 10^5$	$10^6 - 10^8$	Very Low	$\tilde{G}$ decay during or after BBN. Insufficient η generated.
$10^5 \lesssim m_{3/2} \lesssim 10^8$	$10^9 - 10^{10}$ or higher	Depends on m_{LSP} and the ratio $m_{LSP}/m_{3/2}$	LSP annihilations ineffective unless $m_{LSP}/m_{3/2}$ is small. T_R constrained by nonthermal LSP abundance from $\tilde{G}$ decay. Loop-split SUSY works only for $m_{3/2} \sim 10^5$ GeV. More general split SUSY theories can be successful.
$10^8 \lesssim m_{3/2} \lesssim 10^{10}$	None	Excellent	Ω_{LSP} is thermal, since $\tilde{G}$ decays before LSP freeze-out. $M_{\Phi_1} > 10^{11}$ GeV allowed. ν spectrum requirements compatible with CHDL.
$10^{10} \lesssim m_{3/2} \lesssim 10^{12}$	None	Questionable (depends on gluino properties)	ν sector and baryogenesis okay, but model may have a cosmological gluino problem.
$10^{12} \lesssim m_{3/2}$	None	Very Low	Potential gluino problem becomes a serious concern.

Table 7.1: The various gravitino mass regimes for split supersymmetry models and the viability of thermal Constrained Hierarchical Dirac Leptogenesis (CHDL) in each case.

It should be mentioned that there are a number of experimental checks on the viability of Dirac leptogenesis in general and on the specific model we have dubbed CHDL. The major prediction of Dirac leptogenesis is that neutrinoless double-beta decay will not be observed to any degree, for this process relies on the existence of a Majorana mass term for right-handed neutrinos. The discovery of such a process experimentally would rule the theory out. In addition, forthcoming results from MiniBooNE [125] should either confirm or deny the LSND result, which will reveal whether or not the neutrino spectrum produced by CHDL is in fact the one present in nature (if MiniBooNE confirms the LSND result, Dirac leptogenesis should still be workable, albeit in a more complicated manifestation than CHDL). Finally, CHDL places constraints on the neutrino mixing parameter $\sin\theta_{13}$ (see figure 3.4), the value of which will be measured in future experiments.

APPENDICES

APPENDIX A

Effective Couplings for Flavor-Violating Calculations

For completeness, we list here the results used in our analysis for lepton flavor violating processes. The amplitudes A^L and A^R in equation (3.44) were computed in [83] and, with a trivial extension to include three right-handed sneutrinos, are given by

$$A^L = A^{(c),L} + A^{(n),L} \qquad \text{and} \qquad A^R = A^{(c),R} + A^{(n),R}, \tag{A.1}$$

where the individual amplitudes $A^{(c),L}$, $A^{(n),L}$, $A^{(c),R}$, and $A^{(n),R}$ are

$$\begin{aligned} A^{(n)L} &= \frac{1}{32\pi^2}\sum_{A=1}^{4}\sum_{X=1}^{6}\frac{1}{m^2_{\tilde{\ell}_X}}\left[N^L_{iAX}N^{L*}_{jAX}\frac{1}{6(1-x_{AX})^4}\right. \\ &\quad \times(1-6x_{AX}+3x^2_{AX}+2x^3_{AX}-6x^2_{AX}\ln x_{AX}) \\ &\quad \left.+N^L_{iAX}N^{R*}_{jAX}\frac{M_{\tilde{\chi}^0_A}}{m_{l_j}}\frac{1}{(1-x_{AX})^3}(1-x^2_{AX}+2x_{AX}\ln x_{AX})\right], \end{aligned} \tag{A.2}$$

$$\begin{aligned} A^{(c)L} &= -\frac{1}{32\pi^2}\sum_{A=1}^{2}\sum_{X=1}^{6}\frac{1}{m^2_{\tilde{\nu}_X}}\left[C^L_{iAX}C^{L*}_{jAX}\frac{1}{6(1-x_{AX})^4}\right. \\ &\quad \times(2+3x_{AX}-6x^2_{AX}+x^3_{AX}+6x_{AX}\ln x_{AX}) \\ &\quad \left.+C^L_{iAX}C^{R*}_{jAX}\frac{M_{\tilde{\chi}^-_A}}{m_{l_j}}\frac{1}{(1-x_{AX})^3}(-3+4x_{AX}-x^2_{AX}-2\ln x_{AX})\right], \end{aligned} \tag{A.3}$$

$$A^{(n,c)R} = A^{(n,c)L}|_{L\leftrightarrow R}. \tag{A.4}$$

Here, the indices A and X respectively label the gaugino (chargino or neutralino) and slepton (sneutrino or charged slepton) mass eigenstates, $x_{AX} \equiv m^2_{\chi_A}/m^2_{\phi_X}$, and $C^{L,R}_{iAX}$ ($N^{L,R}_{iAX}$) denote the effective couplings of charged lepton i to chargino (neutralino) A and sneutrino (charged slepton) X. The flavor mixing terms in (3.38) - (3.40) enter into the overall rate (3.44) through $C^{L,R}_{iAX}$ and $N^{L,R}_{iAX}$, which contain elements of the matrices U_ν and U_ℓ that diagonalize the mass-squared matrices for sneutrinos and charged sleptons, respectively. The slepton masses also enter into the partial amplitudes (A.2-A.4).

The effective couplings $N^{L,R}_{iAX}$ and $C^{L,R}_{iAX}$ are

$$\begin{aligned}
N^R_{iAX} &= -\frac{g_2}{\sqrt{2}}\left([-(U_N)_{A2} - (U_N)_{A1}\tan\theta_W]U^\ell_{X,i} + \frac{m_{l_i}}{m_W\cos\beta}(U_N)_{A3}U^\ell_{X,i+3}\right), \\
N^L_{iAX} &= -\frac{g_2}{\sqrt{2}}\left(\frac{m_{l_i}}{m_W\cos\beta}(U_N)_{A3}U^\ell_{x,i} + 2(U_N)_{A1}\tan\theta_W U^\ell_{X,i+3}\right), \\
C^R_{iAX} &= -g_2(O_R)_{A1}U^\nu_{X,i}, \quad \text{and} \\
C^L_{iAX} &= g_2\frac{m_{l_i}}{\sqrt{2}m_W\cos\beta}(O_L)_{A2}U^\nu_{X,i}
\end{aligned} \tag{A.5}$$

in terms of the chargino mixing matrices $(O_R)_{A,i}$ and $(O_L)_{A,i}$ the neutralino mixing matrix $U^N_{X,i}$, and the sneutrino and charged slepton mixing matrices $U^\nu_{X,i}$ and $U^\ell_{X,i}$. The chargino mixings matrices are defined by the relation

$$M_c^{diag} = (O_R)M_c(O_L)^T, \tag{A.6}$$

where

$$M_c = \begin{pmatrix} 0 & X \\ X^T & 0 \end{pmatrix}, \quad \text{where} \quad X = \begin{pmatrix} M_2 & \sqrt{2}M_W\cos\beta \\ \sqrt{2}M_W\sin\beta & \mu \end{pmatrix} \tag{A.7}$$

and M_c^{diag} is diagonal. The sneutrino mixing matrix $U^\nu_{X,i}$ and the charged slepton mixing matrix $U^\ell_{X,i}$ are defined by the relations

$$(m^2_{\tilde{\ell}^\pm})^{diag} = U^\ell m^2_{\tilde{\ell}^\pm}U^\dagger_\ell \quad , \quad (m^2_{\tilde{\nu}^\pm})^{diag} = U^\ell m^2_{\tilde{\nu}}U^\dagger_\ell, \tag{A.8}$$

where the matrices $m^2_{\tilde{\ell}^\pm}$ and $m^2_{\tilde{\nu}}$ are given by the sum of the MSSM contribution and the respective Dirac leptogenesis contributions in (3.41). The neutralino mixing matrix U_N is defined by the relation

$$(m_{\tilde{N}})^{diag} = U_N m_{\tilde{N}} U_N^\dagger, \tag{A.9}$$

where

$$m_{\tilde{N}} = \begin{pmatrix} M_1 & 0 & -M_Z \sin\theta_w \cos\beta & M_Z \sin\theta_w \sin\beta \\ 0 & M_2 & M_Z \cos\theta_w \cos\beta & -M_Z \cos\theta_w \cos\beta \\ -M_Z \sin\theta_w \cos\beta & M_Z \cos\theta_w \cos\beta & 0 & -\mu \\ M_Z \sin\theta_w \sin\beta & -M_Z \cos\theta_w \sin\beta & -\mu & 0 \end{pmatrix}. \tag{A.10}$$

APPENDIX B

Derivation of the Boltzmann Equations for Dirac Leptogenesis

In this appendix, we derive the Boltzmann equations (4.2) - (4.3) for the evolution of baryon and lepton number in Dirac leptogenesis, following the methods and notation of [126]. We begin by observing that the Boltzmann equation for any particle species a in the early universe can be written in terms of the number density n_a of a as

$$\begin{aligned}\frac{dn}{dt}_a + 3Hn_a &= \int \frac{d^3p_a}{(2\pi)^3}\frac{d^3p_i}{(2\pi)^3}\frac{d^3p_j}{(2\pi)^3}\cdots\frac{d^3p_k}{(2\pi)^3}(2\pi)^4\delta(\sum_{n=a,i,j,\ldots k} p_n) \\ &\quad \left[\sum_{int.} |\mathcal{M}(a\ldots i \to j\ldots k)|^2 (f_a\ldots f_i)\right. \\ &\quad \left. - \sum_{int.} |\mathcal{M}(j\ldots k \to a\ldots i)|^2 (f_j\ldots f_k)\right], \end{aligned} \tag{B.1}$$

where f_i is the phase-space distribution function of particle i, $|\mathcal{M}(a\ldots i \to j\ldots k)|^2$ are the squared matrix elements for particle-number-changing interactions involving a, and the sums are over all interaction processes which create or destroy a. The term proportional to the Hubble parameter H can be absorbed by rewriting equation (B.1) in terms of the ratio $Y_a \equiv n_a/s$, where s is the

entropy density of the unverse [42]:

$$\frac{dY_A}{dt} = \frac{1}{s}\int \frac{d^3p_a}{(2\pi)^3}\frac{d^3p_i}{(2\pi)^3}\frac{d^3p_j}{(2\pi)^3}\cdots\frac{d^3p_k}{(2\pi)^3}(2\pi)^4\delta(\sum_{n=a,i,j,\ldots k} p_n) \left[\sum_{int.}|\mathcal{M}(a\ldots i\to j\ldots k)|^2(f_a\ldots f_i) - \sum_{int.}|\mathcal{M}(j\ldots k\to a\ldots i)|^2(f_j\ldots f_k)\right], \quad \text{(B.2)}$$

In the high temperature limit $T \gg m_a$, the ratio Y_a is well-approximated by

$$Y_a = n_a/s \simeq \frac{1}{2}\frac{g_a}{g_{*s}(T)}e^{\mu_a/T}, \quad \text{(B.3)}$$

where g_a and μ_a respectively denote the the number of degrees of freedom and chemical potential of species a and $g_{*s}(T)$ represents the total number of relativistic interacting degrees of freedom at temperature T.[1] If an asymmetry $A_a = Y_a - Y_{a^c}$ develops between a and its antiparticle a^c, the chemical potential μ_a can be expressed in terms of this asymmetry (assuming μ_a, $A_a \ll 1$) using the relation

$$A_a \simeq \frac{1}{2}\frac{g_a}{g_{*s}}e^{-\mu_a/T}(e^{2\mu_a/T}-1) \simeq \frac{1}{2}\frac{g_a}{g_{*s}}(e^{2\mu_a/T}-1), \quad \text{(B.4)}$$

which implies that

$$e^{\mu_a/T} \simeq 1 + A_a\frac{g_{*s}}{g_a}. \quad \text{(B.5)}$$

In deriving Boltzmann equations for the heavy fields, we will begin with those for the scalars ϕ and ϕ^c. To first order in these fields, the leading processes include only decays and inverse decays, the Boltzmann equations for the abundances Y_ϕ and $Y_{\overline{\phi}}$ are given by

$$\frac{dY_{\phi_\Phi}}{dt} = -\frac{1}{s}\Lambda_{12}^{\phi_\Phi}\left[f_{\phi_\Phi}\,|\mathcal{M}(\phi_\Phi\to\tilde{\ell}\phi_\chi)|^2 + f_{\phi_\Phi}\,|\mathcal{M}(\phi_\Phi\to\nu_R^c\widetilde{H}_u^c)|^2 - f_{\phi_\chi}f_{\tilde{\ell}}\,|\mathcal{M}(\widetilde{\ell}\phi_\chi\to\phi_\Phi)|^2 - f_{\nu_R^c}f_{\widetilde{H}_u^c}\,|\mathcal{M}(\nu_R^c\widetilde{H}_u^c\to\phi_\Phi)|^2\right] \quad \text{(B.6)}$$

[1] During the epoch of interest, $g_{*s}(T)$ remains constant, and thus we will henceforth drop the T-dependence in our notation.

and

$$\frac{dY_{\phi^c_\Phi}}{dt} = -\frac{1}{s}\Lambda_{12}^{\phi^c_\Phi}\Big[f_{\phi^c_\Phi}\ |\mathcal{M}(\phi^c_\Phi \to \widetilde{\ell}^c\phi^c_\chi)|^2 + f_{\phi^c_\Phi}\ |\mathcal{M}(\phi^c_\Phi \to \nu_R\widetilde{H}_u)|^2 - f_{\phi^c_\chi} f_{\widetilde{\ell}^c}\ |\mathcal{M}(\widetilde{\ell}^c\phi^c_\chi \to \phi^c_\Phi)|^2 - f_{\nu_R} f_{\widetilde{H}_u}\ |\mathcal{M}(\nu_R\widetilde{H}_u \to \phi^c_\Phi)|^2\Big], \tag{B.7}$$

where $\Lambda^{a\ldots i}_{j\ldots k}$ has been used as a shorthand to denote the appropriate phase-space integral and we use the notation ℓ and H_u to denote the usual Lepton and Higgs-up doublets of $SU(2)$. These equations can be simplified by noting that energy conservation implies that the inverse decay processes of the form $(a + i \to b)$ appearing in equations (B.6) and (B.7), in which particle i is in chemical equilibrium with other particles in the thermal bath (i.e. $\mu_i = 0$), the previous relation allows us to write

$$f_a\ f_i \simeq f_b^{eq}(1 + \frac{s}{n_\gamma}\frac{A_a}{g_a}), \tag{B.8}$$

where f_a^{eq} is the equilibrium distribution of a. The assumption of CPT-invariance also simplifies these expressions by enforcing the relation

$$|\mathcal{M}(a \to ij)|^2 = |\mathcal{M}(i^c j^c \to a^c)|^2. \tag{B.9}$$

The particle asymmetries with which we will be concerned here are the lepton number abundances $L_i = Q_{L_i}(n_i - n_i^c)/s$ carried by each field i in the theory with lepton number charge

Q_{L_i}. From the charge assignments given in table 2.1 the nonzero L_i are given by

$$L_\ell = Y_\ell - Y_{\ell^c} \tag{B.10}$$

$$L_{\nu_R} = -(Y_{\nu_R} - Y_{\nu_R^c}) \tag{B.11}$$

$$L_{\widetilde{\ell}} = Y_{\widetilde{\ell}} - Y_{\widetilde{\ell}^c} \tag{B.12}$$

$$L_{\widetilde{\nu}_R} = -(Y_{\widetilde{\nu}_R} - Y_{\widetilde{\nu}_R^c}) \tag{B.13}$$

$$L_{\phi_\Phi} = Y_{\phi_\Phi} - Y_{\phi_\Phi^c} \tag{B.14}$$

$$L_{\phi_{\overline{\Phi}}} = -(Y_{\phi_{\overline{\Phi}}} - Y_{\phi_{\overline{\Phi}}^c}) \tag{B.15}$$

Using these definitions and relations (B.8) and (B.9), the Boltzmann equations for ϕ and ϕ^c become

$$\frac{dY_{\phi_\Phi}}{dt} = -\frac{1}{s}\int \frac{d^3p_{\phi_\Phi}}{(2\pi)^3}\left[(f_{\phi_\Phi} - f^{eq}_{\phi_\Phi})\Gamma_D - \frac{s}{2n_\gamma} f^{eq}_{\phi_\Phi}\left(\frac{L_{\widetilde{\ell}}}{2}\,\Gamma^c_L + L_{\nu_R}\,\Gamma^c_R\right)\right] \tag{B.16}$$

$$\frac{dY_{\phi^c_\Phi}}{dt} = -\frac{1}{s}\int \frac{d^3p_{\phi_\Phi}}{(2\pi)^3}\left[(f_{\phi^c_\Phi} - f^{eq}_{\phi_\Phi})\Gamma_D + \frac{s}{2n_\gamma} f^{eq}_{\phi_\Phi}\left(\frac{L_{\widetilde{\ell}}}{2}\,\Gamma_L + L_{\nu_R}\,\Gamma_R\right)\right], \tag{B.17}$$

where the interaction rates $\Gamma_L = \Gamma(\phi \to \widetilde{\ell} + \chi)$ and $\Gamma_R = \Gamma(\phi \to \nu^c_R + \tilde{H}^c_u)$ are defined by the relations

$$\Gamma_L = \int \frac{d^3p_i}{(2\pi)^3}\frac{d^3p_i}{(2\pi)^3}|\mathcal{M}(\phi \to \ell\chi)|^2 \tag{B.18}$$

$$\Gamma_R = \int \frac{d^3p_i}{(2\pi)^3}\frac{d^3p_i}{(2\pi)^3}|\mathcal{M}(\phi \to \nu^c_R\tilde{H}^c_u)|^2, \tag{B.19}$$

with Γ^c_L, R being the rates of the conjugate processes and $\Gamma_D = \Gamma_L + \Gamma_R$ is the total decay rate for ϕ, $\overline{\phi}$, etc. given in (2.6). Because of supersymmetry, the total decay rate of the fermion components of the heavy supermultiplets Φ and $\overline{\Phi}$ will also be Γ_D, with the same Γ_L and Γ_R as their partial rates.

It will be more convenient for our purposes to express the Boltzmann equations in terms of $Y_{\phi^c_\Phi}$ and L_{ϕ_Φ}. Subtracting (B.17) from (B.16) yields

$$\begin{aligned}\frac{dL_{\phi_\Phi}}{dt} &= -\frac{1}{s}\int \frac{d^3p_{\phi_\Phi}}{(2\pi)^3}\left[(f_{\phi_\Phi}-f^c_{\phi_\Phi})\Gamma_D\right. \\ &\left. -\frac{s}{2n_\gamma}f^{eq}_{\phi_\Phi}\left(\frac{L_{\widetilde{\ell}}}{2}\left(\Gamma_L+\Gamma^c_L\right)+L_{\nu_R}\left(\Gamma_R+\Gamma^c_R\right)\right)\right] \qquad \text{(B.20)}\end{aligned}$$

After integrating equations (B.17) and (B.20) over the incoming momentum $\vec{p}_\phi$, using relations (2.2) - (2.5) to express the result in terms of the decay asymmetry ϵ, and averaging over time-dilation factors [126] we obtain

$$\begin{aligned}\frac{dL_{\phi_\Phi}}{dz} &= -\langle\Gamma_D\rangle\left[L_{\phi_\Phi}-\frac{s}{2n_\gamma}Y^{eq}_{\phi_\Phi}\epsilon\left(\frac{L_{\widetilde{\ell}}}{2}-L_{\nu_R}\right)\right] \\ &\quad +Y^{eq}_{\phi_\Phi}\frac{s}{n_\gamma}\left[\frac{L_{\widetilde{\ell}}}{2}\langle\Gamma_L\rangle+L_{\nu_R}\langle\Gamma_R\rangle\right] \qquad \text{(B.21)}\\ \frac{dY_{\phi^c_\Phi}}{dt} &= -\left[(Y_{\phi^c_\Phi}-Y^{eq}_{\phi_\Phi})\langle\Gamma_D\rangle+\frac{s}{2n_\gamma}Y^{eq}_{\phi_\Phi}\left(\frac{L_{\widetilde{\ell}}}{2}\langle\Gamma_L\rangle+L_{\nu_R}\langle\Gamma_R\rangle\right)\right],, \qquad \text{(B.22)}\end{aligned}$$

were, the time-dilation-averaged rates $\langle\Gamma_i\rangle$ are given in terms of the naive rates Γ_i factors [126]:

$$\langle\Gamma_i\rangle = \frac{K_1(M_\Phi/T)}{K_2(M_\Phi/T)}\,\Gamma_i \qquad \text{(B.23)}$$

where $K_1(x)$ and $K_2(x)$ are modified Bessel functions.

The Boltzmann equations for the scalar component of the $\overline{\Phi}$ superfield (and its conjugate), as well as the ones for the fermion components of Φ and $\overline{\Phi}$, are obtained in a similar manner. They turn out to be

$$\begin{aligned}\frac{dL_{\phi_{\overline{\Phi}}}}{dt} &= -\langle\Gamma_D\rangle\left[L_{\phi_{\overline{\Phi}}}+\frac{s}{2n\gamma}\epsilon\,Y^{eq}_{\phi_\Phi}\left(\frac{L_\ell}{2}-L_{\tilde{\nu}_R}\right)\right] \\ &\quad +Y^{eq}_{\phi_\Phi}\left[\frac{L_\ell}{2}\langle\Gamma^c_L\rangle+L_{\tilde{\nu}_R}\langle\Gamma^c_R\rangle\right)] \qquad \text{(B.24)}\\ \frac{dY_{\phi_{\overline{\Phi}}}}{dt} &= -\left[(Y_{\phi_{\overline{\Phi}}}-Y^{eq}_{\phi_\Phi})\langle\Gamma_D\rangle-\frac{s}{2n_\gamma}Y^{eq}_{\phi_\Phi}\left(\frac{L_\ell}{2}\langle\Gamma_L\rangle-L_{\tilde{\nu}_R}\langle\Gamma_R\rangle\right)\right. \\ &\quad \left.+\frac{s}{2n_\gamma}\epsilon\langle\Gamma_D\rangle Y^{eq}_{\phi_\Phi}\left(\frac{L_\ell}{2}-L_{\tilde{\nu}_R}\right)\right], \qquad \text{(B.25)}\end{aligned}$$

where we have used the fact that $Y^{eq}_{\phi_\Phi} = Y^{eq}_{\phi_{\overline{\Phi}}}$. Dropping negligibly small terms proportional to ϵL_i, we notice that Boltzmann equations for the combinations $Y^+_{\phi_\Phi} \equiv= Y_{\phi_\Phi} + Y_{\phi^c_\Phi}$ and $Y^+_{\phi_{\overline{\Phi}}} \equiv= Y_{\phi_{\overline{\Phi}}} + Y_{\phi^c_{\overline{\Phi}}}$

$$\frac{dY^+_{\phi_\Phi}}{dt} = -\langle\Gamma_D\rangle\left(Y^+_{\phi_\Phi} - 2Y^{eq}_{\phi_\Phi}\right) \tag{B.26}$$

$$\frac{dY^+_{\phi_{\overline{\Phi}}}}{dt} = -\langle\Gamma_D\rangle\left(Y^+_{\phi_{\overline{\Phi}}} - 2Y^{eq}_{\phi_\Phi}\right) \tag{B.27}$$

$$\tag{B.28}$$

are redundant. We thus only require three equations to describe the dynamics of the heavy field sector.

We now turn to address the evolution of the Lepton number abundance of the particle species ℓ, ν_R, $\tilde{\ell}$, and $\tilde{\nu_R}$, in which we must take into account the effect of $2 \leftrightarrow 2$ processes which transfer lepton number between L_ℓ, L_{ν_R}, $L_{\widetilde{\ell}}$, and $L_{\widetilde{\nu}_R}$. For the moment, we will not concern ourselves with the exact form these interaction terms will take, but will will make one important observation: the rates for interactions which shuffle lepton number between ℓ, $\tilde{\ell}$, and the right-handed charged lepton and sleptons fields e_R and $\tilde{e}_R$ will be much larger than those for the interactions which shuffle lepton number between ν_R and any of these other fields. This is because the ν_R interact only via processes pictured in figure 4.1, which involve a virtual ϕ_Φ, $\phi_{\overline{\Phi}}$, etc. while all of the other fields either take part in $SU(2)$ and/or $U(1)_Y$ gauge interactions. We will represent the effects of these rapid equilibration processes by including terms Σ_A (where A is the relevant particle asymmetry) to represent them in the Boltzmann equations. The slower $2 \leftrightarrow 2$ processes through which right handed neutrinos ν_R interact with lepton doublets ℓ and $\widetilde{\ell}$ and with right handed sneutrino $\tilde{\nu}_R$ will be included separately as $C_{\nu_R \leftrightarrow \ell}$, $C_{\nu_R \leftrightarrow \tilde{\ell}}$ and $C_{\nu_R \leftrightarrow \tilde{\nu}_R}$. As discussed in chapter IV and elsewhere, $\tilde{\nu}_R$ may or may not also take part in rapid

equilibration processes, depending on the value of $\langle F_\chi \rangle$.

To simplify further the notation we will define the terms F_A to account for the collective contribution from decays (and inverse decays) of the fermionic components of Φ and $\overline{\Phi}$ (which we will not write explicitly, being of similar form to the contribution from the scalar components).

Expressed in the above notation, the equations for the left-handed lepton field ℓ and its conjugate ℓ^c are

$$\begin{aligned}
\frac{dY_\ell}{dt} &= \frac{1}{n_\gamma}\Lambda_{12}^{\phi^c_{\overline{\Phi}}}\left[f_{\phi^c_{\overline{\Phi}}}\,|\mathcal{M}(\phi^c_{\overline{\Phi}} \to \ell\psi_{_\chi})|^2 - f_{\phi_{_\chi}} f_\ell\,|\mathcal{M}(\ell\psi_{_\chi} \to \phi^c_{\overline{\Phi}})|^2\right] \\
&\quad + F_L(\psi^c_{_\Phi}) + \Sigma_L. \qquad \text{(B.29)} \\
\frac{dY_{\ell^c}}{dt} &= \frac{1}{n_\gamma}\Lambda_{12}^{\phi_{\overline{\Phi}}}\left[f_{\phi_{\overline{\Phi}}}\,|\mathcal{M}(\phi_{\overline{\Phi}} \to \ell^c\psi^c_{_\chi})|^2 - f_{\psi^c_{_\chi}} f_{\ell^c}\,|\mathcal{M}(\ell^c\psi^c_{_\chi} \to \phi_{\overline{\Phi}})|^2\right] \\
&\quad + F^c_L(\psi_{_\Phi}) + \Sigma^c_L \qquad \text{(B.30)}
\end{aligned}$$

The lepton number abundance L_ℓ is obtained by subtracting the second of these equations from the first, and the result is

$$\begin{aligned}
\frac{dL_\ell}{dt} &= -\frac{1}{n_\gamma}\int d^3p_{\phi_{_\Phi}}\left[f_{\phi_{\overline{\Phi}}}\,\Gamma^{\overline{\phi}}_{\ell^c\tilde{\chi}^c} - f^{eq}_{\phi_{\overline{\Phi}}}(1-L/4)\Gamma^{\overline{\phi}^c}_{\ell\tilde{\chi}} - f_{\phi^c_{\overline{\Phi}}}\,\Gamma^{\overline{\phi}^c}_{\ell\tilde{\chi}}\right. \\
&\quad \left. + f^{eq}_{\phi_{_\Phi}}(1+L/4)\Gamma^{\overline{\phi}}_{\ell^c\tilde{\chi}^c}\right] + (F_L - F^c_L) + (\Sigma_L - \Sigma^c_L) \\
&= -\epsilon\,\langle\Gamma_D\rangle\left(Y_{\phi^c_{\overline{\Phi}}} + Y^{eq}_{\phi_{_\Phi}}\right) + L_{\phi_{\overline{\Phi}}}\langle\Gamma_L\rangle - Y^{eq}_{\phi_{_\Phi}}\frac{s}{n_\gamma}L_\ell\,\left(\langle\Gamma_L\rangle - \frac{1}{2}\epsilon\langle\Gamma_D\rangle\right) \\
&\quad + F_\ell + \Sigma_\ell + C_{_{\nu_R\leftrightarrow\ell}} \qquad \text{(B.31)}
\end{aligned}$$

The equations for L_{ν_R}, $L_{\widetilde{\nu}_R}$, and $L_{\widetilde{\ell}}$ are determined in a similar manner:

$$\begin{aligned}
\frac{dL_{\nu_R}}{dt} &= \epsilon\,\langle\Gamma_D\rangle\Big(Y^c_{\phi_\Phi}+Y^{eq}_{\phi_\Phi}\Big)-L_{\phi_\Phi}\langle\Gamma_R\rangle+Y^{eq}_{\phi_\Phi}\frac{s}{n_\gamma}L_{\nu_R}\Big(\langle\Gamma_R\rangle-\frac{1}{2}\epsilon\Gamma_D)\Big)\\
&\quad +F_{\nu_R}-C_{\nu_R\leftrightarrow\widetilde{\ell}}-C_{\nu_R\leftrightarrow\widetilde{\nu}_R}-C_{\nu_R\leftrightarrow\ell} \qquad \text{(B.32)}\\
\frac{dL_{\widetilde{\ell}}}{dt} &= -\epsilon\,\langle\Gamma_D\rangle(Y_{\phi^c_\Phi}+Y^{eq}_{\phi_\Phi})+L_{\phi_\Phi}\langle\Gamma_L\rangle-Y^{eq}_{\phi_\Phi}\frac{s}{n_\gamma}L_{\widetilde{\ell}}\Big(\frac{1}{2}\langle\Gamma_L\rangle+\frac{1}{2}\epsilon\langle\Gamma_D\rangle\Big)\\
&\quad +F_{\widetilde{\ell}}+\Sigma_{\tilde{\ell}}+\ C_{\nu_R\to\widetilde{\ell}} \qquad \text{(B.33)}\\
\frac{dL_{\widetilde{\nu}_R}}{dt} &= \epsilon\,\langle\Gamma_D\rangle(Y_{\phi^c_{\overline{\Phi}}}+Y^{eq}_{\phi_{\overline{\Phi}}})-L_{\phi_{\overline{\Phi}}}\langle\Gamma_R\rangle-Y^{eq}_{\phi_{\overline{\Phi}}}\frac{s}{n_\gamma}L_{\widetilde{\nu}_R}\Big(\langle\Gamma_R\rangle+\frac{1}{2}\epsilon\Gamma_D\Big)\\
&\quad +F_{\widetilde{\nu}_R}+\Sigma_{\widetilde{\nu}_R}+C_{\nu_R\to\widetilde{\nu}_R}. \qquad \text{(B.34)}
\end{aligned}$$

Before going any further we still need to compute the terms $C_{\nu_R\leftrightarrow\widetilde{\ell}}$, $C_{\nu_R\leftrightarrow\widetilde{\nu}_R}$ and $C_{\nu_R\leftrightarrow\ell}$ corresponding to the $2\leftrightarrow 2$ processes mediated by heavy fields. We begin by calculating $C_{\nu_R\leftrightarrow\tilde{L}}$, which is given by

$$\begin{aligned}
C_{\nu_R\leftrightarrow\widetilde{\ell}} &= \frac{2}{n_\gamma}\Lambda^{34}_{12}e^{-(E_1+E_2)/T}\Bigg[\Big(|\mathcal{M}'(\widetilde{H}^c_u\nu^c_R\to\widetilde{\ell}\chi)|^2-|\mathcal{M}'(\widetilde{\ell}\chi\to\nu^c_R\widetilde{H}^c_u)|^2\Big)\\
&\quad +\frac{(L_{\nu_R}-\frac{1}{2}L_{\widetilde{\ell}})}{2}\Big(|\mathcal{M}'(\widetilde{H}^c_u\nu^c_R\to\widetilde{\ell}\chi)|^2+|\mathcal{M}'(\widetilde{\ell}\chi\to\nu^c_R\widetilde{H}^c_u)|^2\Big)\Bigg] \qquad \text{(B.35)}
\end{aligned}$$

$\mathcal{M}'$ here refers to the amplitude for the specified $2\leftrightarrow 2$ process to which we have substracted the contribution from the resonant intermediate state (RIS) in which a real field ϕ_Φ is produced and then decayed into the 2 particle final state. The RIS contribution must be substracted since we have already counted contributions from decays of real ϕ_Φ fields.

The leading term in the difference between a $2\leftrightarrow 2$ process of the form $ab\to ij$ involving a heavy intermediary k and its conjugate process depends on the contribution of the on-shell (resonant) intermediate state:

$$|\mathcal{M}'(ab\to ij)|^2-|\mathcal{M}'(ij\to ab)|^2=|\mathcal{M}_{\mathcal{RIS}}(ij\to ab)|^2-|\mathcal{M}_{\mathcal{RIS}}(ab\to ij)|^2 \qquad \text{(B.36)}$$

with

$$|\mathcal{M}_{\mathcal{RIS}}(ab \to ij)|^2 \simeq \frac{\pi}{m_\phi \Gamma_D}\delta(s - m_\phi^2)|\mathcal{M}(ab \to k)|^2 \times |\mathcal{M}(k \to ij)|^2 \tag{B.37}$$

where k represents the intermediate-state particle, and s is the usual kinematic variable $s = (p_1^{in} + p_2^{in})^2$. In our case, making use of the equality $\Gamma_L^c \Gamma_R - \Gamma_L \Gamma_R^c = \epsilon \Gamma_D$ we find

$$|\mathcal{M}_{\mathcal{RIS}}(\widetilde{\ell}\chi \to \nu_R^c \widetilde{H}_u^c)|^2 - |\mathcal{M}_{\mathcal{RIS}}(\widetilde{H}_u^c \nu_R^c \to \widetilde{\ell}\chi)|^2 \simeq \epsilon \frac{\pi}{m_\phi \Gamma_D}\delta(s - m_\phi^2)|\mathcal{M}_{tot}^\phi|^4 \tag{B.38}$$

and substituting this result in eq. (B.35) we finally obtain

$$C_{\nu_R \leftrightarrow \widetilde{\ell}} \;=\; 2\epsilon Y_{\phi_\Phi}^{eq} \langle \Gamma_D \rangle + (L_{\nu_R} - \frac{1}{2} L_{\widetilde{\ell}})\; n_\gamma \langle v\sigma_{\nu_R \to \widetilde{\ell}} + v\sigma_{\widetilde{\ell} \to \nu_R} \rangle. \tag{B.39}$$

For the other sets of $2 \leftrightarrow 2$ processes, $C_{\nu_R \to \widetilde{\nu}_R}$ and $C_{\nu_R \to \ell}$, the procedure is essentially the same. The rates $\langle \Gamma_{\nu_R \leftrightarrow \widetilde{\ell}} \rangle \equiv n_\gamma \langle v\sigma_{\nu_R \to \widetilde{\ell}} + v\sigma_{\widetilde{\ell} \to \nu_R} \rangle$, $\langle \Gamma_{\nu_R \leftrightarrow \ell} \rangle \equiv n_\gamma \langle v\sigma_{\nu_R \to \ell} + v\sigma_{\ell \to \nu_R} \rangle$ and $\langle \Gamma_{\nu_R \leftrightarrow \widetilde{\nu}_R} \rangle \equiv n_\gamma \langle v\sigma_{\nu_R \to \widetilde{\nu}_R} + v\sigma_{\widetilde{\nu}_R \to \nu_R} \rangle$, associated with these interactions are calculated in section 4.2. We will denote the total contribution from these processes as $\langle \Gamma_{2 \leftrightarrow 2} \rangle$.

At this point, the full Boltzmann system comprises fifteen individual differential equations: four to represent the evolution of ϕ_Φ, $\phi_{\overline{\Phi}}$, and their conjugates (in whatever basis we choose); an additional four for the fermionic superpartners in the Φ and $\overline{\Phi}$ supermultiplets; six for the the Lepton asymmetries L_ℓ, L_{ν_R}, $L_{\widetilde{\ell}}$, $L_{\widetilde{\nu}_R}$, $L_{e_R} \equiv e_R^c - e_R$, and $L_{\widetilde{e}_R}$ stored in various individual lepton and slepton species; and one for the overall baryon number B of the universe, which interacts with L_ℓ via sphaleron processes of the form given in equation 1.17.[2] We have already noted that equations (B.22) and (B.25) are redundant up to terms of $\mathcal{O}(\epsilon L_i)$, and the assumption of unbroken supersymmetry during the leptogenesis epoch allows us to equate the abundances of the fermionic and bosonic components of Φ_1 and $\overline{\Phi}_1$, which reduces the number of equations in

[2]Keeping track of individual baryon numbers is unnecessary, since QCD gauge interactions among the quarks are rapid.

our system to ten. As discussed in section 4.1, we can also make use of the fact that many of the light fields in our theory will be brought into chemical equilibrium by rapid $SU(2) \times U(1)_Y$ gauge interactions, Yukawa interactions, A-terms, etc. whose collective rates we have denoted Σ_A. In this case, any lepton number stored in ℓ, $\tilde{\ell}$, e_R, or $\tilde{e}_R$ should be rapidly distributed among all of these particles in proportion to the relative number of degrees of freedom for each field. Whether $\tilde{\nu}_R$ is also in equilibrium with these fields depends on the size of the effective A-term (2.11) induced by $\langle F_\chi \rangle$: if $\langle F_\chi \rangle$ is large, the $\tilde{\nu}_R$ fields will equilibrate chemically with the left-handed leptons and sleptons; if $\langle F_\chi \rangle$ is small (or zero), they will not, but can be seen as part of the hidden sector which contains the right-handed neutrino fields. In either case, we can define two aggregate lepton numbers L_{vis} and L_{hid} for the fields in the visible and hidden sectors respectively and reduce the number of equations in our Boltzmann system to six. In the case where $\langle F_\chi \rangle$ is large and $\tilde{\nu}_R$ is in the visible sector, we have

$$L_{vis} = L_\ell + L_{\tilde{\nu}_R} + L_{\tilde{\ell}} + L_{e_R} + L_{\tilde{e}_R} \tag{B.40}$$

$$L_{hid} = L_{\nu_R}, \tag{B.41}$$

When $\tilde{\nu}_R$ is in the hidden sector, we have

$$L_{vis} = L_\ell + L_{\tilde{\nu}_R} + L_{\tilde{\ell}} + L_{e_R} \tag{B.42}$$

$$L_{hid} = L_{\nu_R} + L_{\tilde{e}_R}. \tag{B.43}$$

In either case, chemical equilibrium enforces that the lepton number stored in each individual particle species be distributed evenly among them in proportion to the number of degrees of freedom of each, or in other words

$$\frac{7}{2} L_\ell = \frac{7}{2} L_{\tilde{\ell}} = 7 L_{\tilde{\nu}_R} = 7 L_{e_R} = 7 L_{\tilde{e}_R} = L_{vis} \tag{B.44}$$

in the large-$\langle F_\chi \rangle$ scenario, and

$$3L_\ell = 3L_{\tilde{\ell}} = 6L_{e_R} = L_{\tilde{e}_R} = L_{vis} \tag{B.45}$$

in the small-$\langle F_\chi \rangle$ scenario. In the latter case, if chemical equilibrium is established among the fields in the hidden sector (for example, via the gauge interactions of the gauged $U(1)_Y$ discussed in section 5.3), one obtains the similar relation

$$\frac{1}{2}L_{\nu_R} = \frac{1}{2}L_{\tilde{e}_R} = L_{hid}. \tag{B.46}$$

In the large-$\langle F_\chi \rangle$ scenario, the Boltzmann equation that describes the evolution of L_{vis}, which is obtained by summing equations (B.31) - (B.34) with the appropriate numerical prefactor from (B.44), is

$$\begin{aligned} \frac{dL_{vis}}{dt} &= -\epsilon\langle\Gamma_D\rangle\left(Y^c_{\phi_\Phi} - Y^{eq}_{\phi_\Phi}\right) + \langle\Gamma_L\rangle\left(L_{\phi_\Phi} + L_{\phi_{\overline{\Phi}}}\right) + \langle\Gamma_R\rangle L_{\phi_{\overline{\Phi}}} \\ &\quad -Y^{eq}_{\phi_\Phi}\frac{s}{2n_\gamma}L_{vis}\Big(\langle\Gamma_D\rangle + \langle\Gamma_L\rangle\Big) + \left(L_{hid} - \frac{1}{7}L_{vis}\right)\langle\Gamma_{2\leftrightarrow 2}\rangle, \end{aligned} \tag{B.47}$$

where small terms proportional to ϵ times L_ℓ, L_{ν_R}, $L_{\widetilde{\ell}}$ or $L_{\tilde{\nu}_R}$ have been dropped. Here, we have used the fact that the Boltzmann equations for L_{e_R} and $L_{\tilde{e}_R}$ are trivial, consisting of only Σ_A terms, which all cancel after taking the sum of all Lepton abundances.

In the event that annihilation processes of the form $\phi_\Phi \phi^c_\Phi \to X$, where X represents some final state comprising light fields, are effective in reducing the abundance of ϕ_Φ and its conjugate, equation (B.22) must be modified slightly to account for the presence of source and sink terms

$$\frac{dY_{\phi^c_\Phi}}{dt} = \ldots\ -\frac{1}{s}\Lambda^{34}_{12}\left[f_{\phi_\Phi}f_{\phi^c_\Phi}\ |\mathcal{M}(\phi_\Phi\phi^c_\Phi \to ij)|^2 - f_i f_j\ |\mathcal{M}(ij \to \phi_\Phi\phi^c_\Phi)|^2\right]. \tag{B.48}$$

Here, i and j represent the unspecified final states products of $\phi_\Phi - \phi^s_\Phi$ annihilation (in which $2 \leftrightarrow 2$ processes will again dominate) and Λ^{34}_{12} is the appropriate four-particle phase-space

integral. Ignoring negligible CP-violation effects and invoking conservation of momentum, we obtain the relation $f_i f_j = (f^{eq}_{\phi_\Phi})^2$, which leads to the result

$$\frac{dY_{\phi^c_\Phi}}{dt} = \ldots \; - \langle \sigma(\phi_\Phi \phi^c_\Phi \to X)|v| \rangle \left[Y^2_{\phi^c_\Phi} - (Y^{eq}_{\phi_\Phi})^2 \right]. \tag{B.49}$$

Using equation (4.18), this can be written in terms of the effective annihilation rate Γ_A.

The only task left is to couple the Bolztmann equations for B and L_{vis} via electroweak sphaleron interactions. The high-temperature rate for these interactions, Γ_{sph}, is given in equation (1.20), and the proportionality constant between B and L_{vis} is given, in the supersymmetric case, by equation (1.35), and since B is otherwise conserved, the equation for its evolution is

$$\frac{dB}{dt} = -\langle \Gamma_{sph} \rangle \left(B + \frac{8}{15} L_{vis} \right) \tag{B.50}$$

We are now ready to write down the complete Boltzmann system for the evolution of baryon and lepton number in Dirac leptogenesis. Collecting equations (B.21) - (B.22), (B.24), (B.32), (B.47), and (B.50) and defining the shorthand expressions

$$\langle \Gamma_D \rangle_{ID} = \frac{1}{7} \frac{n^{eq}_{\phi_\Phi}}{n_\gamma} \langle \Gamma_D \rangle \qquad \langle \Gamma_L \rangle_{ID} = \frac{1}{7} \frac{n^{eq}_{\phi_\Phi}}{n_\gamma} \langle \Gamma_L \rangle \qquad \langle \Gamma_R \rangle_{ID} = \frac{n^{eq}_{\phi_\Phi}}{n_\gamma} \langle \Gamma_D \rangle \tag{B.51}$$

for the inverse decay rates, we obtain the following result:

$$\frac{dB}{dt} = -\langle\Gamma_{sph}\rangle\Big(B + \frac{8}{15}L_{vis}\Big) \tag{B.52}$$

$$\begin{aligned}\frac{dL_{vis}}{dt} &= -2\epsilon\langle\Gamma_D\rangle(Y_{\phi^c_\Phi} - Y^{eq}_{\phi_\Phi}) + \langle\Gamma_L\rangle(L_{\phi_\Phi} + L_{\phi_{\overline{\Phi}}}) + \langle\Gamma_R\rangle L_{\phi_{\overline{\Phi}}} \\ &\quad -2L_{vis}\Big(\langle\Gamma_D\rangle_{ID} + \langle\Gamma_L\rangle_{ID}\Big) + (L_{hid} - \frac{1}{7}L_{vis})\langle\Gamma_{2\leftrightarrow 2}\rangle \\ &\quad -\langle\Gamma_{sph}\rangle\Big(B + \frac{8}{15}L_{vis}\Big)\end{aligned} \tag{B.53}$$

$$\begin{aligned}\frac{dL_{hid}}{dt} &= 2\epsilon\langle\Gamma_D\rangle(Y_{\phi^c_\Phi} - Y^{eq}_{\phi_\Phi}) + L_{\phi_\Phi}\langle\Gamma_R\rangle - 2L_{hid}\langle\Gamma_R\rangle_{ID} \\ &\quad -(L_{hid} - \frac{1}{7}L_{vis})\langle\Gamma_{2\leftrightarrow 2}\rangle\end{aligned} \tag{B.54}$$

$$\begin{aligned}\frac{dY_{\phi^c_\Phi}}{dt} &= -\langle\Gamma_D\rangle(Y_{\phi^c_\Phi} - Y^{eq}_{\phi_\Phi}) + \frac{1}{2}L_{vis}\langle\Gamma_L\rangle_{ID} + \frac{1}{2}L_{hid}\ \langle\Gamma_R\rangle_{ID} \\ &\quad -\langle\Gamma_A\rangle\left[\Big(Y_{\phi^c_\Phi}/Y^{eq}_{\phi_\Phi}\Big)^2 - 1\right]\end{aligned} \tag{B.55}$$

$$\frac{dL_{\phi_\Phi}}{dt} = -\langle\Gamma_D\rangle L_{\phi_\Phi} + 2L_{vis}\langle\Gamma_L\rangle_{ID} + 2L_{hid}\langle\Gamma_R\rangle_{ID} \tag{B.56}$$

$$\frac{dL_{\phi_{\overline{\Phi}}}}{dt} = -\langle\Gamma_D\rangle L_{\phi_{\overline{\Phi}}} + 2L_{vis}\langle\Gamma_D\rangle_{ID}, \tag{B.57}$$

where once again, negligibly small terms proportional to ϵL_{vis} or ϵL_{hid} have been dropped. Changing variables from t to $z = M_{\Phi_i}/T$, one obtains equations (4.2) - (4.7).

In the "drift and decay" limit, in which all the rates in $\langle\Gamma_A\rangle$ and $\langle\Gamma_{2\leftrightarrow 2}\rangle$ are assumed to be much smaller than the rate of expansion of the universe H, we note that this system simplifies considerably. In this case

$$\frac{dL_{vis}}{dt} = -2\epsilon\langle\Gamma_D\rangle(Y_{\phi^c_\Phi} - Y^{eq}_{\phi_\Phi}) \tag{B.58}$$

$$\frac{dL_{hid}}{dt} = 2\epsilon\langle\Gamma_D\rangle(Y_{\phi^c_\Phi} - Y^{eq}_{\phi_\Phi}) \tag{B.59}$$

$$\frac{dY^c_{\phi_\Phi}}{dt} = -\langle\Gamma_D\rangle(Y_{\phi^c_\Phi} - Y^{eq}_{\phi_\Phi}), \tag{B.60}$$

and since the right sides of these expressions are proportional to one another, the Boltzmann

system reduced to a single differential equation, whose solution is

$$L_{hid}(t \to \infty) = -L_{vis}(t \to \infty) = 2\epsilon Y^{eq}_{\phi_\Phi}(t = t_0), \tag{B.61}$$

given the boundary conditions $L_{vis}(t = 0) = L_{hid}(t = 0) = 0$ and $Y^{eq}_{\phi_\Phi}(t \to \infty) = 0$ and approximating $Y_{\phi^c_\Phi}$ by its equilibrium abundance at time t_0, defined as the time at which $T = M_{\Phi_1}$.

APPENDIX C

Derivation of the Boltzmann Equations for Hidden Sector Dark Matter

Here we present a derivation of the Boltzmann equations for right-handed sneutrino dark matter, using the methods of [126]. We begin by writing down the equations in terms of the abundances: $Y_{\tilde{\nu}_R} = n_{\tilde{\nu}_R}/s$ and $Y_{\tilde{\nu}^c_R} = n_{\tilde{\nu}^c_R}/s$:

$$\begin{aligned}
\frac{dY_{\tilde{\nu}_R}}{dt} &= \frac{1}{s}\Lambda^{34}_{12}\left[2f_{\nu_R}f_{\nu_R}\,|\mathcal{M}(\nu_R\nu_R \to \tilde{\nu}_R\tilde{\nu}_R)|^2 - 2f_{\tilde{\nu}_R}f_{\tilde{\nu}_R}\,|\mathcal{M}(\tilde{\nu}_R\tilde{\nu}_R \to \nu_R\nu_R)|^2\right. \\
&\qquad \left. + f_{\nu^c_R}f_{\nu_R}\,|\mathcal{M}(\nu^c_R\nu_R \to \tilde{\nu}_R\tilde{\nu}^c_R)|^2 - f_{\tilde{\nu}^c_R}f_{\tilde{\nu}_R}\,|\mathcal{M}(\tilde{\nu}^c_R\tilde{\nu}_R \to \nu^c_R\nu_R)|^2\right] \qquad \text{(C.1)} \\
\frac{dY_{\tilde{\nu}^c_R}}{dt} &= \frac{1}{s}\Lambda^{34}_{12}\left[2f_{\nu^c_R}f_{\nu^c_R}\,|\mathcal{M}(\nu^c_R\nu^c_R \to \tilde{\nu}^c_R\tilde{\nu}^c_R)|^2 - 2f_{\tilde{\nu}^c_R}f_{\tilde{\nu}^c_R}\,|\mathcal{M}(\tilde{\nu}^c_R\tilde{\nu}^c_R \to \nu^c_R\nu^c_R)|^2\right. \\
&\qquad \left. + f_{\nu^c_R}f_{\nu_R}\,|\mathcal{M}(\nu^c_R\nu_R \to \tilde{\nu}_R\tilde{\nu}^c_R)|^2 - f_{\tilde{\nu}^c_R}f_{\tilde{\nu}_R}\,|\mathcal{M}(\tilde{\nu}^c_R\tilde{\nu}_R \to \nu^c_R\nu_R)|^2\right]. \qquad \text{(C.2)}
\end{aligned}$$

Here the phase space integral Λ^{34}_{12} is defined as in equation (B.6). The energy-conservation condition (B.8) implies that

$$\begin{aligned}
f_{\nu_R}f_{\nu_R} &= e^{-(E_{N_{R1}}+E_{N_{R2}})/T}(1 + g_{*s}L_{\nu_R}) \qquad \text{(C.3)} \\
f_{\nu^c_R}f_{\nu^c_R} &= e^{-(E_{N_{R1}}+E_{N_{R2}})/T}(1 - g_{*s}L_{\nu_R}) \qquad \text{(C.4)} \\
f_{\nu_R}f_{\nu^c_R} &= e^{-(E_{N_{R1}}+E_{N_{R2}})/T}, \qquad \text{(C.5)}
\end{aligned}$$

and we also will neglect CP violation (a good assumption at scales $T \ll M_{\Phi_1}$, and define

$$|\mathcal{M}(\nu_R^c \nu_R^c \to \tilde{\nu}_R^c \tilde{\nu}_R^c)|^2 = |\mathcal{M}(\nu_R \nu_R \to \tilde{\nu}_R \tilde{\nu}_R)|^2 = |\mathcal{M}_{RR}|^2 \tag{C.6}$$

$$|\mathcal{M}(\nu_R \nu_R^c \to \tilde{\nu}_R \tilde{\nu}_R^c)|^2 = |\mathcal{M}_{RR^c}|^2. \tag{C.7}$$

With these simplifications, the Boltzmann equations become

$$\frac{dY_{\tilde{\nu}_R}}{dt} = \frac{1}{s}\Lambda_{12}^{34}\, e^{-\left(E_{N_{R_1}}+E_{N_{R_2}}\right)/T}\left[2\,|\mathcal{M}_{RR}|^2\left(1+g_{*s}L_{\nu_R}-\left(\frac{n_{\tilde{\nu}_R}}{n_{\tilde{\nu}_R}^{MB}}\right)^2\right)\right.$$
$$\left. +\,|\mathcal{M}_{RR^c}|^2\left(1-\frac{n_{\tilde{\nu}_R}n_{\tilde{\nu}_R^c}}{n_{\tilde{\nu}_R^c}^{MB}n_{\tilde{\nu}_R}^{MB}}\right)\right] \tag{C.8}$$

$$\frac{dY_{\tilde{\nu}_R^c}}{dt} = \frac{1}{s}\Lambda_{12}^{34}\, e^{-\left(E_{N_{R_1}}+E_{N_{R_2}}\right)/T}\left[2\,|\mathcal{M}_{RR}|^2\left(1-g_{*s}L_{\nu_R}-\left(\frac{n_{\tilde{\nu}_R^c}}{n_{\tilde{\nu}_R^c}^{MB}}\right)^2\right)\right.$$
$$\left. +\,|\mathcal{M}_{RR^c}|^2\left(1-\frac{n_{\tilde{\nu}_R}n_{\tilde{\nu}_R^c}}{n_{\tilde{\nu}_R^c}^{MB}n_{\tilde{\nu}_R}^{MB}}\right)\right] \tag{C.9}$$

It will be more convenient for our purposes (to relate the dark matter abundance to the hidden-sector lepton asymmetry L_{hid}) to write these equations in terms of $L_{\tilde{\nu}_R} = Y_{\tilde{\nu}_R} - Y_{\tilde{\nu}_R^c}$ and $Y_{DM} = Y_{\tilde{\nu}_R} + Y_{\tilde{\nu}_R^c}$. We also define the effective rates

$$\Gamma_{\tilde{\nu}\tilde{\nu}} = \frac{1}{(Y_{\tilde{\nu}_R}^{eq})^2}\Lambda_{12}^{34}\, e^{-\left(E_{N_{R_1}}+E_{N_{R_2}}\right)/T}|\mathcal{M}_{RR}|^2 = \frac{\gamma_{\tilde{\nu}_R\tilde{\nu}_R}}{(Y_{\tilde{\nu}_R}^{eq})^2} \tag{C.10}$$

$$\Gamma_{\tilde{\nu}\tilde{\nu}}^* = \frac{1}{(Y_{\tilde{\nu}_R}^{eq})^2}\Lambda_{12}^{34}\, e^{-\left(E_{N_{R_1}}+E_{N_{R_2}}\right)/T}|\mathcal{M}_{RR^c}|^2 = \frac{\gamma_{\tilde{\nu}_R\tilde{\nu}_R^c}}{(Y_{\tilde{\nu}_R}^{eq})^2}, \tag{C.11}$$

where $Y^{eq}_{\tilde{\nu}_R} \equiv Y^{MB}_{\tilde{\nu}_R}(\mu = 0)$, in terms of which the Boltzmann equations become

$$\begin{aligned}
\frac{dL_{\tilde{\nu}_R}}{dt} &= \frac{2}{s}\Lambda^{34}_{12}\, e^{-\left(E_{N_{R1}}+E_{N_{R2}}\right)/T}|\mathcal{M}_{RR}|^2\left(2g_{*s}L_{\nu_R} + \left(\frac{n_{\tilde{\nu}^c_R}}{n^{MB}_{\tilde{\nu}^c_R}}\right)^2 - \left(\frac{n_{\tilde{\nu}_R}}{n^{MB}_{\tilde{\nu}_R}}\right)^2\right) \\
&= -\frac{2}{s}\Gamma_{\tilde{\nu}_R\tilde{\nu}_R}\left(L_{\tilde{\nu}_R}Y_{DM} - 2g_{*s}L_{\nu_R}(Y^{eq}_{\tilde{\nu}_R})^2\right) \qquad \text{(C.12)} \\
\frac{dY_{DM}}{dt} &= \frac{2}{s}\Lambda^{34}_{12}\, e^{-\left(E_{N_{R1}}+E_{N_{R2}}\right)/T}\left[|\mathcal{M}_{RR}|^2\left(2 - \left(\frac{n_{\tilde{\nu}_R}}{n^{MB}_{\tilde{\nu}_R}}\right)^2 - \left(\frac{n_{\tilde{\nu}^c_R}}{n^{MB}_{\tilde{\nu}^c_R}}\right)^2\right)\right. \\
&\qquad \left. + |\mathcal{M}_{RR^c}|^2\left(1 - \frac{n_{\tilde{\nu}_R}n_{\tilde{\nu}^c_R}}{n^{MB}_{\tilde{\nu}^c_R}n^{MB}_{\tilde{\nu}_R}}\right)\right] \\
&= \frac{2}{s}\left[\left(\Gamma_{\tilde{\nu}_R\tilde{\nu}^*_R} + 2\Gamma_{\tilde{\nu}_R\tilde{\nu}_R}\right)\left(Y^{eq2}_{\tilde{\nu}_R} - \frac{Y^2_{DM}}{4}\right) + \left(\Gamma_{\tilde{\nu}_R\tilde{\nu}^*_R} - 2\Gamma_{\tilde{\nu}_R\tilde{\nu}_R}\right)\frac{L^2_{\tilde{\nu}_R}}{4}\right] \qquad \text{(C.13)}
\end{aligned}$$

Defining the quantities $\Gamma^{(\pm)} = \Gamma_{\tilde{\nu}_R\tilde{\nu}^c_R} \pm 2\Gamma_{\tilde{\nu}_R\tilde{\nu}_R}$ and $Y^{eq}_{DM} = 2Y^{eq}_{\tilde{\nu}_R}$, these two equations take the far more manageable form

$$\begin{aligned}
\frac{dL_{\tilde{\nu}_R}}{dt} &= -\frac{2}{s}\Gamma_{\tilde{\nu}_R\tilde{\nu}_R}\left(L_{\tilde{\nu}_R}Y_{DM} - 2g_{*s}(L^{tot}_R - L_{\tilde{\nu}_R})Y^{eq^2}_{\tilde{\nu}_R}\right) \qquad \text{(C.14)} \\
\frac{dY_{DM}}{dt} &= \frac{1}{2s}\left[\Gamma^{(+)}\left({Y^{eq}_{DM}}^2 - Y^2_{DM}\right) + \Gamma^{(-)}\, L^2_{\tilde{\nu}_R}\right] \qquad \text{(C.15)}
\end{aligned}$$

given in (5.26 - 5.27).

APPENDIX D

Thermally Averaged Cross Sections

Here we provide a computation of $\hat{\sigma}(\tilde{\nu}\tilde{\nu})$ and $\hat{\sigma}(\tilde{\nu}\tilde{\nu}^*)$. Let us begin with $\hat{\sigma}(\tilde{\nu}\tilde{\nu})$. For a right-handed sneutrino LSP, the only relevant process is annihilation into neutrinos via t-channel exchange of hidden sector neutralinos χ_j^0 shown in figure D.1. It it the $\tilde{Z}'$ component of each neutralino that mediates this exchange, hence neutralino mass mixing will introduce factors of U_{1j}, where U_{ij} is unitary matrix that diagonalizes (5.19). The squared amplitude for this process is

$$\sum_{s,s'} |\mathcal{M}|^2 = 4g^4 \sum_{i,j} m_{\chi_i}^2 \, s \left(\frac{1}{t - m_{\chi_i}^2} + \frac{1}{u - {\chi_i}^2} \right) \left(\frac{1}{t - m_{\chi_j}^2} + \frac{1}{u - {\chi_j}^2} \right). \tag{D.1}$$

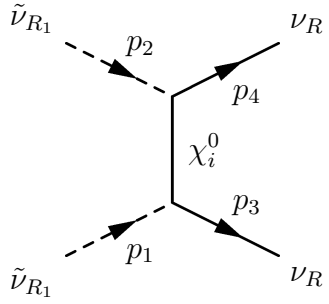

Figure D.1: Processes contributing to $\hat{\sigma}(\tilde{\nu}\tilde{\nu})$ in the right-handed sneutrino dark matter scenario.

in terms of the Mandelstam variables s, t, and u; the $U(1)_N$ gauge coupling g and the neutralino masses m_{χ_i}. Let us assume that $m_{\chi_1} \ll m_{\chi_i}$ for all $i > 1$. Then if we define the the quantities $x_{\chi_1} = s/m_{\chi_1}^2$, $x_n = s/m_{\tilde{\nu}_R}^2$, $A = (2x_n^{-1} - 2x_\chi^{-1} - 1)$, this expression simplifies to

$$\begin{aligned} \sum_{s,s'} |\mathcal{M}|^2 &= 4g^4 m_{\chi_i}^2 \, s \left(\frac{1}{t - m_{\chi_i}^2} + \frac{1}{u - {\chi_i}^2} \right)^2 \\ &= 64 g^4 \frac{m_{\chi_i}^2}{s} \left(\frac{A}{A^2 - Y^2} \right)^2 . \end{aligned} \tag{D.2}$$

Using equation (4.17) and defining $r \equiv \sqrt{1 - 4m_{\tilde{\nu}_R}^2/s}$, we find

$$\hat{\sigma}(s) = \frac{g^4}{\pi} \frac{1}{x_\chi} \left(\frac{1}{A} \ln \left(\frac{A + r}{A - r} \right)^2 - 4 \frac{r}{r^2 - A^2} \right) \tag{D.3}$$

where the s-dependence comes in through both A and r.

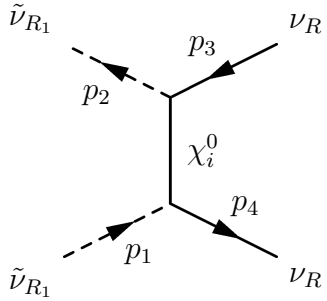

$$= \quad -i\, 2\, g^2\, Q_N^2\, |U_{1i}|^2 \left(\tfrac{1}{t - m_i^2} \right) \bar{u}(p_3) \gamma^\mu P_L \, v(p_4) \, q_\mu$$

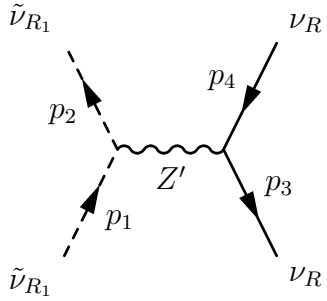

$$= \quad -i\, g^2\, Q_N^2 \left(\tfrac{1}{s - M_{Z'}^2} \right) \bar{u}(p_3) \gamma^\mu P_L \, v(p_4) \, (p_2 - p_1)_\mu$$

Figure D.2: Processes contributing to $\hat{\sigma}(\tilde{\nu}\tilde{\nu}^*)$ in the right-handed sneutrino dark matter scenario.

The reduced cross-section $\hat{\sigma}(\tilde{\nu}\tilde{\nu}^*)$ for $L_{\tilde{\nu}}$-conserving processes is slightly more complicated, as we have not only a t-channel contribution from neutralino exchange, but also an s-channel contribution mediated by the Z' gauge boson of $U(1)_N$, as shown in figure D.2. The squared amplitude for each of these processes is

$$\sum_{s,s'} |\mathcal{M}_{Z'Z'}|^2 = g^4 \left(\frac{1}{s - M_Z^2}\right)^2 s^2(r^2 - Y^2) \tag{D.4}$$

$$\begin{aligned} \sum_{s,s'} |\mathcal{M}_{\chi_1\chi_1}|^2 &= g^4 \left(\frac{1}{u - M_\chi^2}\right)^2 s^2(r^2 - Y^2) \\ &= 4g^4 \frac{r^2 - Y^2}{(A+Y)^2}, \end{aligned} \tag{D.5}$$

and the interference term between them is

$$\begin{aligned} \sum_{s,s'} |\mathcal{M}_{Z'\chi_1}|^2 &= g^4 \frac{1}{u - M_\chi^2} \frac{1}{s - M_Z^2} s^2(r^2 - Y^2) \\ &= 2g^4 \frac{s}{s - M_Z^2} \frac{r^2 - Y^2}{A + Y}. \end{aligned} \tag{D.6}$$

Straightforward calculation yields the reduced cross-section contributions

$$\hat{\sigma}_{Z'Z'} = \frac{g^4}{12\pi} \left(\frac{s}{s - M_Z^2}\right)^2 r^3 \tag{D.7}$$

$$\hat{\sigma}_{\chi\chi} = \frac{g^4}{4\pi} \left(-4r + A \ln\left(\frac{A+r}{A-r}\right)^2\right) \tag{D.8}$$

$$\hat{\sigma}_{Z'\chi_1} = \frac{g^4}{8\pi} \left(\frac{s}{s - M_Z^2}\right) \left(2Ar + \frac{(r^2 - A^2)}{2} \ln\left(\frac{A+r}{A-r}\right)^2\right), \tag{D.9}$$

the sum of which appears in equations (5.29) - (5.30).

BIBLIOGRAPHY

BIBLIOGRAPHY

[1] C. L. Bennett *et al.*, "First Year Wilkinson Microwave Anisotropy Probe (WMAP) Observations: Preliminary Maps and Basic Results," Astrophys. J. Suppl. **148**, 1 (2003) [astro-ph/0302207].

[2] A. D. Sakharov, "Violation Of CP Invariance, C Asymmetry, and Baryon Asymmetry of the Universe," Pisma Zh. Eksp. Teor. Fiz. **5**, 32 (1967) [JETP Lett. **5**, 24 (1967 SOPUA,34,392-393.1991 UFNAA,161,61-64.1991)].

[3] A. Riotto and M. Trodden, Ann. Rev. Nucl. Part. Sci. **49**, 35 (1999) [arXiv:hep-ph/9901362].

[4] A. G. Cohen and D. B. Kaplan, "Thermodynamic Generation of the Baryon Asymmetry," Phys. Lett. B **199**, 251 (1987).

[5] G. L. Alberghi, R. Casadio and A. Tronconi, Mod. Phys. Lett. A **22**, 339 (2007) [arXiv:hep-ph/0310052].

[6] H. Davoudiasl, R. Kitano, G. D. Kribs, H. Murayama and P. J. Steinhardt, Phys. Rev. Lett. **93**, 201301 (2004) [arXiv:hep-ph/0403019].

[7] S. M. Carroll and J. Shu, Phys. Rev. D **73**, 103515 (2006) [arXiv:hep-ph/0510081].

[8] R. Carosi *et al.* [NA31 Collaboration], Phys. Lett. B **237**, 303 (1990).

[9] B. Schwingenheuer *et al.*, Phys. Rev. Lett. **74**, 4376 (1995).

[10] I. Affleck and M. Dine, "A New Mechanism for Baryogenesis," Nucl. Phys. B **249**, 361 (1985).

[11] M. Fukugita and T. Yanagida, "Baryogenesis without Grand Unification," Phys. Lett. B **174**, 45 (1986).

[12] M. A. Luty, "Baryogenesis via Leptogenesis," Phys. Rev. D **45**, 455 (1992).

[13] G. 't Hooft, "Computation of the Quantum Effects Due to a Four-Dimensional Pseudoparticle," Phys. Rev. D **14**, 3432 (1976) [Erratum-ibid. D **18**, 2199 (1978)].

[14] W. Buchmuller, "Neutrinos, Grand Unification and Leptogenesis," [hep-ph/0204288]; W. Buchmuller, P. Di Bari and M. Plumacher, "Leptogenesis for Pedestrians," Annals Phys. **315**, 305 (2005) [hep-ph/0401240]; W. Buchmuller, P. Di Bari and M. Plumacher, "Some Aspects of Thermal Leptogenesis," New J. Phys. **6**, 105 (2004) [hep-ph/0406014].

[15] J. Wess and B. Zumino, Nucl. Phys. B **70**, 39 (1974).

[16] M. J. G. Veltman, Acta Phys. Polon. B **12**, 437 (1981).

[17] P. Langacker and M. x. Luo, Phys. Rev. D **44**, 817 (1991).

[18] U. Amaldi, W. de Boer and H. Furstenau, Phys. Lett. B **260**, 447 (1991).

[19] J. R. Ellis, J. S. Hagelin, D. V. Nanopoulos, K. A. Olive and M. Srednicki, Nucl. Phys. B **238**, 453 (1984).

[20] T. Yanagida, "Horizontal Gauge Symmetry and Masses of Neutrinos," *In Proceedings of the Workshop on the Baryon Number of the Universe and Unified Theories, Tsukuba, Japan, 13-14 Feb 1979*; M. Gell-Mann, P. Ramond and R. Slansky, in *Supergravity* (North Holland, Amsterdam, 1979) eds. P. Van Nieuenhuizen, D. Freedman, p. 315.

[21] J. Schechter and J. W. F. Valle, Phys. Rev. D **22**, 2227 (1980); J. Schechter and J. W. F. Valle, Phys. Rev. D **25**, 774 (1982).

[22] J. Schechter and J. W. F. Valle, Phys. Rev. D **25**, 2951 (1982).

[23] W. Buchmuller, R. D. Peccei and T. Yanagida, Ann. Rev. Nucl. Part. Sci. **55**, 311 (2005) [arXiv:hep-ph/0502169].

[24] G. 't Hooft, Phys. Rev. Lett. **37**, 8 (1976).

[25] P. Arnold and L. D. McLerran, Phys. Rev. D **36**, 581 (1987).

[26] P. Arnold, D. Son and L. G. Yaffe, Phys. Rev. D **55**, 6264 (1997) [arXiv:hep-ph/9609481].

[27] P. Arnold, D. T. Son and L. G. Yaffe, Phys. Rev. D **59**, 105020 (1999) [arXiv:hep-ph/9810216].

[28] P. Huet and D. T. Son, Phys. Lett. B **393**, 94 (1997) [arXiv:hep-ph/9610259]; D. T. Son, arXiv:hep-ph/9707351; P. Arnold, Phys. Rev. D **55**, 7781 (1997) [arXiv:hep-ph/9701393].

[29] D. Bodeker, Phys. Lett. B **426**, 351 (1998) [arXiv:hep-ph/9801430].

[30] G. D. Moore, C. r. Hu and B. Muller, Phys. Rev. D **58**, 045001 (1998) [arXiv:hep-ph/9710436].

[31] D. Bodeker, G. D. Moore and K. Rummukainen, Phys. Rev. D **61**, 056003 (2000) [arXiv:hep-ph/9907545].

[32] J. M. Cline, arXiv:hep-ph/0609145.

[33] M. C. Chen, arXiv:hep-ph/0703087.

[34] P. Vogel, arXiv:hep-ph/0611243.

[35] J. Giedt, G. L. Kane, P. Langacker and B. D. Nelson, Phys. Rev. D **71**, 115013 (2005) [arXiv:hep-th/0502032].

[36] K. Dick, M. Lindner, M. Ratz and D. Wright, "Leptogenesis with Dirac Neutrinos," Phys. Rev. Lett. **84**, 4039 (2000) [hep-ph/9907562].

[37] H. Murayama and A. Pierce, "Realistic Dirac Leptogenesis," Phys. Rev. Lett. **89**, 271601 (2002) [hep-ph/0206177].

[38] B. Thomas and M. Toharia, Phys. Rev. D **73**, 063512 (2006) [arXiv:hep-ph/0511206].

[39] M. B. Green and J. H. Schwarz, "Anomaly Cancellation in Supersymmetric D=10 Gauge Theory and Superstring Theory," Phys. Lett. B **149**, 117 (1984).

[40] M. Flanz, E. A. Paschos, U. Sarkar and J. Weiss, "Baryogenesis through Mixing of Heavy Majorana Neutrinos," Phys. Lett. B **389**, 693 (1996) [hep-ph/9607310].

[41] F. Borzumati and Y. Nomura, "Low-scale See-saw Mechanisms for Light Neutrinos," Phys. Rev. D **64**, 053005 (2001) [hep-ph/0007018].

[42] E. W. Kolb and M. S. Turner, "The Early Universe,"

[43] B. Thomas and M. Toharia, Phys. Rev. D **75**, 013013 (2007) [arXiv:hep-ph/0607285].

[44] K. A. Olive, G. Steigman and T. P. Walker, "Primordial Nucleosynthesis: Theory and Observations," Phys. Rept. **333**, 389 (2000) [astro-ph/9905320].

[45] T. Moroi, "Effects of the Gravitino on the Inflationary Universe," arXiv:hep-ph/9503210.

[46] M. Y. Khlopov and A. D. Linde, Phys. Lett. B **138**, 265 (1984); M. Kawasaki, K. Kohri and T. Moroi, "Big-bang Nucleosynthesis and Hadronic Decay of Long-lived Massive Particles," Phys. Rev. D **71**, 083502 (2005) [astro-ph/0408426].

[47] D. N. Spergel *et al.* [WMAP Collaboration], "First Year Wilkinson Microwave Anisotropy Probe (WMAP) Observations: Determination of Cosmological Parameters," Astrophys. J. Suppl. **148**, 175 (2003) [astro-ph/0302209].

[48] G. F. Giudice and A. Romanino, "Split Supersymmetry," Nucl. Phys. B **699**, 65 (2004) [Erratum-ibid. B **706**, 65 (2005)] [hep-ph/0406088].

[49] G. F. Giudice and R. Rattazzi, Phys. Rept. **322**, 419 (1999) [arXiv:hep-ph/9801271].

[50] T. Gherghetta, G. F. Giudice and A. Riotto, Phys. Lett. B **446**, 28 (1999) [arXiv:hep-ph/9808401].

[51] M. Bolz, W. Buchmuller and M. Plumacher, Phys. Lett. B **443**, 209 (1998) [arXiv:hep-ph/9809381].

[52] M. Kawasaki and T. Moroi, "Gravitino Production in the Inflationary Universe and the Effects on Big Bang Nucleosynthesis," Prog. Theor. Phys. **93**, 879 (1995) [hep-ph/9403364].

[53] T. Moroi and L. Randall, "Wino Cold Dark Matter from Anomaly-mediated SUSY Breaking," Nucl. Phys. B **570**, 455 (2000) [hep-ph/9906527].

[54] A. Arvanitaki, C. Davis, P. W. Graham, A. Pierce and J. G. Wacker, "Limits on Split Supersymmetry from Gluino Cosmology," [hep-ph/0504210].

[55] R. Allahverdi, S. Hannestad, A. Jokinen, A. Mazumdar and S. Pascoli, "Supermassive Gravitinos, Dark Matter, Leptogenesis and Flat Direction Baryogenesis," [hep-ph/0504102].

[56] N. Arkani-Hamed and S. Dimopoulos, "Supersymmetric Unification without Low Energy Supersymmetry and Signatures for Fine-tuning at the LHC," JHEP **0506**, 073 (2005) [hep-th/0405159]; N. Arkani-Hamed, S. Dimopoulos, G. F. Giudice and A. Romanino, "Aspects of Split Supersymmetry," Nucl. Phys. B **709**, 3 (2005) [hep-ph/0409232].

[57] J. D. Wells, "Implications of Supersymmetry Breaking with a Little Hierarchy Between Gauginos and Scalars," [hep-ph/0306127]; J. D. Wells, "PeV-scale Supersymmetry," [hep-ph/0411041].

[58] L. Randall and R. Sundrum, "Out of This World Supersymmetry Breaking," Nucl. Phys. B **557**, 79 (1999) [hep-th/9810155]; G. F. Giudice, M. A. Luty, H. Murayama and R. Rattazzi, "Gaugino Mass without Singlets," JHEP **9812**, 027 (1998) [hep-ph/9810442].

[59] A. Masiero, S. Profumo and P. Ullio, "Neutralino Dark Matter Detection in Split Supersymmetry Scenarios," [hep-ph/0412058].

[60] A. Arvanitaki and P. W. Graham, "Indirect Signals from Dark Matter in Split Supersymmetry," [hep-ph/0411376].

[61] B. Thomas, "Requirements to Detect the Monoenergetic Photon Signature of Thermal Cold Dark Matter in PeV-scale Split Supersymmetry," [hep-ph/0503248].

[62] M. Toharia and J. D. Wells, "Gluino Decays with Heavier Scalar Superpartners," [hep-ph/0503175].

[63] P. Gambino, G. F. Giudice and P. Slavich, "Gluino Decays in Split Supersymmetry," Nucl. Phys. B **726**, 35 (2005) [hep-ph/0506214].

[64] G. F. Giudice, M. A. Luty, H. Murayama and R. Rattazzi, JHEP **9812**, 027 (1998) [arXiv:hep-ph/9810442].

[65] M. Ibe, R. Kitano, H. Murayama and T. Yanagida, "Viable Supersymmetry and Leptogenesis with Anomaly Mediation," Phys. Rev. D **70**, 075012 (2004) [hep-ph/0403198].

[66] L. J. Hall and S. J. Oliver, "Why are neutrinos light? An alternative," Nucl. Phys. Proc. Suppl. **137**, 269 (2004) [arXiv:hep-ph/0409276].

[67] H. Goldberg, G. Perez and I. Sarcevic, "Mini Z' burst from relic supernova neutrinos and late neutrino masses," arXiv:hep-ph/0505221.

[68] G. L. Fogli, E. Lisi, D. Montanino and A. Palazzo, "Model-dependent and Independent Implications of the First Sudbury Neutrino Observatory Results," Phys. Rev. D **64**, 093007 (2001) [hep-ph/0106247].

[69] J. N. Bahcall, M. C. Gonzalez-Garcia and C. Pena-Garay, "Global Analysis of Solar Neutrino Oscillations Including SNO CC Measurement," JHEP **0108**, 014 (2001) [hep-ph/0106258].

[70] C. Hagedorn and W. Rodejohann, "Minimal Mass Matrices for Dirac Neutrinos," [hep-ph/0503143].

[71] A. Davidson and K. C. Wali, "Symmetric Versus Antisymmetric Mass Matrices in Grand Unified Theories," Phys. Lett. B **94**, 359 (1980).

[72] R. Barbieri, L. J. Hall, S. Raby and A. Romanino, Nucl. Phys. B **493**, 3 (1997) [arXiv:hep-ph/9610449]; R. Barbieri, L. J. Hall and A. Romanino, Phys. Lett. B **401**, 47 (1997) [arXiv:hep-ph/9702315]; R. Barbieri, L. Giusti, L. J. Hall and A. Romanino, Nucl. Phys. B **550**, 32 (1999) [arXiv:hep-ph/9812239].

[73] S. F. King, I. N. R. Peddie, G. G. Ross, L. Velasco-Sevilla and O. Vives, "Kaehler Corrections and Softly Broken Family Symmetries," JHEP **0507**, 049 (2005) [hep-ph/0407012].

[74] C. D. Froggatt and H. B. Nielsen, "Hierarchy of Quark Masses, Cabibbo Angles and CP Violation," Nucl. Phys. B **147**, 277 (1979).

[75] C. Jarlskog, "Commutator of The Quark Mass Matrices in the Standard Electroweak Model and a Measure of Maximal CP Violation," Phys. Rev. Lett. **55**, 1039 (1985).

[76] I. Dunietz, O. W. Greenberg and D. d. Wu, "A Priori Definition of Maximal CP Violation," Phys. Rev. Lett. **55**, 2935 (1985).

[77] S. Eidelman *et al.* [Particle Data Group], Phys. Lett. B **592**, 1 (2004).

[78] MEG Collaboration: http://meg.psi.ch

[79] Y. Kuno, Nucl. Phys. Proc. Suppl. **149**, 376 (2005).

[80] L. Calibbi, A. Faccia, A. Masiero and S. K. Vempati, arXiv:hep-ph/0605139.

[81] S. P. Martin, arXiv:hep-ph/9709356.

[82] S. P. Martin and M. T. Vaughn, Phys. Rev. D **50**, 2282 (1994) [arXiv:hep-ph/9311340].

[83] J. Hisano, T. Moroi, K. Tobe and M. Yamaguchi, "Lepton-Flavor Violation via Right-Handed Neutrino Yukawa Couplings in Phys. Rev. D **53**, 2442 (1996) [arXiv:hep-ph/9510309].

[84] S. T. Petcov, W. Rodejohann, T. Shindou and Y. Takanishi, "The see-saw mechanism, neutrino Yukawa couplings, LFV decays l(i) $\to$ l(j) Nucl. Phys. B **739**, 208 (2006) [arXiv:hep-ph/0510404].

[85] T. Hambye, M. Raidal and A. Strumia, Phys. Lett. B **632**, 667 (2006) [arXiv:hep-ph/0510008].

[86] E. J. Chun and S. Scopel, Phys. Lett. B **636**, 278 (2006) [arXiv:hep-ph/0510170].

[87] L. Covi and E. Roulet, Phys. Lett. B **399**, 113 (1997) [arXiv:hep-ph/9611425].

[88] A. Pilaftsis, Nucl. Phys. B **504**, 61 (1997) [arXiv:hep-ph/9702393].

[89] A. Pilaftsis, Phys. Rev. D **56**, 5431 (1997) [arXiv:hep-ph/9707235].

[90] P. Ullio, JHEP **0106**, 053 (2001) [hep-ph/0105052].

[91] L. J. Hall, T. Moroi and H. Murayama, "Sneutrino cold dark matter with lepton-number violation," Phys. Lett. B **424**, 305 (1998) [arXiv:hep-ph/9712515].

[92] N. Arkani-Hamed, L. J. Hall, H. Murayama, D. R. Smith and N. Weiner, "Small neutrino masses from supersymmetry breaking," Phys. Rev. D **64**, 115011 (2001) [arXiv:hep-ph/0006312].

[93] D. Hooper, J. March-Russell and S. M. West, Phys. Lett. B **605**, 228 (2005) [arXiv:hep-ph/0410114].

[94] D. E. Morrissey and J. D. Wells, Phys. Rev. D **74**, 015008 (2006) [arXiv:hep-ph/0512019].

[95] K. Griest and D. Seckel, Phys. Rev. D **43**, 3191 (1991).

[96] E. A. Mirabelli and M. E. Peskin, Phys. Rev. D **58**, 065002 (1998) [arXiv:hep-th/9712214].

[97] D. E. Kaplan, G. D. Kribs and M. Schmaltz, Phys. Rev. D **62**, 035010 (2000) [arXiv:hep-ph/9911293].

[98] Z. Chacko, M. A. Luty, A. E. Nelson and E. Ponton, JHEP **0001**, 003 (2000) [arXiv:hep-ph/9911323].

[99] M. Schmaltz and W. Skiba, Phys. Rev. D **62**, 095004 (2000) [arXiv:hep-ph/0004210].

[100] L. Bergstrom and P. Ullio, Nucl. Phys. B **504**, 27 (1997) [hep-ph/9706232]; Z. Bern, P. Gondolo and M. Perelstein, Phys. Lett. B **411**, 86 (1997) [hep-ph/9706538].

[101] B. Moore, T. Quinn, F. Governato, J. Stadel and G. Lake, Mon. Not. Roy. Astron. Soc. **310**, 1147 (1999) [astro-ph/9903164].

[102] B. Moore, F. Governato, T. Quinn, J. Stadel and G. Lake, Astrophys. J. **499**, L5 (1998) [arXiv:astro-ph/9709051].

[103] J. F. Navarro, C. S. Frenk and S. D. M. White, Astrophys. J. **462**, 563 (1996) [astro-ph/9508025].

[104] S. Casertano and J. H. van Gorkom, Astron. J. **101**, 1231 (1991).

[105] J. Edsjo, M. Schelke and P. Ullio, JCAP **0409**, 004 (2004) [arXiv:astro-ph/0405414].

[106] A. Burkert, IAU Symp. **171**, 175 (1996) [Astrophys. J. **447**, L25 (1995)] [astro-ph/9504041].

[107] Y. P. Jing and Y. Suto, Astrophys. J. **574**, 538 (2002) [arXiv:astro-ph/0202064].

[108] P. Gondolo and J. Silk, Phys. Rev. Lett. **83**, 1719 (1999) [astro-ph/9906391].

[109] T. C. Weekes, *Very High-Energy Gamma-Ray Astronomy*, IOP Publishing LTD, Philadelphia, 2003.

[110] G. Bertone, D. Hooper and J. Silk, Phys. Rept. **405**, 279 (2005) [hep-ph/0404175].

[111] J. A. Hinton [The HESS Collaboration], New Astron. Rev. **48**, 331 (2004) [arXiv:astro-ph/0403052].

[112] The VERITAS Collaboration, http://veritas.sao.arizona.edu.

[113] The GLAST Collaboration, http://www-glast.stanford.edu.

[114] S. D. Hunger *et al.*, Astrophys. J. **481** (1997) 205.

[115] P. Sreekumar *et al.* [EGRET Collaboration], Astrophys. J. **494**, 523 (1998) [astro-ph/9709257].

[116] A. W. Strong, I. V. Moskalenko and O. Reimer, Astrophys. J. **613**, 962 (2004) [astro-ph/0406254].

[117] L. Bergstrom, P. Ullio and J. H. Buckley, Astropart. Phys. **9**, 137 (1998) [astro-ph/9712318].

[118] P. Ullio, L. Bergstrom, J. Edsjo and C. G. Lacey, Phys. Rev. D **66**, 123502 (2002) [arXiv:astro-ph/0207125].

[119] J. E. Taylor and J. Silk, Mon. Not. Roy. Astron. Soc. **339**, 505 (2003) [arXiv:astro-ph/0207299].

[120] S. Ando, Phys. Rev. Lett. **94**, 171303 (2005) [arXiv:astro-ph/0503006].

[121] T. Oda, T. Totani and M. Nagashima, Astrophys. J. **633**, L65 (2005) [arXiv:astro-ph/0504096].

[122] S. Ghigna, B. Moore, F. Governato, G. Lake, T. Quinn and J. Stadel, Mon. Not. Roy. Astron. Soc. **300**, 146 (1998) [arXiv:astro-ph/9801192].

[123] A. A. Klypin, A. V. Kravtsov, O. Valenzuela and F. Prada, Astrophys. J. **522**, 82 (1999) [arXiv:astro-ph/9901240].

[124] W. H. Press and P. Schechter, Astrophys. J. **187**, 425 (1974).

[125] H. L. Ray [MiniBooNE Collaboration], arXiv:hep-ex/0701040.

[126] E. W. Kolb and S. Wolfram, "Baryon Number Generation in the Early Universe," Nucl. Phys. B **172**, 224 (1980) [Erratum-ibid. B **195**, 542 (1982)].

[127] S. P. Ahlen *et al.*, Phys. Rev. Lett. **61**, 145 (1988).

[128] S. M. Carroll, J. A. Harvey, V. A. Kostelecky, C. D. Lane and T. Okamoto, Phys. Rev. Lett. **87**, 141601 (2001) [arXiv:hep-th/0105082].

[129] N. Arkani-Hamed, H. C. Cheng, M. A. Luty and S. Mukohyama, JHEP **0405**, 074 (2004) [arXiv:hep-th/0312099].

[130] S. R. Elliott and J. Engel, J. Phys. G **30**, R183 (2004) [arXiv:hep-ph/0405078].

[131] D. G. Cerdeno, A. Dedes and T. E. J. Underwood, "The minimal phantom sector of the standard model: Higgs phenomenology and arXiv:hep-ph/0607157.

[132] S. Abel and V. Page, JHEP **0605**, 024 (2006) [arXiv:hep-ph/0601149].

[133] T. Asaka, K. Ishiwata and T. Moroi, Phys. Rev. D **73**, 051301 (2006) [arXiv:hep-ph/0512118].